NATIONAL ACADEMY OF SCIENCES OF UKRAINE
Palladin Institute of Biochemistry

BIOTECHNOLOGIA ACTA

Vol. 16, No 5, 2023

BIMONTHLY

Editorial address:
Palladin Institute of Biochemistry of the NAS of Ukraine, 9, Leontovich Street, Kyiv, 01054, Ukraine;
Tel.: +3 8 044–235–14–72; ***E-mail:*** biotech@biochem.kiev.ua; ***Web-site***: www.biotechnology.kiev.ua

According to the resolution of the Presidium of the National Academy of Sciences of Ukraine from 27.05.2009 №1-05 / 2 as amended on 25.04.2013 number 463 Biotechnologia Acta has been included in High Attestation Certification Commission list of Ukraine for publishing dissertations on specialties "Biology" and "Technology".

Certificate of registration of print media КВ series №19650-9450ПР on 01.30.2013

Literary editor — H. **Shevchenko**; Computer-aided makeup — **O. Melezhyk**
Authorized for printing 2023/10/31, Format — 210×297. Paper 115 g/m^2. Gaqrn. SchoolBookC. Print — digital. Sheets 9.7. An edition of 100 copies. Order 5.6. Make-up page is done in Palladin Institute of Biochemistry of the National Academy of Sciences of Ukraine. Print — **O. Moskalenko** FOP

NATIONAL ACADEMY OF SCIENCES OF UKRAINE
Palladin Institute of Biochemistry

BIOTECHNOLOGIA ACTA

Scientific journal

Bimonthly

Vol. 16, No 5, 2023

REVIEWS

EXPERIMENTAL ARTICLES

НАЦІОНАЛЬНА АКАДЕМІЯ НАУК УКРАЇНИ
Інститут біохімії ім. О. В. Палладіна

BIOTECHNOLOGIA ACTA

Науковий журнал

Том 16, № 4, 2023

ОГЛЯДИ

ЕКСПЕРИМЕНТАЛЬНІ СТАТТІ

UDC 606:577.112:551.583 https://doi.org/10.15407/biotech16.05.005

BIOCATALYTIC CARBON DIOXIDE CAPTURE PROMOTED BY CARBONIC ANHYDRASE

O. K. ZOLOTAREVA, N. M. TOPCHIY, O. M. FEDIUK

Kholodny Institute of Botany of the National Academy of Sciences of Ukraine, Kyiv

E-mail: olgamuronivna@ukr.net

Received 2023/08/25
Revised 2023/09/14
Accepted 2023/10/31

The rapid and steady increase in the concentration of CO_2, the most abundant greenhouse gas in the atmosphere, leads to extreme weather and climate events. Due to the burning of fossil fuels (oil, coal and natural gas), the concentration of CO_2 in the air has been increasing in recent decades by more than 2 ppm per year, and in the last year alone — by 3.29 ppm. To prevent the "worst" scenarios of climate change, immediate and significant reductions in CO_2 emissions through carbon management are needed.

Aim. Analysis of the current state of research and prospects for the use of carbonic anhydrase in environmental decarbonization programs.

Results. Carbonic anhydrase (CA) is an enzyme that accelerates the exchange of CO_2 and HCO_3^- in solution by a factor of 10^4 to 10^6. To date, 7 types of CAs have been identified in different organisms. CA is required to provide a rapid supply of CO_2 and HCO_3^- for various metabolic pathways in the body, explaining its multiple independent origins during evolution. Enzymes isolated from bacteria and mammalian tissues have been tested in CO_2 sequestration projects using carbonic anhydrase (CA). The most studied is one of the isoforms of human CAz — hCAII — the most active natural enzyme. Its drawbacks have been instability over time, high sensitivity to temperature, low tolerance to contaminants such as sulphur compounds and the impossibility of reuse. Molecular modelling and enzyme immobilisation methods were used to overcome these limitations. Immobilisation was shown to provide greater thermal and storage stability and increased reusability.

Conclusions. Carboanhydrases are involved in biological CO_2 assimilation. Therefore, the study of such enzymes and the conditions of their participation in atmospheric CO_2 sequestration provides a basis for the development of biocatalytic means to enhance atmospheric decarbonization.

Key words: climate; decarbonization; biosequestration of CO_2; carbonic anhydrase; immobilization of enzymes.

The processes of carbon sequestration, deposition and release from biological and geological sources are well balanced, thanks to which the balance of the ecosystem is maintained [1]. With the beginning of industrialisation, the global climate balance was disturbed, the concentration of CO_2 in the atmosphere began to increase rapidly [2]. At the end of the 19th century, the Swedish scientist Svante Arrhenius was one of the first to study the relationship between the level of atmospheric carbon dioxide (CO_2) and the Earth's temperature, focusing on understanding the role of CO_2 in climate regulation on a geological time scale. His work played an important role in the development of modern climatology [3]. The concept of anthropogenic global warming emerged much later, mainly in the second half of the 20th century, as a result of the development of climatology and the accumulation of factual data.

In the 1960s, Charles David Keeling demonstrated that the amount of anthropogenic carbon dioxide emitted into the air was sufficient to cause global warming [3]. and a broader understanding of the greenhouse effect. The increase in greenhouse gas (GHG) levels in the atmosphere over the past five decades is considered to be the main cause of global warming. Although carbon dioxide is not the only greenhouse gas in the atmosphere, its share is 65% of the total volume of global emissions, it is the largest contributor to the total GHG in the atmosphere and is responsible for 60% of the effects of global warming.

Today, 22 billion tonnes of CO_2 are emitted into the atmosphere from anthropogenic sources. The emission of GHG as a result of the use of fossil fuels is the main reason why the concentration of CO_2 has increased from the pre-industrial level of 270 ppm to the current level of 420 ppm. Over the next hundred years, energy demand is expected to more than double, which experts predict will lead to a doubling of CO_2 emissions by 2050 [4]. Data from ice cores in Greenland and Antarctica show that such high concentrations of CO_2 have not been observed for more than 400,000 years. The consequences of such an unprecedented increase in CO_2 concentrations may include: ocean acidification, sea level rise, climate disruption and ecosystem destruction [5–7].

Currently, CO_2 concentrations continue to increase by about 2 ppm per year, and by 2.53 ppm in the last year alone: from 417.15 ppm in August 2022 to 419.68 ppm in August 2023 according to https://gml.noaa.gov/ccgg/trends/. In order to reduce GHG emissions into the atmosphere, there is an urgent need for strategies to mitigate the consequences of CO_2 emissions. GHG emissions can be reduced by reducing the use of fossil fuels and promoting CO_2 sequestration [2, 8]. Atmospheric CO_2 can be sequestered using physical, chemical and biological approaches [1]. Depending on the chosen conversion method, CO_2 is captured and converted into value-added products [9, 10]. One of the most effective approaches for sustainable development is the biological sequestration of CO_2. Plants and microorganisms can capture atmospheric CO_2 using the carbon concentration mechanism (CCM) and convert the captured carbon into bioproducts [11]. However, these biological accumulators are only temporary carbon sinks, since CO_2 is released again during respiration, decomposition of dead organisms, and also during fires.

Decarbonisation programmes are being developed to remove carbon from the atmosphere and sequester it for indefinite or very long periods (thousands to millions of years) [4]. These include chemical adsorption from flue gases followed by storage in deep geological repositories, or conversion of CO_2 to insoluble carbonate salts [12–15].

The conversion of CO_2 into mineral carbonates offers the prospect of a safe, stable and environmentally benign product for long-term carbon sequestration [12, 16, 17], as significant reservoirs of carbonate minerals have existed for millions of years.

Under natural conditions, carbon sequestration in mineral carbonates is a very slow process. To speed up the reaction, decarbonisation technologies use an enzyme known as carbonic anhydrase (CA), which radically accelerates CO_2 hydration [18, 19].

Carbonic anhydrases catalyze the reaction of the reversible hydration of carbon dioxide:

$$CA + CO_2 + H_2O \underset{k_{-1}}{\overset{k_1}{\rightleftharpoons}} CA{\cdot}CO_2 \underset{k_{-2}}{\overset{k_{cat}}{\rightleftharpoons}}$$

$$\underset{k_{-2}}{\overset{k_{cat}}{\rightleftharpoons}} CA + HCO_3^- + H^+ \qquad (1)$$

The rate of interconversion of CO_2 and HCO_3^- in the absence of enzyme is relatively low: the value of the rate constant for the non-catalytic hydration of CO_2 is ~ 0.037 s^{-1} at 25 °C and an ionic strength of 0.2 [20]. This reaction has a second order rate constant k_1 of 0.0027 $M^{-1} \cdot s^{-1}$ at 37 °C and neutral pH, which corresponds to a pseudo first order rate constant of 0.15 s^{-1}. The dehydration reaction constant k_{-1} is equal to 50 s^{-1}. These constants determine the $[CO_2]/[H_2CO_3]$ ratio in aqueous solutions of 340 : 1. Carbonic acid H_2CO_3 dissociates in aqueous solution with pK 1 6.35 and pK 2 10.25, i.e. at neutral pH inorganic carbon in the form of bicarbonate ion (HCO_3^-) predominates. Carbonic anhydrases (CA) significantly accelerate both reactions, especially the hydration reaction. The most active human carbonic anhydrase II enzyme has a k_{cat} of the CO_2 hydration reaction of more than $10^6 \cdot s^{-1}$, and the rate constant of the dehydration reaction is $2.5–10^5 \cdot s^{-1}$ [21] (Table 1).

Carbonic anhydrases are ubiquitous in both prokaryotes and eukaryotes [22, 23]. They play important roles in numerous physiological processes such as respiration, pH and CO_2 homeostasis, secretion and gluconeogenesis. There are seven different classes of CAs (α,

β, γ, δ, ζ, η, θ, ι) that differ in their role in various important physiological processes, amino acid sequences and three-dimensional tertiary structure [24]. Despite structural differences, all CAs share the same catalytic mechanism involving a central metal atom (most commonly zinc).

Recently, CAs have been the target of environmental studies as enzyme accelerators to significantly improve CO_2 capture in the aqueous phase [25, 26].

Types of Carbonic Anhydrases and Their Features

α-Carbonic anhydrases

α-CAs are widespread and are found in vertebrates [27], algae [28, 29], higher plants [30, 31], eubacteria [32–34], some species of fungi and protozoa, as well as some bacteria and cyanobacteria [35, 24]. However, α-CA has not been detected in archaea [36]. Most α-CAs are monomers with a molecular mass of about 30 kDa (Fig 1, *A*). Most α-CAs are active as approximately 30 kDa monomers with three histidines coordinating the zinc atom [30] (Fig. 1, *B*).

Historically, α-CAs were the first carboanhydrases to be described, isolated from animal erythrocytes. They are considered to be the evolutionary youngest group of CAs [39] found in mammals, including humans, and have a limited distribution in prokaryotes [22].The alpha class includes all 16 mammalian CA isoforms with different organ-tissue distribution and subcellular location, 15 of which have been found in humans (HCAs) [24], and several new isoenzymes have also been identified in non-mammalian vertebrates, among which HCAII is the best studied and characterised CA. The tertiary structure of HCAII consists of a unique domain containing ten β-bands that twist to form a β-sheet (eight of which are antiparallel, the other two parallel). Around these β-sheets are up to eight more α-helices on the surface of the protein (Fig. 1, *A*).

The α-CA isoenzymes differ in their kinetic properties, tissue distribution and subcellular localisation, and sensitivity to different inhibitors. In general, there are three distinct groups of CA isoenzymes in the α-CA gene family. One of these groups contains cytoplasmic CA, which includes mammalian CAs I, II, III, V, VII, and XIII. These isoenzymes are found in the cytoplasm of various tissues, with the exception of mitochondrial CA V. Another group of isoenzymes called membrane bound CAs consists of mammalian CAs IV, IX, XII, XIV and XV [40]. These isoenzymes are associated with the plasma membranes of many different tissue types. The latter group contains some very unusual isoenzymes, CA VIII, X and XI, which have lost the classical CA activity of CO_2 hydration/dehydration and are referred to as CA-related proteins [41].

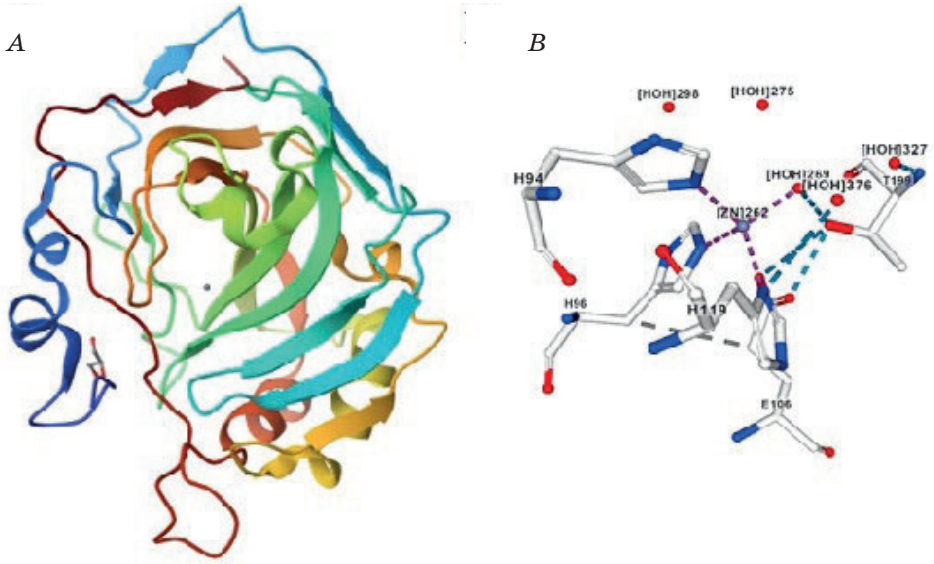

Fig. 1. **Structure of human CAII enzymes retrieved from PDB 3U45 (*A*). The human CAII monomer mostly consists of beta strands (*B*) a single active site with three zinc-coordinating histidine residues [37, 38]**

β–*Carbonic anhydrases*

β-CAs were first identified as carbonic anhydrases in higher plants [42, 43]. Subsequently, β-CAs were discovered in cyanobacteria [28, 44], microalgae [45], eubacteria [46], archaeubacteria [22] and fungi [47]. This CA family is not represented in any vertebrate genome. The active site of β-CAs contains histidine and two cysteine residues that act as zinc ligands [48, 49]. β-CAs are usually active as dimers or multimers. In *Pisum sativum*, CA dimers form tetramers (Fig. 2, 3), which are held together by their C-termini to form octamers [50]. An active center is formed at the interface between the two subunits.

β-CA's were discovered after α-CAs in plants and other organisms. The quaternary organisation of β-CAs is more diverse: they can form different oligomeric structures such as dimers, tetramers and octamers. The molecular masses of these oligomers range from 45 to 200 kDa. Among them, the dimer is the catalytically active unit responsible for the carboanhydrase activity of the enzyme. Individual β-CA subunits have molecular masses of 25 to 30 kDa (Fig. 2). These subunits have a unique α/β folded structure that allows them to associate and form dimers, which are the main structural units in the catalytic mechanism. The structure of the β-CA monomer consists mainly of helices surrounding a β-sheet of four parallel β-strands. A fifth C-terminal β-strand is also involved in the oligomerisation of β-CA [5].

Initially, it was thought that the β-class of CAs consisted exclusively of enzymes localised in the chloroplasts of higher plants, and they were commonly referred to as 'plant CAs'. However, with the accumulation of new data since the 1990s, it has become clear that β-CAs are much more widespread and are found in different organisms in all three superkingdoms: eukaryotes, bacteria and archaea. β-CAs have been identified in a wide range of organisms including microalgae, cyanobacteria, bacteria, fungi, archaea, higher C3 and C4 plants and invertebrates.

This wide distribution suggests that β–CAs play an important role in a variety of biological processes in different life forms. Phylogenetic analyses by Smith and Ferry [22] of 76 β-CAs from a variety of organisms belonging to different domains of life revealed distinct patterns. Unicotyledonous and dicotyledonous plants formed monophyletic groups, suggesting a common evolutionary origin. However, the remaining β-CAs formed four distinct subgroups or clades, including two clades formed by enzymes from Eukarya and Bacteria, and two exclusively prokaryotic clades: one comprising enzymes from Gram-negative bacteria, and the other consisting predominantly of sequences from Archaea and Gram-positive bacterial species.

The functional unit of β-CA is the dimer (Fig. 2), although the most common oligomeric form of β-CA is the tetramer [50, 53]. The β-CA dimer is formed by extensive interactions created by the two N-terminal α-helices of one monomer wrapping around the second monomer and a minor hydrogen bond between the second β-helices of each monomer [50]. Tetramers are formed by interactions mainly through the fifth, C-terminal β-helix [50]. In pea, chloroplast β-CA forms an octamer. For some β-CA, dicots have a unique C-terminal extension of the fifth β-sequence, whereas unicots do not [50, 53]. Octamers are formed by slightly different interactions with these fifth β-band extensions [50, 53].

The structural diversity observed in β-CA reflects the adaptability of these enzymes to different environments and physiological

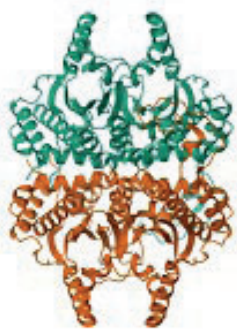

Fig. 2. **X-ray structure of a β-carbonic anhydrase from the red alga, *Porphyridium purpureum* R-1 [51]**

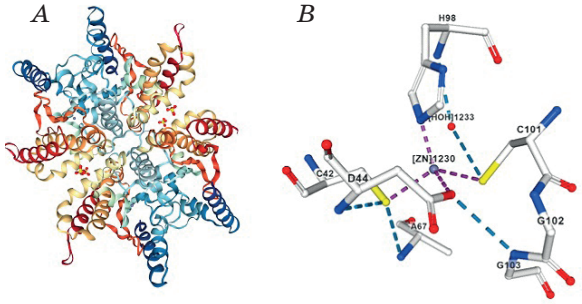

Fig. 3. **Ribbon diagram of the β-CA native tetramer of Haemophilus influenzae β-CA retrieved from PDB 2A8C (*A*) [52].**
The active site of β-CAs containing one histidine and two cysteine residues that act as zinc ligands (*B*)

roles. Understanding the structural features of β-CAs can provide valuable information on their catalytic mechanisms, regulation and potential applications in biotechnology and medicine.

γ-Carbonic anhydrases

γ-CAs were first discovered in the archaea Methanosarcina thermophila [54]. Plants [55] and photosynthetic bacteria [56, 57] also contain γ-carboanhydrases, while reports detailing γ-CA in animals have not appeared. The amino acid sequence of Cam showed no significant homology with known representatives of α- or β-class carboanhydrases [55].

Similar to the active centre of α-CAs, the active centre of Archaebacterium γ-carboanhydrases has zinc in the active centre coordinated by three histidine residues and one water molecule [59] (Fig 4, *B*). However, in contrast to the structure of carboanhydrases, which are monomers, the functional unit of γ-carboanhydrases is a trimer with three active centres spanning the monomer-monomer interfaces.

The zinc ion is coordinated by his residues represented by two different subunits [59]. The β-chain region dominates the structure of γ-carboanhydrase and consists of seven complete turns forming a left-handed β-helix [59]. Each complete turn contains three β-chains, making the β-helix look like an equilateral triangle when viewed from above [59]. In photosynthetic organisms, γ-carboanhydrase may contain additional domains, as seen in the cyanobacterial CcmM proteins of cyanobacteria, which have two or three repeating C-terminal domains with high similarity to the *Rubisco* small subunit [60]. In cyanobacteria, CcmM sometimes acts as an active carboanhydrase, but some CcmM proteins lack activity [57, 61]. However, CcmM is thought to organise the packaging of Rubisco in the carboxysome even though it does not have carboanhydrase activity.

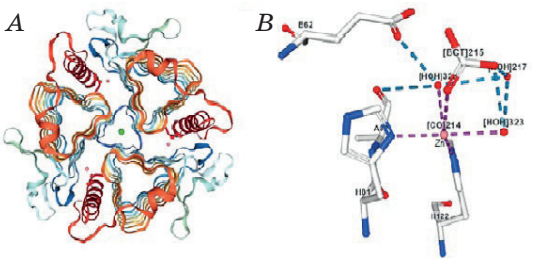

Fig. 4. **Structure of γ-CA from *Methanosarcina thermophila* 1QRE [58, 59]**

It has been shown that γ- or γ-like CAs are part of complex I of the mitochondrial electron transport chain in plants and algae [62, 63].

δ-Carbonic anhydrases

To date, δ-CAs have only been described in a few diatoms [64]. Like the first three CA families, the δ-CA families represent a case of convergent evolution, with almost no sequence similarity to α-, β- and γ–CAs [65]. The structure and geometry of the ~34 kDa enzyme was found to be similar to that of α- and γ-CA [66].

ζ-Carbonic anhydrases

This family of CA genes, also restricted to marine protists, is somewhat similar to the β-CA family [67–69]. What distinguishes this CA family from the β-CA family is that other metals, such as Cd or Co, can replace Zn in the active site [67–69].

ζ-CA, also called cadmium CA, was first isolated from the marine diatom *T. weissflogii* [68]. Seawater is mainly depleted in Zn^{2+} ions. Therefore, under strict Zn^{2+} limitation, the activity of the Zn-dependent δ-CA TWCA1 decreases sharply and is replaced by another CA using Cd^{2+} ions in its active centre. The amino acid sequence of CDCA and its exact molecular mass (69 kDa) were later determined. CDCA had no significant homology to proteins from other known classes of CAs and was therefore assigned to the new ζ-class CAs. Genes encoding CDCA homologues have been found in a number of other diatoms [67]. CDCA is a monomer with an amino acid sequence of consists of three repeats (R1-R3) that share 85% identity, while the coding DNA sequences share a much lower percentage of homology [69]. Each of the R1-R3 repeats contains an active site that structurally mimics the type I β-CA site [70].

η-Carbonic anhydrases

The η-family has been found in the protozoan parasite, *Plasmodium falciparum*, which causes human malaria [71]. This is a group of enzymes previously thought to belong to the alpha family of CAs, but it has been demonstrated that η-CAs have unique features, such as the structure of metal ion coordination. De Simone et al. [72]. showed that the metal ion coordination structure of this CA is unique among all six other gene families encoding such enzymes. In the active centre of η-CA, zinc is coordinated by two His residues and one Gln, in addition to a water molecule/hydroxide ion (Fig. 5), which acts as

a nucleophile in the catalytic cycle. Despite the fact that η- and α-CAs share the same three-dimensional structure, strongly suggesting the evolutionary origin of the former from the latter, there are significant differences between the two families, which will allow the design of selective inhibitors of the parasite to be optimised without harming the host enzymes.

ι-Carbonic anhydrases

The iota class, the newest class of CAs, was discovered in the marine diatom *Thalassiosira pseudonana* and is widespread in marine phytoplankton [73]. In diatoms, ι-CA is localised in chloroplasts and is only expressed at low CO_2 concentrations, suggesting an important role for this enzyme in CO_2 concentration mechanisms. Unlike other classes, ι-CA can use manganese instead of zinc as a metal cofactor, which has potential ecological significance since Mn^{2+} is more abundant in the ocean than Zn^{2+}. Its homologues are present in several sequenced diatoms and other algae, bacteria and archaea. Homologues of ι-CA have also been identified in Gram-negative bacteria, where they may be present as the protein homodimer CA. Thus, ι-CA is phylogenetically widespread, as confirmed by analysis of the Tara Oceans database [73]. This suggests that CAs are likely to play an important role in the global biogeochemical carbon cycle.

Structure of the active center and catalytic mechanism of carbonic anhydrases

The catalytic mechanism of CA was first described for human α-CA II (hCA II) [74]. The discovered catalytic mechanism was termed 'Zn hydroxide' because the catalytically active group of hCA II is Zn-bound water ionised to a hydroxide ion. The metal ion itself is not a nucleophile to act as a catalyst. It was later found that all classes of CAs utilise a metal hydroxide mechanism, using divalent metal hydroxide derivatives as catalytically active structures [24].

Crystallographic studies have shown that the active centres of CAs are usually a tetrahedral cavity formed by three amino acid residues and a deprotonated water molecule (hydroxide ion), which act as coordinating ligands for Me^{2+} (Fig. 5). The metal ion (usually Zn^{2+}) is hydrogen-bonded to the amino acids surrounding the active site [24].

These ligands, as well as the amino acids involved either in catalysis or in forming the correct structure of the active site, are strictly conserved within each class of CAs. In α-, γ- and δ-CA, three his residues coordinate the Me^{2+} ion and the fourth ligand is a hydroxide ion.

All β-CAs are divided into two types depending on the nature of the fourth ligand in the active centre and the adjacent amino acid residues [24, 75] (Fig. 5). In type I β-CAs (so-called "open active site" enzymes), Me^{2+} is coordinated by one His, two Cys and one hydroxide ion. Type II β-CAs (enzymes with a "closed active site") use an Asp instead of a hydroxide ion (Fig. 5). These enzymes are only active at pH above 8.3. It is this environment that favours the transition from a "closed active site" to an "open site" where the water molecule (hydroxide ion) occupies the position of the fourth ligand required for catalysis. All β-cases require dimerisation for catalysis [75], so a single catalytically active subunit has two active centres, each carrying Me^{2+}.

The structure of the ζ-CAS active centre is similar to that of the type I β-CA active centre [76]. In η-CA, Me^{2+} is coordinated by two His residues and one Gln residue in addition to the hydroxide ion [72].

The catalysis takes place in two steps [77]. In the first step, CO_2 is converted to HCO_3^-.

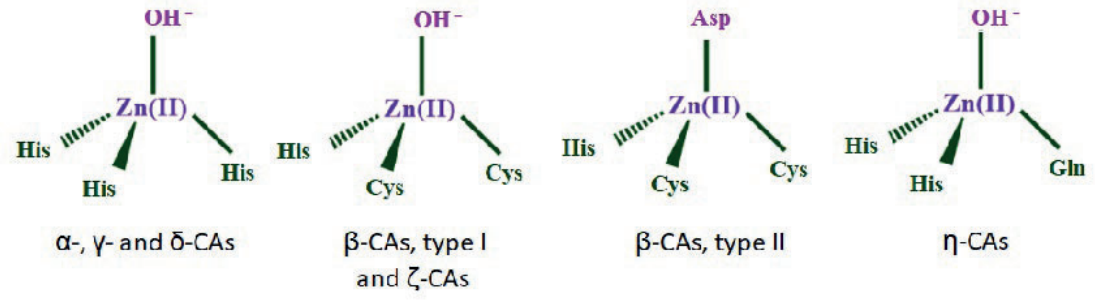

Fig. 5. **Schematic representation of active sites of different classes of CAs. Ligands coordinating metal ion (Zn^{2+}) in the active centre of enzymes are shown**

The metal hydroxide derivative in the active site of the enzyme (E) is a strong nucleophile that attacks the CO_2 molecule. This step results in the formation of a bicarbonate ion bound to Me^{2+} (Equation 2). The bicarbonate ion is replaced by a water molecule and released into solution.

$$E\text{-}Me^{2+}\text{-}OH^- + CO_2 \rightleftharpoons E\text{-}Me^{2+}\text{-}HCO_3^- \overset{H_2O}{\rightleftharpoons} \rightleftharpoons E\text{-}Me^{2+}\text{-}H_2O + HCO_3^- \quad (2)$$

This results in the formation of an inactive acid form of the enzyme in which water is coordinated to Me^{2+}.

In the second step, the active basic form of the enzyme is regenerated by ionisation of the water molecule bound to the metal and removal of a proton from the active centre to an external buffer (Equation 3).

$$E\text{-}Me^{2+}\text{-}H_2O \rightleftharpoons E\text{-}Me^{2+}\text{-}OH- + H^+ \quad (3)$$

In some cases, this step is facilitated by individual amino acid residues close to the active site of the enzyme that act as intermediates in the proton transfer [23]. The removal of protons from the active site and the reduction of the metal-bound hydroxide is the limiting step in the catalytic process.

In the highly active hCA II, the proton-translocating residues are complemented by a His cluster protruding from deep within the active centre to the enzyme surface. This cluster promotes even more efficient proton removal.

This makes hCA II the most active enzyme known to date — the rate of its catalysis is essentially limited only by the rate of ion diffusion [78].

A characteristic feature of all CAs, at least of those proteins, is the "bipolar" architecture of the active site: one half of the active site is covered with hydrophobic residues and the other half, the opposite half, is covered with hydrophilic amino acids [79].

This dual nature is due to the fact that the enzyme substrates, CO_2 and HCO_3^-, have different chemical properties. At the beginning of the reaction, the CO_2 molecule binds to a specific part of the hydrophobic region of the active centre of the CA site (hydrophobic pocket]; this facilitates the subsequent nucleophilic attack [79]. The hydrophilic moieties ensure regeneration of the active site by removing a proton from the zinc-bound water and releasing it to the external environment by means of proton-translocating groups. Table 1 summarizes typical kinetic parameters of the many carbonic anhydrase isozymes.

The data, which include enzymes from all six CA families, show that hCA II (α-class CA) or ZnCA1-R1 (ζ-class CA) are among the enzymes with the highest turnover numbers described so far.

The table shows data on α-class CAs: human cytosolic isoenzyme hCA II; bovine (wtbCAII) and the bacterium SazCA (from SulfuriHydrogenibium azorense); the β-class includes the enzyme Can2 from the fungus

Table 1. **Kinetic parameters for the CO_2 hydration reaction catalysed by various CAs belonging to the various families**

	Class	Organism	k_{cat} (s^{-1})	k_{cat}/KM [$(Ms)^{-1}$]	References
hCA I	α	Human	2.0×10^5	5.0×10^7	[78]
hCA II	α	Human	1.4×10^6	1.5×10^8	[70]
wtbCAII	α	Bovini	9.3×10^4	1.198×10^8	[80]
SazCA	α	Bacterium	4.4×10^6	3.5×10^8	[81]
Can2	β	Fungus	3.9×10^5	4.3×10^7	[82]
FbiCA1	β	Plant	1.2×10^5	7.5×10^6	[83]
PgiCA	γ	Bacterium	4.1×10^5	5.4×10^7	[84]
CdCA1-R1	ζ	Diatom	1.5×10^6	1.4×10^8	[85]
ZnCA1-R1	ζ	Diatom	1.4×10^6	1.6×10^8	[70]
TweCA	δ	Diatom	1.3×10^5	3.3×10^7	[76]
PfCA	η	Protozoa	1.4×10^5	5.4×10^6	[71]

Cryptococcus neoformans FbiCA1 from the plant *Flaveria bidentis*; γ-class enzyme — PgiCA from the anaerobic bacterium *Porphyromonas gingivalis*; δ- and ζ-class enzymes from the diatom *Thalassiosira weissflogii*; ζ-class CA with zinc (ZnCA1-R1) and cadmium (CdCA1-R1); η-CA (PfCA) from *Plasmodium falciparum*.

As the most active enzyme, hCA II is often tested in CO_2 capture projects from industrial gas emissions [20, 25, 77]. Carbonic anhydrase from bovine erythrocytes, although less active than the hCA II isoform, is one of the most studied forms of CA and is promising for use in flue gas decarbonisation programmes [86–88].

The combustion of fossil fuels produces not only CO_2 but also nitrogen and sulphur oxides, from which nitrates, nitrites, sulphates and sulphites are formed in the aquatic environment. The influence of these anions on the activity of CA is of interest when designing reactors for CO_2 sequestration. The results of the study of these effects show that the enzymatic activity of hCA II is only slightly inhibited by NO_3^-, NO_2^-, SO_4^{2-}, HSO^{3-} [89]. η-CA (PfCA) proved to be much more sensitive to these anions [71].

Other impurities of flue gases are heavy metal ions that inhibit to varying degrees carbonic anhydrases hCAII, hCAI and α-CA from different vertebrate and invertebrate species [90].

Comparative analysis of the results obtained when studying the effects of heavy metals on plants [91] and multiple forms of plant carbonic anhydrases [92–94] allows us to conclude that plant β-carbonic anhydrases are more sensitive to the inhibitory effects of heavy metals than animal α-CAs. The reason for the high susceptibility of β-CAs to Me^{2+} seems to be the presence of SH-containing amino acids (cys) in their active centre (Fig. 5), which have a high affinity for heavy metal ions. Obviously, these characteristics should be taken into account in the design of reactors, depending on the composition of the flue gases to be decarbonised, for which one or other CA will be used.

Influence of temperature on the structure and activity of carbonic anhydrases

At high temperature, enzymes lose their biological activity and are irreversibly denatured by denaturation. This inactivation by thermal denaturation has a profound effect on enzyme productivity [95]. The temperature limitation of enzymes is an important parameter for industrial applications, affecting the cost of the process if the enzyme cannot be reused. Lavecchia and Zugaro studied the effect of thermal denaturation on the catalytic properties of carbonic anhydrase from bovine erythrocytes [96]. It was found that at temperatures below 60 °C the enzyme is very stable, whereas at temperatures between 60 and 65 °C there is a sharp decrease in biological activity followed by irreversible loss of activity.

Below 60 °C the enzyme recovers almost completely its biological activity, whereas in the range 60–65 °C a considerable decrease in the catalytic activity takes place, above 65 °C the residual activity drops to zero after few minutes. Thermal transition between native and partially unfolded carbonic anhydrase is a highly cooperative process. The observed loss of activity appears to be a consequence of large conformational changes affecting all the molecule and causing the unfolding of the protein. When the enzyme solution is cooled down to 25 °C in order to measure the catalytic activity, the structural rearrangements of the polypeptide chain are likely to result in an uncorrected reconstitution of the active site region.

As the turnover rate of hCA II is much higher than that of other types of CAs, it is attracting increasing attention in CO_2 capture projects. However, its hydratase activity is very sensitive to temperature, and the enzyme is inactivated at 45 °C [97]. This greatly complicates its use as a potential catalyst for accelerating CO_2 absorption from flue gases [98], i.e. at high temperatures and in the presence of trace amounts of pollutants [16, 99].

Recently, many authors have reported a decrease in enzyme activity with prolonged exposure to high temperatures [89, 100, 101]. It became clear that the development of enzymatic CO_2 capture technologies would be impossible without solving the problem of the thermal stability of CAs.

To solve this problem,

1) In thermophilic organisms, enzymes are being sought that maintain high activity as the temperature rises [22, 55, 58, 59, 95, 97, 102, 103];

2) Molecular modelling methods are used with directed replacement of critical amino acids in the CA molecule [72, 77, 95, 99, 101, 104, 105];

3) Developing methods and carriers for immobilizing CA to increase its thermal stability, improve enzyme recovery and reuse, and reduce the overall cost of the process [15, 100, 106–108];

4) Scaling up research to develop enzymatic CO_2 sequestration technologies for subsequent industrial implementation [107, 109].

CAs from *Methanobacterium thermoautotrophicum* (CAB) and *Caminibacter mediaatlanticus* DSM 16658 are able to retain more than 40% of their initial hydratase activity at 85 °C when reduced to 1.7×10^4 s^{-1} [22]. Enzymes from *Bacillus subtilis* and *Citrobacter freundii* are stable at ≤ 60 °C but lack hydratase activity [17].

In recent years, four highly thermally stable α-CAs, SspCA from *Sulfurihydrogenibium yellowstonense* YO3AOP1, SazCA from *Sulfurihydrogenibium azorense*, *Thermovibrio ammonificans* (TaCA) and *Persephonella marina* EX-H1 (PmCA), have been extensively studied.

Capasso et al, [110] reported a highly thermally stable recombinant α-CA (SspCA), which was identified and characterised from the thermophilic bacterium *Sulfurihydrogenibium yellowstonense* sp. YO3AOP1. It retains its high catalytic activity for the CO_2 hydration reaction even after heating at 70 °C for several hours.

Russo et al, [100] developed a novel recombinant CA, SspCA, isolated from the thermophilic bacterium *Sulfurihydrogenibium yellowstonense* sp. YO3AOP1. They also reported that the half-life of the enzyme at pH ≈ 8.3 was 53 days at 40 °C and 8 days at 70 °C.

De Luca et al. and Vullo et al. [102] reported the biochemical properties, thermostability and inhibition of a novel α-CA enzyme, SazCA, obtained by translational analysis of the genome of the thermophilic bacterium *Sulfurihydrogenibium azorense*. The SazCA enzyme is highly thermostable, withstanding incubation temperatures of 90–100 °C for several hours without loss of activity. However, SazCA is highly sensitive to most inorganic anions (except sulphate), which inhibit the enzyme at concentrations of about 1 mM.

So for today, SazCA has the highest catalytic hydratase activity of 3.5×10^8 $M^{-1}\cdot s^{-1}$ at 20 °C [102], which is more than twice the activity of hCA II. The enzyme retains high hydratase c after 3 h incubation even at 100 °C, which may be due to the substitution of two amino acids involved in proton transfer: Glu2 for His2 and Gln207 for His207 [72]. These two mutations could affect the pKa of the proton shuttle and consequently its ability to transfer the proton [72].

Using the methods of molecular modeling, it was possible to increase the thermal stability of the spacecraft due to such strategies as increasing the stiffness of the surface loop [104] and compactness of the surface [105, 111], reducing surface hydrophobicity [99] and introducing a conservative disulfide bridge [77].

Enzyme immobilisation

CA enzymes are rather unstable molecules with a limited range of working conditions, and their use in their free form is not recommended because they cannot be extracted from the reaction environment [108], which severely limits their large-scale industrial applications. Also, the use of free enzyme dissolved in the solution phase is not favourable due to the significant amount of enzyme required in enzymatic processes. Enzyme denaturation is another challenge, resulting in the loss of enzyme CO_2 hydration activity over time. Enzyme immobilisation allows mobile enzymes to be confined by attaching them to an inert, insoluble material. This can provide increased resistance to changes in pH or temperature. It also allows the enzyme to remain in a stabilised state throughout the reaction, after which it can be easily separated from the products and reused. This greatly increases the efficiency of the process and is therefore widely used in industry for reactions dependent on enzymatic activity [112]. Therefore, enzyme immobilization is a rational approach to overcome these limitations and develop a viable CO_2 capture system using aqueous solvents.

Immobilisation of carbonic anhydrase can offer several advantages, including improved stability, reusability and easier separation of the enzyme from the reaction medium. Various supports and immobilisation strategies have been explored to immobilise carbonic anhydrase with the aim of achieving good activity and stability compared to free enzyme in solution [15, 107].

The immobilisation strategy is crucial for maintaining the activity and stability of immobilised carbonic anhydrase. Various strategies such as physical entrapment (encapsulation), covalent binding and adsorption have been used to immobilise carbonic anhydrase [112, 113].

Physical entrapment involves the encapsulation of the enzyme within the carrier matrix, which provides protection and maintains the enzyme activity. Enzyme encapsulation is an irreversible immobilisation method in which enzymes are entrapped within the fibre, either in polymer membranes or in lattice structures of the material, which supply the substrate and remove products from the enzyme. Capture involves the physical confinement of the enzyme within a limited

network space. Mechanical stability, enzyme leaching and chemical interaction with the polymer are generally improved when the enzyme is immobilised by encapsulation. This method modifies the encapsulating material to provide an optimal microenvironment for the enzyme. An ideal microenvironment with optimal pH, polarity or amphiphilicity can be achieved by using different support materials [113].

Adsorption. Adsorption involves the non-covalent binding of the enzyme onto the surface of the carrier, which can be reversible and allows for enzyme release. This method is based on physical interactions between proteins and solid support surfaces through van der Waals forces, hydrogen bridges and electrostatic interactions. Adsorption immobilisation of enzymes is relatively simple and can have higher commercial potential, lower cost and higher efficiency with relatively weak (non-covalent) binding of the enzyme.

However, the physical binding is generally too weak for the enzyme to remain attached to the support and not be subject to enzyme leaching, resulting in significant substrate contamination [108, 113].

Covalent binding and cross-linking. Covalent binding involves the formation of covalent bonds between the enzyme and the carrier, which provides strong attachment and stability. The technique of covalent enzyme immobilisation is one of the most prominent. The formation of covalent bonds is required for more stable binding, and these are generally formed by reaction with functional groups present on the protein surface. The functional groups that contribute to enzyme binding include side chains of lysine (amino group), cysteine (thiol group) and aspartic and glutamic acids (carboxyl group) [114]. The activity of the covalently bound enzyme depends on the coupling method, the composition of the carrier material, as well as its size and shape and the specific conditions during coupling [15,107].

Support materials for CA immobilization. The choice of the support material is an important factor which must be considered, as it has an important effect on the performance of biocatalytic system [108]. Some features should be considered for support material selection such as availability, low cost, functional group availability, mechanical stability, and compatibility with the enzyme.

1. *Polymer-based materials:* Polymers such as polyvinyl alcohol (PVA), polyvinyl acetate (PVA), polyethyleneimine (PEI), polyurethane (PU), and polyethyleneglycol (PEG)have been widely used as support materials for CA immobilization. These polymers have high mechanical stability, tunable porosity and can provide a stable matrix for the enzyme.

2. *Silica-based materials:* Silica-based materials, such as silica gels, mesoporous silica, and silica nanoparticles, have been extensively studied for CA immobilization. They have a high surface area, which provides a large amount of immobilization sites for the enzyme. Silica-based materials also have good compatibility with the enzyme and can provide a stable environment for its activity.

Inorganic materials, such as silica nanoparticles, gold nanoparticles, and titanium dioxide nanoparticles, offer unique properties for enzyme immobilization. They provide stability and controlled release of the enzyme, which can enhance the overall performance of the CO_2 capture process.

3. *Metal-organic frameworks (MOFs):* MOFs are a class of porous materials composed of metal ions connected by organic ligands. These materials have shown great potential as support materials for CA immobilization due to their high porosity and tunable structures. MOFs can provide a controlled environment for the enzyme and improve its stability and catalytic activity.

4. *Mesoporous materials*: Mesoporous materials, such as silica, alumina, and zeolites, have attracted attention for enzyme immobilization. These materials provide a high surface area and a well-defined pore structure, allowing for efficient loading and dispersion of CA enzyme [115].

5. *Magnetic nanoparticles*: Nanoparticles, such as magnetic nanoparticles and gold nanoparticles, have been explored as carriers for immobilizing carbonic anhydrase. These nanoparticles can provide high surface area-to-volume ratios and can be easily separated from the reaction medium using external magnetic fields or centrifugation.

6. *Carbon-based materials*: Carbon-based materials, such as activated carbon, carbon nanotubes, and graphene oxide, have been investigated for CA immobilization. These materials have a large surface area, good mechanical stability, and are chemically inert, making them suitable support materials for enzyme immobilization.

Conclusions

Numerous studies in recent years have shown that the use of carbonic anhydrase for enzymatic CO_2 capture has significant potential

to create a cost-effective technology. However, the industrial application of enzymes in carbon capture processes is limited by their high cost, low catalytic activity, poor stability over time, high sensitivity to temperature, low tolerance to pollutants such as sulphur compounds and reusability. To overcome these limitations, further developments are needed to improve the economics. Carbonic anhydrases are found in all organisms, from protozoa to humans. Not all of them have been studied, so the search for new stable enzymes among organisms with enormous genetic diversity remains an urgent task. The use of molecular modelling has already led to impressive successes in the design of thermostable enzymes, and further developments in this area are expected. Enzyme immobilisation offers great potential for the industrial production of carbonic anhydrase in captured CO_2. Advances in support materials, immobilisation strategies and reactor design could lead to the development of efficient and cost-effective enzymatic CO_2 capture systems.

Significant progress is also expected in areas such as the conversion of captured carbon dioxide into chemicals such as carbon monoxide, methanol, formic acid, glucose or methane, and fuels by chemical, electrochemical and enzymatic methods.

Few laboratory processes have been tested on a large scale, and refinement of their details on an industrial scale is necessary to create sustainable technologies.

In summary, the research carried out confirms the remarkable potential of some CAs as biocatalysts and gives hope for the feasibility of introducing biomimetic processes into CO_2 sequestration technology.

Financing

This review was prepared as a part of research No. 0121U114515 "Polyenzyme complexes and metabolons in providing photosynthetic assimilation of inorganic carbon in chloroplasts" supported by the National Academy of Sciences of Ukraine.

REFERENCES

1. *Prentice I. C., Farquhar G. D., Fasham M. J. R., Goulden M. L., Heimann M., Jaramillo V. J., ..., Yool A.* 2001, The carbon cycle and atmospheric carbon dioxide.
2. *Bosok B., Bazeev E.* Global warming: problems, discussions and forecasts ISSN 1819-7329. *Svitohliad, 2020, 6 (86).*
3. *Dessler A. E.* Introduction to modern climate change. *Cambridge University Press*. 2021.
4. *Benson S. M., Surles T.* Carbon dioxide capture and storage: An overview with emphasis on capture and storage in deep geological formations. Proc. IEEE. 2006, 94 (10), 1795–1805.
5. *Sabine C. L., Feely R. A., Gruber N., Key R. M., Lee K., Bullister J. L., ..., Rios A. F.* The oceanic sink for anthropogenic CO_2. Science, 2004, 305 (5682), 367–371. https://doi.org/10.1126/science.1097403
6. *Thomas C. D., Cameron A., Green R. E., Bakkenes M., Beaumont L. J., Collingham, Y. C., ..., Williams S. E.* Extinction risk from climate change. *Nature.* 2004, 427 (6970), 145–148. https://doi.org/10.1038/nature02121
7. *Wigley T. M., Richels R., Edmonds J. A.* Economic and environmental choices in the stabilization of atmospheric CO_2 concentrations. Nature. 1996, 379 (6562), 240–243. https://doi.org/10.1038/379240a0
8. *Zolotaryova O., Shnyukova E.* Where biofuel industry goes to. *Visnyk NAN Ukrainy,* 2010, 4, 10–20.
9. *Mazari S. A., Ali B. S., Jan B. M., Saeed I. M., Nizamuddin S.* An overview of solvent management and emissions of amine-based CO_2 capture technology. *International Journal of Greenhouse Gas Control.* 2015, 34, 129–140.
10. *Olajire A. A.* Valorization of greenhouse carbon dioxide emissions into value-added products by catalytic processes. *Journal of CO_2 Utilization*. 2013, 3, 74–92. https://doi.org/10.1016/j.jcou.2013.10.004
11. *Raven J. A., Beardall J.* CO_2 concentrating mechanisms and environmental change. *Aquatic Botany,* 2014, 118, 24–37. https://doi.org/10.1016/j.aquabot.2014.05.008
12. *Hills C. D., Tripathi N., Carey, P. J.* Mineralization technology for carbon capture, utilization, and storage. *Frontiers in Energy Research*, 2020, 8,142. https://doi.org/10.3389/fenrg.2020.00142
13. *Lee S. W., Park S. B., Jeong S. K., Lim K. S., Lee S. H., Trachtenberg M. C.* On carbon dioxide storage based on biomineralization strategies. *Micron,* 201041 (4), 273–282. https://doi.org/10.1016/j.micron.2009.11.012
14. *Koytsoumpa E. I., Bergins C., Kakaras E.* The CO_2 economy: Review of CO_2 capture and reuse technologies. *The Journal of Supercritical Fluids.* 2018,132 (1), 3–16. https://doi.org/10.1016/j.supflu.2017.07.029
15. *Ren S., Jiang S., Yan X., Chen R., Cui H.* Challenges and opportunities:

porous supports in carbonic anhydrase immobilization. *Journal of CO_2 Utilization,* 2020, 42, 101305. https://doi.org/10.1016/j.jcou.2020.101305
16. *Bond G. M., Stringer J., Brandvold D. K., Simsek F. A., Medina M. G., Egeland G.* Development of integrated system for biomimetic CO_2 sequestration using the enzyme carbonic anhydrase. *Energy & Fuels.* 2001, 15 (2), 309–316. https://doi.org/10.1021/ef000246p
17. *Ramanan R., Kannan K., Sivanesan S. D., Mudliar S., Kaur S., Tripathi A. K. Chakrabarti T.* Bio-sequestration of carbon dioxide using carbonic anhydrase enzyme purified from *Citrobacter freundii*. World *Journal of Microbiology and Biotechnology,* 2009, 25, 981–987. https://doi.org/10.1007/s11274-009-9975-8
18. *Favre N., Christ M. L., Pierre A. C.* Biocatalytic capture of CO_2 with carbonic anhydrase and its transformation to solid carbonate. *Journal of Molecular Catalysis B: Enzymatic,* 2009, 60 (3–4), 163–170. https://doi.org/10.1016/j.molcatb.2009.04.018
19. *Mirjafari P., Asgha, K., Mahinpey N.* Investigating the application of enzyme carbonic anhydrase for CO_2 sequestration purposes. *Industrial & engineering chemistry research,* 2007, 46 (3), 921–926. https://doi.org/10.1021/ie060287u
20. *Khalifah R. G.*The carbon dioxide hydration activity of carbonic anhydrase: I. Stop-flow kinetic studies on the native human isoenzymes B and C. *Journal of Biological Chemistry*, 1971, 246 (8), 2561–2573. https://doi.org/10.1016/S0021-9258(18)62326-9
21. *Sanyal G., Pessah N. I., Maren T. H.* Kinetics and inhibition of membrane-bound carbonic anhydrase from canine renal cortex. *Biochimica et Biophysica Acta (BBA)-Enzymology,* 1981, 657 (1), 128–137. https://doi.org/10.1016/0005-2744(81)90136-4
22. *Smith K. S., Ferry J. G.* A plant-type (β-class) carbonic anhydrase in the thermophilic methanoarchaeon *Methanobacterium thermoautotrophicum*. *Journal of bacteriology*, 1999, 181 (20), 6247–6253. https://doi.org/10.1128/jb.181.20.6247-6253.1999
23. *Tripp B. C., Smith K. S., Ferry J. G.* Carbonic anhydrase: New insightsfor an ancient enzyme, a minireview. *Journal of Biological Chemistry,* 2001, 276, 48615–48618. https://doi.org/10.1074/jbc.R100045200
24. *Supuran C. T.* Structure and function of carbonic anhydrases. *Biochemical Journal,* 2016, 473 (14), 2023–2032. https://doi.org/10.1042/BCJ20160115
25. *Boone C. D., Habibzadegan A., Tu C., Silverman D. N., McKenna R.* Structural and catalytic characterization of a thermally stable and acid-stable variant of human carbonic anhydrase II containing an engineered disulfide bond. *Acta Crystallographica Section D: Biological Crystallography*, 2013, 69 (8), 1414–1422. https://doi.org/10.1107/S0907444913008743
26. *Sharma A., Bhattacharya A.* Enhanced biomimetic sequestration of CO_2 into $CaCO_3$ using purified carbonic anhydrase from indigenous bacterial strains. *Journal of molecular catalysis B: Enzymatic,* 2010, 67(1-2), 122–128. https://doi.org/10.1016/j.molcatb.2010.07.016
27. *Meldrum N. U., Roughton F. J.* Carbonic anhydrase. Its preparation and properties. *The Journal of physiology,* 1933, 80 (2), 113. https:// 10.1113/jphysiol.1933.sp003077
28. *Fukuzawa H., Fujiwara S., Yamamoto Y., Dionisio-Sese M. L., Miyachi* S. cDNA cloning, sequence, and expression of carbonic anhydrase in Chlamydomonas reinhardtii: regulation by environmental CO_2 concentration. *Proceedings of the National Academy of Sciences*, 1990, 87 (11), 4383–4387. https://doi.org/10.1073/pnas.87.11.4383
29. *Fujiwara S., Fukuzawa H., Tachiki A., Miyachi S.* Structure and differential expression of 2 genes encoding carbonic-anhydrase in *Chlamydomonas reinhardtii*. *Proc Natl Acad Sci USA,* 1990, 87:9779-9783. https://doi.org/10.1073/pnas.87.24.9779
30. *Moroney J. V., Ma Y., Frey W. D., Fusilier K. A., Pham T. T., Simms T. A., ..., Mukherjee B.* The carbonic anhydrase isoforms of Chlamydomonas reinhardtii: intracellular location, expression, and physiological roles. *Photosynthesis Research,* 2011, 109, 133–149. https://doi.org/10.1007/s11120-011-9635-3
31. *Tuskan G. A., Difazio S., Jansson S., Bohlmann J., Grigoriev I., Hellsten U., Putnam N., ..., Rokhsar D.* The genome of black cottonwood, Populus trichocarpa (Torr. & Gray). *Science,* 2006, 313: 1596–1604. https://doi.org/10.1126/science.1128691
32. *Soltes-Rak E., Mulligan M. E., Coleman J. R.* Identification and characterization of a gene encoding a vertebrate-type carbonic anhydrase in cyanobacteria. *Journal of Bacteriology*, 1997, 179 (3), 769–774. https://doi.org/10.1128/jb.179.3.769-774.1997
33. *Elleby B., Chirica L. C., Tu C., Zeppezauer M., Lindskog S.* Characterization of carbonic anhydrase from Neisseria gonorrhoeae. *European Journal of Biochemistry,* 2001, 268 (6), 1613–1619. https://doi.org/10.1046/j.1432-1327.2001.02031.x
34. *Chirica L. C., Elleby B., Lindskog S.* Cloning, expression and some properties

of α-carbonic anhydrase from Helicobacter pylori. *Biochimica et Biophysica Acta (BBA) — Protein Structure and Molecular Enzymology,* 2001, 1544 (1-2), 55–63. https:// doi:10.1016/s0167-4838(00)00204-1
35. *Elleuche S., Pöggeler S.* Carbonic anhydrases in fungi. *Microbiology,* 2010, 156(1), 23–29. https://doi.org/10.1099/mic.0.032581-0
36. *Kumar R. S. S., Ferry J. G.* Prokaryotic Carbonic Anhydrases of Earth's Environment. In: Frost, S., McKenna, R. (eds) Carbonic Anhydrase: Mechanism, Regulation, Links to Disease, and Industrial Applications. *Subcellular Biochemistry,* 2014, 75. https://doi.org/10.1007/978-94-007-7359-2_5
37. *Mangani S., Hakansson K.* Crystallographic studies of the binding of protonated and unprotonated inhibitors to carbonic anhydrase using hydrogen sulphide and nitrate anions. *Eur. J. Biochem*, 1992, 210, 867–871. https://doi.org/ 10.1111/j.1432-1033.1992.tb17490.x
38. *West D., Kim C. U., Tu C., Robbins A. H., Gruner S. M., Silverman D. N., McKenna R.* Structural and kinetic effects on changes in the CO_2 binding pocket of human carbonic anhydrase II. *Biochemistry,* 2012, 51, 9156–9163. https://doi.org/10.1021/bi301155z
39. *Kupriyanova E., Pronina N., Los D.* Carbonic anhydrase–A universal enzyme of the carbon-based life. *Photosynthetica,* 2017, 55 (1), 3–19. https://doi.org/10.1007/s11099-017-0685-4
40. *Esbaugh A. J., Tufts B. L.* The structure and function of carbonic anhydrase isozymes in the respiratory system of vertebrates. *Respiratory physiology & neurobiology,* 2006, 154 (1–2), 185–198. https://doi.org/10.1016/j.resp.2006.03.007
41. *Tashian R. E., Hewett-Emmett D., Carter N., Bergenhem N. C. H.* Carbonic anhydrase (CA)-related proteins (CA-RPs), and transmembrane proteins with CA or CA-RP domains. In: Chegwidden, W.R., Carter, N.D., Edwards, Y.H. (eds) *The Carbonic Anhydrases. EXS 90,* 2000, vol 90. Birkhäuser, Basel. https://doi.org/10.1007/978-3-0348-8446-4_6
42. *Burnell J. N., Gibbs M. J., Mason J. G.* Spinach chloroplastic carbonic anhydrase: nucleotide sequence analysis of cDNA. *Plant physiology*, 1990, 92 (1), 37–40. https://doi.org/10.1104/pp.92.1.37
43. *Fawcett T. W., Browse J. A., Volokita M., Bartlett S. G.* Spinach carbonic anhydrase primary structure deduced from the sequence of a cDNA clone. *Journal of Biological Chemistry,* 1990, 265 (10), 5414–5417. https://doi.org/10.1016/S0021-9258(19)39375-5
44. *Yu J. W., Price G. D., Song L., Badger M. R.* Isolation of a putative carboxysomal carbonic anhydrase gene from the cyanobacterium Synechococcus PCC7942. *Plant Physiology,* 1992, 100 (2), 794–800. https://doi.org/10.1104/pp.100.2.794
45. *Eriksson M., Karlsson J., Ramazanov Z., Gardestrom P., Samuelsson G.* Discovery of an algal mitochondrial carbonic anhydrase: molecular cloning and characterization of low CO_2 induced polypeptide in *Chlamydomonas reinhardtii. — Proc. nat. Acad. Sci*, 1996, 93: 12031–12034.
46. *Hewett-Emmett D., Tashian R. E.* Functional diversity, conservation and convergence in the evolution of the α-, β- and γ-carbonic anhydrase gene families. *Mol. Phylogenet. Evol,* 1996, 5: 50–77, https://doi.org/10.1006/mpev.1996.0006
47. *Gotz R, Gnann A., Zimmermann F. K.* Deletion of the carbonic anhydrase-like gene NCE103 of the yeast *Saccharomyces cerevisiae* causes an oxygen-sensitive growth defect. *Yeast*, 1999, 15:855–864. https://doi.org/10.1002/(SICI)1097-0061(199907)15:10A<855::AID-YEA425>3.0.CO;2-C
48. *Rowlett R. S., Chance M. R., Wirt M. D., Sidelinger D. E., Royal J. R., Woodroffe M., ..., Lam M. G.* Kinetic and structural characterization of spinach carbonic anhydrase. *Biochemistry*, 1994, 33 (47), 13967–13976. https://doi.org/10.1021/bi00251a003
49. *Bracey M. H., Christiansen J., Tovar P., Cramer S. P., Bartlett S. G.* Spinach carbonic anhydrase: investigation of the zinc-binding ligands by site-directed mutagenesis, elemental analysis, and Exafs. *Biochemistry*, 1994, 33:13126–13131. https://doi.org/10.1021/bi00248a023
50. *Kimber M. S., Pai E. F.* The active site architecture of *Pisum sativum* β-carbonic anhydrase is a mirror image of that of α-carbonic anhydrases. *The EMBO journal,* 2000, 19 (7), 1407–1418. https://doi.org/10.1093/emboj/19.7.1407
51. *Mitsuhashi S., Mizushima T., Yamashita E., Yamamoto M., Kumasaka T., Moriyama H., ..., Tsukihara T.* X-ray structure of β-carbonic anhydrase from the red alga, Porphyridium purpureum, reveals a novel catalytic site for CO_2 hydration. *Journal of Biological Chemistry,* 2000, 275 (8), 5521–5526. https://doi.org/10.1074/jbc.275.8.5521
52. *Cronk J. D., Rowlett R. S., Zhang K. Y., Tu C., Endrizzi J. A., Lee J., Gareiss P. C., Preiss J. R.* Identification of a novel noncatalytic bicarbonate binding site in eubacterial beta-carbonic anhydrase. *Biochemistry*, 2006, 45, 43514361. https://doi.org/10.1021/bi052272q

53. *Rowlett R. S.* Structure and catalytic mechanism of the β-carbonic anhydrases. *Biochimica et Biophysica Acta (BBA)-Proteins and Proteomics*, 2010, 1804 (2), 362–373.https://doi.10.1016/j.bbapap.2009.08.002
54. *Parisi G., Perales M., Fornasari M., Colaneri A., Schain N., Casati D., ..., Zabaleta E.* Gamma carbonic anhydrases in plant mitochondria. *Plant molecular biology*, 2004, 55, 193–207. https://doi.org/10.1007/s11103-004-0149-7
55. *Alber B. E., Ferry J. G.* Characterization of heterologously produced carbonic anhydrase from Methanosarcina thermophile, *J. Bacteriol,* 1996, 178, 3270–3274, https://doi.org/10.1128/jb.178.11.3270-3274.1996.
56. *Price G. D., Howitt S. M., Harrison K., Badger M. R.* Analysis of a genomic DNA region from the cyanobacterium Synechococcus sp. strain PCC7942 involved in carboxysome assembly and function. *Journal of bacteriology,* 1993, 175 (10), 2871–2879. https://doi.org/10.1128/jb.175.10.2871-2879.1993
57. *Peña K. L., Castel S. E., de Araujo C., Espie G. S., Kimber M. S.* Structural basis of the oxidative activation of the carboxysomal γ-carbonic anhydrase, CcmM. *Proceedings of the National Academy of Sciences*, 2010, 107 (6), 2455–2460. https://doi.org/10.1073/pnas.091086610
58. *Iverson T. M., Alber B. E., Kisker C., Ferry J. G., ReesD. C.* A closer look at the active site of gamma-class carbonic anhydrases: High-resolution crystallographic studies of the carbonic anhydrase from *Methanosarcina thermophila*. *Biochemistry*, 2000, 39, 9222–9231. https://doi.org/10.1021/bi000204s
59. *Kisker C., Schindelin H., Alber B. E., Ferry J. G., Rees D. C.* A left-hand beta-helix revealed by the crystal structure of a carbonic anhydrase from the archaeon *Methanosarcina thermophila*. *EMBO J,* 1996, 15, 2323–2330. https://doi.org/10.1002/j.1460-2075.1996.tb00588.x
60. *Long B. M., Badger M. R., Whitney S. M., Price G. D.* Analysis of carboxysomes from Synechococcus PCC7942 reveals multiple Rubisco complexes with carboxysomal proteins CcmM and CcaA. *Journal of Biological Chemistry,* 2007, 282 (40), 29323–29335. https://doi.org/10.1074/jbc.M703896200
61. *de Araujo C., Arefeen D., Tadesse Y., Long B. M., Price G. D., Rowlett R. S., ..., Espie G. S.* Identification and characterization of a carboxysomal γ-carbonic anhydrase from the cyanobacterium Nostoc sp. PCC 7120. *Photosynthesis research,* 2014, 121, 135–150. https://doi.org/10.1007/s11120-014-0018-4
62. *Klodmann J., Sunderhaus S., Nimtz M., Jänsch L., Braun, H. P.* Internal architecture of mitochondrial complex I from *Arabidopsis thaliana*. *The Plant Cell,* 2010, 22 (3), 797–810. https://doi.org/10.1105/tpc.109.073726
63. *Sunderhaus S., Dudkina, N. V., Jänsch L., Klodmann J., Heinemeyer J., Perales M., ..., Braun H. P.* Carbonic anhydrase subunits form a matrix-exposed domain attached to the membrane arm of mitochondrial complex I in plants. *Journal of Biological Chemistry*, 2006, 281 (10), 6482–6488.https://doi.org/10.1074/jbc.M511542200
64. *Roberts S. B., Lane T. W., Morel F. M.* Carbonic anhydrase in the marine diatom *Thalassiosira weissflogii* (Bacillariophyceae) 1. *Journal of Phycology,* 1997, 33 (5), 845–850. https://doi.org/10.1111/j.0022-3646.1997.00845.x
65. *Sawaya M. R., Cannon G. C., Heinhorst S., Tanaka S., Williams E. B., Yeates T. O., Kerfeld C. A.* The structure of β-carbonic anhydrase from the carboxysomal shell reveals a distinct subclass with one active site for the price of two. *Journal of Biological Chemistry*, 2006, 281 (11), 7546–7555. https://doi.org/10.1074/jbc.M510464200
66. *Cox E. H., McLendon G. L., Morel F. M., Lane T. W., Prince R. C., Pickering, I. J., George G. N.* The active site structure of Thalassiosira weissflogii carbonic anhydrase 1. *Biochemistry,* 2000, 39 (40), 12128–12130. https://doi.org/10.1021/bi001416s
67. *Park H., Song B., Morel F. M.* Diversity of the cadmium-containing carbonic anhydrase in marine diatoms and natural waters. *Environmental microbiology,* 2007, 9 (2), 403–413. https://doi.org/10.1111/j.1462-2920.2006.01151.x
68. *Lane T. W., Morel F. M.* Regulation of carbonic anhydrase expression by zinc, cobalt, and carbon dioxide in the marine diatom *Thalassiosira weissflogii*. *Plant physiology*, 2000, 123 (1), 345–352. https://doi.org/10.1104/pp.123.1.345
69. *Lane T. W., Saito M. A., George G. N., Pickering I. J., Prince R. C., Morel F. M.* A cadmium enzyme from a marine diatom. *Nature*, 2005, 435(7038), 42–42. https://doi.org/10.1038/435042a
70. *Alterio V., Di Fiore A., D'Ambrosio K., Supuran C. T., De Simone G.* Multiple binding modes of inhibitors to carbonic anhydrases: how to design specific drugs targeting 15 different isoforms? *Chemical reviews,* 2012, 112 (8), 4421–4468. https://doi.org/10.1021/cr200176r
71. *Del Prete S., Vullo D., Fisher G. M., Andrews K. T., Poulsen S. A., Capasso C., Supuran C. T.* Discovery of a new family of carbonic anhydrases in the malaria pathogen

Plasmodium falciparum – The η-carbonic anhydrases. *Bioorganic & Medicinal Chemistry Letters*, 2014, 24 (18), 4389–4396. https://doi.org/10.1016/j.bmcl.2014.08.015
72. *De Simone G., Monti S. M., Alterio V., Buonanno M., De Luca V., Rossi, M., ..., Di Fiore A.* Crystal structure of the most catalytically effective carbonic anhydrase enzyme known, SazCA from the thermophilic bacterium Sulfurihydrogenibium azorense. *Bioorganic & Medicinal Chemistry Letters*, 2015, 25 (9), 2002–2006. https://doi.org/10.1016/j.bmcl.2015.02.068
73. *Jensen E. L., Clement R., Kosta A., Maberly S. C., Gontero B.* A new widespread subclass of carbonic anhydrase in marine phytoplankton. *The ISME Journal,* 2019, 13 (8), 2094–2106. https://doi.org/10.1038/s41396-019-0426-8
74. *Silverman D. N., Lindskog S.* The catalytic mechanism of carbonic anhydrase: implications of a rate-limiting protolysis of water. *Accounts of Chemical Research*, 1988, 21 (1), 30–36. https://doi.org/10.1021/ar00145a005
75. *Rowlett R. S., Chance M. R., Wirt M. D., Sidelinger D. E., Royal J. R., Woodroffe M., Lam M. G.* Kinetic and structural characterization of spinach carbonic anhydrase. *Biochemistry,* 1994, 33(47), 13967–13976. https://doi.org/10.1021/bi00251a003
76. *Xu Y., Feng, L., Jeffrey P. D., Shi Y., Morel F. M.* Structure and metal exchange in the cadmium carbonic anhydrase of marine diatoms. *Nature,* 2008, 452 (7183), 56–61. https://doi.org/10.1038/nature06636
77. *Boone C. D., Rasi V., Tu C., McKenna R.* Structural and catalytic effects of proline substitution and surface loop deletion in the extended active site of human carbonic anhydrase II. *The FEBS journal*, 2015, 282 (8), 1445–1457. https://doi.org/10.1111/febs.13232
78. *Supuran C. T.* Carbonic anhydrases-an overview. *Current pharmaceutical design,* 2008, 14(7), 603–614. https://doi.org/10.2174/138161208783877884
79. *Domsic J. F., Avvaru B. S., Kim C. U., Gruner S. M., Agbandje-McKenna, M., Silverman, D. N., McKenna R.* Entrapment of Carbon Dioxide in the Active Site of Carbonic Anhydrase II. *Journal of Biological Chemistry*, 2008, 283 (45), 30766–30771. https://doi.org/10.1074/jbc.M805353200
80. *Phan D. T., Burns R. C., Puxty G., Williams M., Haritos V. S., Maeder M.* A study of bovine and human carbonic anhydrases as a model enzyme system for CO_2 hydration in post combustion capture. *International Journal of Greenhouse Gas Control,* 2015, 37, 85–89. https://doi:10.1016/j.ijggc.2015.03.016
81. *Vullo D., De Luca V., Scozzafava A., Carginale V., Rossi M., Supuran C. T., Capasso C.* The first activation study of a bacterial carbonic anhydrase (CA). The thermostable α-CA from Sulfurihydrogenibium yellowstonense YO3AOP1 is highly activated by amino acids and amines. *Bioorganic & medicinal chemistry letters,* 2012, 22 (20), 6324–6327. https://doi.org/10.1016/j.bmcl.2012.08.088
82. *Schlicker C., Hall R. A., Vullo D., Middelhaufe S., Gertz M., Supuran C. T., ..., Steegborn C.* Structure and inhibition of the CO_2-sensing carbonic anhydrase Can2 from the pathogenic fungus Cryptococcus neoformans. *Journal of molecular biology,* 2009, 385 (4), 1207–1220. https://doi.org/10.1016/j.jmb.2008.11.037
83. *Monti S. M., De Simone G., Dathan N. A., Ludwig M., Vullo D., Scozzafava A., Supuran C. T.* Kinetic and anion inhibition studies of a β-carbonic anhydrase (FbiCA 1) from the C4 plant Flaveria bidentis. *Bioorganic & medicinal chemistry letters,* 2013, 23 (6), 1626–1630. https://doi.org/10.1016/j.bmcl.2013.01.087
84. *Del Prete S., Vullo D., De Luca V., Carginale V., Scozzafava A., Supuran, C. T., Capasso, C.* A highly catalytically active γ-carbonic anhydrase from the pathogenic anaerobe Porphyromonas gingivalis and its inhibition profile with anions and small molecules. *Bioorganic & medicinal chemistry letters*, 2013, 23 (14), 4067–4071. https://doi.org/10.1016/10.1016/j.bmcl.2013.05.063
85. *Viparelli F., Monti S.M., De Simone G., Innocenti A., Scozzafava A., Xu, Y., ..., Supuran, C. T.* Inhibition of the R1 fragment of the cadmium-containing ζ-class carbonic anhydrase from the diatom Thalassiosira weissflogii with anions. *Bioorganic & medicinal chemistry letters*, 2010, 20 (16), 4745–4748. https://doi.org/10.1016/j.bmcl.2010.06.139
86. *da Costa Ores J., Sala L., Cerveira G. P., Kalil S. J.* Purification of carbonic anhydrase from bovine erythrocytes and its application in the enzymic capture of carbon dioxide. *Chemosphere*, 2012, 88 (2), 255–259. https://doi.org/10.1016/j.chemosphere.2012.03.059
87. *Vinoba M., Kim D. H., Lim K. S., Jeong S. K., Lee S. W., Alagar M.* Biomimetic sequestration of CO_2 and reformation to $CaCO_3$ using bovine carbonic anhydrase immobilized on SBA-15. *Energy & fuels*, 2011, 25 (1), 438–445. https://doi.org/10.1021/ef101218a
88. *Kernohan.* The pH-activity curve of bovine carbonic anhydrase and its relationship to the inhibition of the enzyme by anions, Biochim. Biophys. *Acta-Enzymol. Biol.* 1965, 96 304–317, https://doi.org/10.1016/0926-6593(65)90014-7.
89. *Ye X., Lu Y.* CO_2 absorption into catalyzed potassium carbonate–bicarbonate solutions: Kinetics and stability of the enzyme carbonic anhydrase as a biocatalyst. *Chemical engineering science*, 2014, 116, 567–575.

90. *Lionetto M. G., Caricato R., Giordano M. E., Erroi E., Schettino T.* Carbonic anhydrase and heavy metals. *Biochemistry. 1st edition. Intech, Rijeka,* 2012, 205–224.
91. *Belyavskaya N.A., Fediuk O. M., Zolotareva E. K.* Plants and heavy metals: perception and signaling. *Bull. Kharkiv Nat. Agrar. Univ. Ser. Biol*, 2018, 3 (45) : 10–30.https://doi.org/10.35550/vbio2018.03.010
92. *Semenihin A. V., Zolotareva O. K.* Carbonic anhydrase activity of integral-functional complexes of thylakoid membranes of spinach chloroplasts. *Ukr. Biochem. J,* 2015, 87(3), 47–56. https://doi.org/10.15407/ubj87.03.047
93. *Polishchuk A. V., Semenikhin A. V., Topchyi N. M., Zolotareva E. K.* Inhibition of multiple forms of carbonic anhydrases of spinach chloroplasts by Cu ions. *Rep Nat Acad Sci Ukraine*, 2018, 4, 94–101. https://doi.org/10.15407/dopovidi2018.04.094
94. *Topchiy N. M., Polishchuk O. V., Zolotareva E. K., Sytnyk S.K.* The influence of Cd^{2+} ions on the activity of stromal carbonic anhydrases of spinach chloroplasts. *Fiziologia rastenij and genetika*, 2019, 51 (2), 172–182. https://doi.org/10.15407/frg2019.02.172
95. *Vieille C., Zeikus G.J.* Hyperthermophilic enzymes: sources, uses, and molecular mechanisms for thermostability. *Microbiology and molecular biology reviews,* 2001, 65(1), 1–43. https://doi.org/10.1128/MMBR.65.1.1-43.2001
96. *Lavecchia R., Zugaro M.* Thermal denaturation of erythrocyte carbonic anhydrase. *FEBS letters*, 1991, 292 (1-2), 162–164. https://doi.org/10.1016/0014-5793(91)80858-Z
97. *Di Fiore A., Capasso C., De Luca V., Monti S. M., Carginale V., Supuran C. T., De Simone G.* X-ray structure of the firstextremo-α-carbonic anhydrase', a dimeric enzyme from the thermophilic bacterium Sulfurihydrogenibium yellowstonense YO3AOP1. *Acta Crystallographica Section D: Biological Crystallography*,2013, 69 (6), 1150–1159. https://doi.org/10.1107/S0907444913007208
98. *Yong J. K., Stevens G. W., Caruso F., Kentish S. E.* The use of carbonic anhydrase to accelerate carbon dioxide capture processes. *Journal of Chemical Technology & Biotechnology,* 2015, 90 (1), 3–10. https://doi.org/10.1002/jctb.4502
99. *Fisher Z., Boone C. D., Biswas S.M., Venkatakrishnan B., Aggarwal M., Tu C., McKenna R.* Kinetic and structural characterization of thermostabilized mutants of human carbonic anhydrase II. *Protein Engineering, Design & Selection*, 2012, 25 (7), 347–355. https://doi.org/10.1093/protein/gzs027
100. *Russo M. E., Capasso C., Marzocchella A., Salatino P.* Immobilization of carbonic anhydrase for CO_2 capture and utilization. *Applied Microbiology and Biotechnology,* 2022, 106 (9-10), 3419–3430. https://doi.org/10.1007/s00253-022-11937-8
101. *Wu S., Chen, J., Ma L., Zhang K., Wang X., Wei Y., Xu X.* Design of carbonic anhydrase with improved thermostability for CO_2 capture via molecular simulations. *Journal of CO_2 utilization,* 2020, 38, 141–147. https://doi.org/10.1016/j.jcou.2020.01.017
102. *De Luca V., Vullo D., Scozzafava A., Carginale V., Rossi M., Supuran C. T., & Capasso C.* An α-carbonic anhydrase from the thermophilic bacterium Sulphurihydrogenibium azorense is the fastest enzyme known for the CO_2 hydration reaction. *Bioorganic & medicinal chemistry,* 2013, 21 (6), 1465–1469. https://doi.org/10.1016/j.bmc.2012.09.047
103. *Effendi S. S. W., Chiu C. Y., Chang Y. K., Ng I. S.* Crosslinked on novel nanofibers with thermophilic carbonic anhydrase for carbon dioxide sequestration. *International journal of biological macromolecules,* 2020,152, 930–938. https://doi.org/10.1016/j.ijbiomac.2019.11.234
104. *Watanabe K., Masuda T., Ohashi H., Mihara H., Suzuki, Y.* Multiple Proline Substitutions Cumulatively Thermostabilize Bacillus Cereus ATCC7064 Oligo 1, 6 Glucosidase: Irrefragable Proof Supporting the Proline Rule. *European journal of biochemistry,* 1994, 226 (2), 277–283. https://doi.org/10.1111/j.1432-1033.1994.tb20051.x.
105. *Villbrandt B., Sagner G., Schomburg D.* Investigations on the thermostability and function of truncated Thermus aquaticus DNA polymerase fragments. *Protein engineering,* 1997, 10 (11), 1281–1288. https://doi.org/10.1128/MMBR.65.1.1-43.2001.
106. *Barbosa O., Torres R., Ortiz C., Berenguer-Murcia Á., Rodrigues R. C.,Fernandez-Lafuente R.* Heterofunctional supports in enzyme immobilization: from traditional immobilization protocols to opportunities in tuning enzyme properties. *Biomacromolecules,* 2013, 14 (8), 2433–2462. https://doi.org/10.1021/bm400762h
107. *Molina-Fernández C., Luis P.* Immobilization of carbonic anhydrase for CO_2 capture and its industrial implementation: a review. *Journal of CO_2 Utilization*, 2021,47, 101475. https://doi.org/10.1016/j.jcou.2021.101475
108. *Rasouli H., Nguyen K.,Iliuta M. C.* Recent advancements in carbonic anhydrase

immobilization and its implementation in CO_2 capture technologies: *A review. Separation and Purification Technology*, 2022, 296, 121299. https://doi.org/10.1016/j.seppur.2022.121299
109. *Mirjafari P., Asghari K., & Mahinpey N.* Investigating the application of enzyme carbonic anhydrase for CO_2 sequestration purposes. *Industrial & engineering chemistry research*, 2007, 46 (3), 921–926. https://doi.org/10.1021/ie060287u
110. *Capasso C., De Luca V., Carginale V., Cannio R., Rossi M.* Biochemical properties of a novel and highly thermostable bacterial α-carbonic anhydrase from Sulfurihydrogenibium yellowstonense YO3AOP1. *Journal of enzyme inhibition and medicinal chemistry*, 2012, 27 (6), 892–897. https://doi.org/10.3109/14756366.2012.703185
111. *Vieille C., Zeikus G. J.* Hyperthermophilic enzymes: sources, uses, and molecular mechanisms for thermostability. *Microbiology and molecular biology reviews*, 2001, 65 (1), 1–43. https://doi.org/10.1128/MMBR.65.1.1-43.2001
112. *Spahn C., Minteer S. D.* Enzyme immobilization in biotechnology. *Recent patents on engineering*, 2008, 2 (3), 195–200. https://doi.org/10.2174/187221208786306333
113. *Boucif N., Roizard D., & Favre E.* The carbonic anhydrase promoted carbon dioxide capture. Membranes for Environmental *Applications*, 2020, 1–44. https://doi.org/10.1007/978-3-030-33978-4
114. *Guisan J. M.* Immobilization of enzymes as the 21st Century begins: an already solved problem or still an exciting challenge?. *Immobilization of enzymes and cells*, 2006, 1–13.
115. *Shao P., Chen H., Ying Q., & Zhang S.* Structure–activity relationship of carbonic anhydrase enzyme immobilized on various silica-based mesoporous molecular sieves for CO_2 absorption into a potassium carbonate solution. *Energy & Fuels*, 2020, 34 (2), 2089–2096. https://doi.org/10.1021/acs.energyfuels.9b03860

БІОКАТАЛІТИЧНЕ УЛОВЛЮВАННЯ ВУГЛЕКИСЛОГО ГАЗУ ЗА УЧАСТЮ КАРБОНГІДРАЗИ

О. К. Золотарьова., Н. М. Топчій., О. М. Федюк

Інститут ботаніки НАН України, Київ

E-mail: olgamuronivna@ukr.net

Швидке та постійне зростання концентрації CO_2, найпоширенішого парникового газу в атмосфері, призводить до екстремальних погодних та кліматичних явищ. Унаслідок спалювання викопного палива (нафти, вугілля та природного газу) концентрація CO_2 в повітрі зростала упродовж останніх десятиліть більше ніж на 2 ppm на рік, і лише за останній рік — на 3,29 ppm. Для запобігання «найгіршим» сценаріям зміни клімату, необхідно негайно та суттєво скоротити викиди CO_2 шляхом управління викидами вуглецевого газу.

Мета. Аналіз сучасного стану досліджень та перспектив використання карбоангідрази в програмах декарбонізації навколишнього середовища.

Результати. Карбоангідраза це — ензим, який прискорює обмін CO_2 та HCO_3^- у розчині від 10^4 до 10^6 разів. На сьогоднішній день в різних організмах ідентифіковано 7 типів карбоангідраз. Карбоангідраза потрібна для забезпечення швидкого постачання CO_2 та HCO_3^- для різних метаболічних шляхів в організмі, що пояснює її багаторазове незалежне походження під час еволюції. Ензими, виділені з бактерій і тканин ссавців, були протестовані в проектах секвестрації CO_2 з використанням карбоангідрази. Найбільш вивченою є одна з ізоформ карбоангідрази людини — hCAII — найбільш активний природний ензим. Його недоліками були нестабільність у часі, висока чутливість до температури, низька толерантність до забруднень, таких як сполуки сірки, і неможливість повторного використання. Найбільш вивченою в цьому відношенні є одна з ізоформ карбоангідрази людини — hCAII — найбільш активний природний ензим. Для подолання цих обмежень використовували методи молекулярного моделювання та іммобілізації ензимів. Показано, що іммобілізація забезпечувала більшу термічну стабільність і стабільність під час зберігання, а також підвищувала можливість повторного використання.

Висновки. Карбоангідрази беруть участь у біологічній асиміляції атмосферного CO_2. Тому, вивчення таких ензимів та умов, необхідних для їх активації та ефективного поглинання CO_2, створює підґрунтя для розроблення біокаталітичних засобів підвищення декарбонізації атмосфери.

Ключові слова: зміна клімату; декарбонізація; біосеквестрація CO_2; карбоангідраза; іммобілізація ензимів.

UDC 578.81: 615.33 https://doi.org/10.15407/biotech16.05.022

PROSPECTS FOR THE CREATION OF LIPOSOMAL ANTIMICROBIALS BASED ON PHAGES

PYLYPENKO D. M.[1], *GRIGORYEVA G. S.*[2], *KRASNOPOLSKY Yu. M.*[3]

[1]State Biotechnological University, Ukraine, Kharkiv
[2]State Institution "Institute of Pharmacology and Toxicology of the National Academy of Medical Sciences of Ukraine", Kharkiv
[3]National Technical University "Kharkiv Polytechnic Institute", Ukraine

E-mail: pdmforwork@gmail.com

Received 2023/09/15
Revised 2023/10/17
Accepted 2023/10/31

The emergence of many pathogenic microorganisms, which are resistant to known antibiotics, indicates the need to find new strategies to fight them.

Aim. The article is devoted to the analysis of modern research on liposomal forms of phages as a promising strategy for fighting microbial infections.

Methods. Analysis of modern national and foreign research devoted to the bacteriophage encapsulation into liposomes and the evaluation of the efficacy of this drug delivery system in antimicrobial therapy.

Results. Bacteriophage encapsulation into liposomal nanoparticles protects phages from the negative effects of external factors, increases the period of circulation in the organism, ensures increased bioavailability of phage particles and, as a result, increases the efficacy of antimicrobial treatment. Liposomal forms of phages have demonstrated their effectiveness in fighting many common pathogenic bacteria, including *Staphylococcus aureus*, *Klebsiella pneumoniae*, *Mycobacterium tuberculosis*, *Salmonella*, etc.

Conclusions. Liposomal phages have prospects as antimicrobial drugs, however, for their widespread use in clinical practice, preclinical and clinical studies are required to confirm their effecace and safety.

Key words: nanobiotechnology; drug delivery system; liposome; bacteriophage; phage therapy; antimicrobial drug.

Increasing resistance of pathogenic microorganisms to antibiotics has led to the emergence of new generation of drugs, such as liposomal (LS) forms of antimicrobials. LS is a promising strategy for treatment options for currently untreatable infections [1–3]. There are FDA-approved LS forms of antibiotics on the pharmaceutical market, such as amphotericin B, amikacin, nystatin, etc. LS forms of polymyxin B, vancomycin, gentamicin, tobramycin, norfloxacin, azithromycin, and carbapenem are at various stages of research. In addition, antitumor antibiotics in the LS form, daunorubicin and doxorubicin hydrochloride, are widely used in the clinic, that make it possible to fight resistant forms of tumors [1–3].

The use of LSs as components of drug delivery system allows to change the pharmacokinetics of the encapsulated active pharmaceutical ingredient (API), increase its bioavailability and efficiency [4–7]. LS forms of APIs have undeniable advantages in the development of antimicrobial drugs. In terms of practical use, LS drug delivery systems are the most successful in nanomedicine. The creation of LS drugs is one of the promising areas of modern medicine and nanopharmacology due to the following advantages of LSs [1, 2, 8–10]:

– to prolong the circulation of the API in the body;

– to change the pharmacokinetics of drugs, significantly increasing their pharmacological effect;

– to protect the API from the degradation by external factors in the body (enzymes, pH, oxidation, etc.);

–- to suppress API-resistant forms of bacteria and tumor cells;

– to protect the cells and tissues of the body from the toxic effects of drugs;

– to increase the bioavailability of lipophilic APIs;

– to provide direct interaction or fusion of LS lipid bilayers and membranes of bacterial or tumor cells, increasing the concentration of antibiotic in bacteria or tumor cells and thus improving the therapeutic effect of the antibiotic;

– to penetrate through the blood-brain barrier and deliver the LS encapsulated API to the cells of microorganisms or tumor cells;

– to be administrated intravenously, orally, inhalation and other ways, as sterile dosage forms that do not contain endotoxins and toxic substances.

The emergence of resistant forms of microorganisms has led to a resurgence of interest in bacteriophage, or phage therapy. The relevance of phage therapy is also explained by the fact that every year there are very few new antibiotics or new dosage forms of known antibiotic APIs, while humanity is facing an increase in resistant forms of infectious agents. Phages are recognized as safe for use in the clinic and do not lead to significant specific side effects [11–17]. The action of a lytic bacteriophage is as follows: the lytic phage binds to a specific surface receptor and introduce the phage DNA into bacterium, where early gene expression, particle assembly and release of phage from the host cell is carried out. A full lytic cycle typically creates 100–200 new phage particles and is completed in about the same time as the doubling time of the bacterial host cell.

Bacteriophages as antibacterial agents

The development of modern science has revived interest in drugs based on phages. Biotechnology allows to introduce phages into our daily lives in new ways. Approved preparations based on bacteriophages prevent contamination of a number of products, such as meat, fish, fruits, vegetables, dairy products [18, 19], with pathogenic bacteria, such as *Listeria monocytogenes*, *Salmonella enterica*, *Chigella*, *Escherichia coli*. Sprayable phage solutions are approved for protecting growing plants and animals from bacterial diseases, phage-based biocides can penetrate biofilms to treat and protect surfaces from contamination or bacterial corrosion. Biotechnological methods are constantly being developed and allows to use bacteriophages for gene delivery and carriers of vaccine antigens. In addition, lytic phages can act as selective and specific probes for the detection of pathogenic bacteria, such as *Staphylococcus aureus* [20–21].

The possibility of using bacteriophages in the treatment of infectious diseases is limited by a number of factors, we are going to focus only on the main problems [22–25]:

1. The instability of phages is associated with their physical and chemical properties as well as external environmental factors. Despite the fact that phage preparations are stable in buffer-salt solutions for at least 1–2 years at a temperature of 2–8 °C, when taken orally, intravenously or intramuscularly, phage suspensions enter the environment with high temperature, non-optimal pH value, different osmotic conditions, enzymes in the stomach and intestines, that leads to instability of phage particles. In addition, the phage stability can be affected by the shape and size of phages, namely the size of the head, and the length and thickness of the tail. The loss of stability of phage naturally leads to a loss of titer, and consequently to a loss of infectivity of it. It should also be noted that it is proposed to use a mixture of phage particles (a phage cocktail) for phage therapy to prevent bacterial infections in clinic. The administration of phage cocktails may effectively prevent bacterial resistance and improve clinical outcomes. According to a number of authors, a mixture of phage cocktails is less stable.

2. The loss of specificity of phages is associated with bacterial resistance and emergence of resistance to phages.

3. The emergence of phage-neutralizing antibodies is one of factors that reduce the activity of phage therapy. Furthermore, the phage therapy requires repeated administration of phages, that in turn leads to an increase in the level of phage-neutralizing antibodies.

4. The phage therapy is low effective for patients infected with intracellular pathogens (*Mycobacterium tuberculosis*, *Salmonella*, *Staphylococcus*) located, for example, in phagocytic cells.

Perspectives of liposomal forms of phages

The encapsulation of phages into LS nanoparticles is one of the strategies for increasing the efficacy of phage therapy, as it has been demonstrated for antibiotic therapy.

Having the experience in LS drugs creation, we believe that LS drugs are the most promising direction of drug delivery systems today.

By analyzing the problems related to the use of phages, advantages of LS forms and our knowledge in the liposomology, we believe that there is a real opportunity to use LSs as drug delivery system in phage therapy in the field of oncology and infectious diseases. In this case, the LS system of phage therapy will significantly overcome these problems. Taking into account that a number of viruses were successfully encapsulated in LSs while maintaining their high cell transfection efficiency, the creation of LS forms of bacteriophage preparations is quite realistic [26–29]. Oncolytic viruses, polioviruses, retroviruses, and others were encapsulated in LSs of various compositions, and LSs containing the virus were able to infect cells by merging with the cell membrane. The transfection efficiency of LS form of adenovirus was 4 times higher compared to non-encapsulated one. Unlike the viruses, the encapsulation of phages into LSs will require another lipid compositions of LS nanoparticles and another technological schemes, because of different size and properties of phages and other viruses. However, it could be used the same technological principles for obtaining of LS forms of phages, lyophilization or spray drying, and cryoprotectant selection as for obtaining LS forms of other preparations.

In recent years, research efforts have been focused on the possibility of using LSs for phage therapy, for example, against *Staphylococcus aureus*, *Klebsiella pneumoniae*, *Pseudomonas aeruginosa*, *Enterococcus faecium*, *Mycobacterium tuberculosis*, *Salmonella*, *Listeria monocytogenes*, etc. Various methods have been proposed for obtaining bacteriophages-containing LS nanoparticles [30, 31]. The following paragraphs are devoted to research describing the production and properties of LS phages.

Bacteriophages against *Salmonella*

Salmonellosis is one the main intestinal infections in humans and animals, caused by bacteria of the family *Enterobacteriaceaee* — *Salmonella*, which colonizes the intestinal cells, resulting in intoxication and damage of the gastrointestinal tract. Salmonella phages were among the first to be used for phage therapy and encapsulated in LSs. Bacteriophages UAB_Phi20, UAB_Phi78, UAB_Phi87 against *Salmonella* strains were encapsulated in positively charged LSs (31.6 mV) with a diameter of 309 to 326 nm. LSs were prepared by the lipid film method followed by hydration and extrusion. LSs consisted of 1,2-dilauroyl-sn-glycero-3-phosphocholine (DLPC), cholesteryl-PEG600, cholesterol, and cholesteryl-3β-N(dimethylaminoethyl) carbamate hydrochloride in a molar ratio of 1 : 0.1 : 0.2 : 0.7. In order to study the stability of phages, LSs were subjected to the action of stomach acid (pH 2.8), and the phage titer decreased from 3.7 to 5.4 log units, whereas the titer of non-encapsulated phages decreased from 5.7 to 7.8 log units in stomach acid, that confirms the protection of the phage activity in LS form in low pH conditions. Both LS phages and free phage suspension protected salmonella-infected chickens *in vivo* when administered daily for 6 days. However, LS phages protection was maintained up to 1 week after treatment was stopped, and free phage activity was completely lost by this time [32].

Using salmonella phage, two different methodologies for bacteriophage encapsulating using two biocompatible materials were offered, a cationic lipid mixture and a combination of alginate with anthracite $CaCO_3$ [33]. The purified phage lysate with concentration of 10^{10}–10^{11} PFU/ml was used for phage encapsulation. Both techniques have been successfully applied to encapsulate salmonella phages with different morphologies, and what is important the used material does not change the antibacterial action of phages. The authors believe that both technologies can also be adapted to encapsulation and stabilization of any bacteriophage for, that will allow to protect phages from critical environmental conditions. Orally administered LS form of salmonella phages was stable in the stomach in mice.

Bacteriophages against *Mycobacterium tuberculosis*

The discovery of phages specific to *Mycobacterium* gives hope that phage therapy will be safe and effective against extracellular bacteria [34]. The phage penetration into intracellular and granulomatous media, as well as synergistic effects with antibiotics, are important issues in the treatment of tuberculosis. The use of LSs can provide an effective intracellular penetration of bacteriophages [35]. Mycobacteriophage TM4 encapsulated LSs were prepared from 1,2-dipalmitoyl-sn-glycero-3-phosphocholine

(DPPC), 1,2-dioleoyl-sn-glycero-3-phosphocholine (DOPC), and the fluorescent lipid Texas Red™ 1,2-dihexadecanoyl-*sn*-glycero-3-phosphoethanolamine (DHPE). The resulting LS size was less than 5 μm, and the possibility of inhalation delivery of mycobacteriophage containing LSs to lungs was shown. In addition, phages encapsulated in LSs penetrated monocyte cells more efficiently than free phages. According to the authors, LS phages can make it possible to fight off intracellular pathogens due to their penetration into eukaryotic cells [36].

LS form of lytic mycobacteriophage D29 for the treatment of tuberculosis infection was prepared from phosphatidylcholine (PC) and cholesterol in a ratio of 3:1 by two methods: extrusion and chromatography on Sephadex G-75 using sodium deoxycholate in 20% ethanol [37]. The first method gives LSs with a size of 0.8 μm and a phage encapsulation of about 40%, and the second method gives LSs with a size of 0.25 μm and a phage encapsulation of about 25%. The lytic effect of the LS form of mycobacteriophage D29 was established both on the model of tuberculous granuloma formed in the presence of *M. tuberculosis* in human mononuclear blood cells *in vitro*, and on the model of tuberculous infection in C57Bl/6 mice. The use of the LS form of lytic mycobacteriophages D29 with a size of 0.8 μm showed the most pronounced significant antimycobacterial effect.

The macrophage cell culture RAW264-7 was infected for 24 hours with *M. tuberculosis* H37RV at a concentration of 10^7 CFU/ml, and macrophages were isolated by centrifugation in a Ficoll density gradient [38]. Phage D29 in a concentration at least 10^8 PFU/ml was purified on an ion exchange column packed with Q-sepharose, and then shaken with a phospholipid film containing PC and cholesterol, the obtained lipid particles containing mycobacteriophage were homogenized by 20-fold extrusion and filtered through filters with pore size of 0.4 μm. The phage encapsulation into LSs was controlled by PCR analysis of phage DNA. There were 82 colonies of *M. tuberculosis* H37RV in control sample, 17 colonies in the sample treated with free mycobacteriophage, and 7 colonies in the sample treated with LS form of phage, that proves a higher antibacterial effect of mycobacteriophages encapsulated in LSs with a size of about 400 nm. In the following research the antimycobacterial action of lytic bacteriophage D29 both in free and LS forms was shown to varying degrees in cell models of intracellularly infected macrophages RAW264-7 and tuberculous granuloma formed by human blood mononuclear cells [39].

Bacteriophages against *Klebsiella pneumoniae*

Nosocomial infections caused by *K. pneumoniae* are the main cause of morbidity and mortality among burn patients [40]. The phage therapy is a safe and effective strategy for fighting against antibiotic resistant pathogens. Despite the fact that the promise of the phage therapy has been confirmed in a number of studies [41–43], to date, none of the phage-based treatments has been comprehensively studied in patients and has not reached commercialization. One of the reasons is the rapid clearance of phages from our body by reticuloendothelial system and a poor pharmacokinetic profile, that negatively affects the treatment efficacy. In this regard, attempts are being made to create LS forms of bacteriophages, in particular, for the treatment of diseases caused by *K. pneumoniae*. For example, a decrease in pro-inflammatory and a significant increase in anti-inflammatory cytokines in the lung homogenates of mice treated with the LS form of lytic bacteriophage T7 was shown, which indicates an increased effectiveness of the LS phages in the treatment of pneumonia in a model of *K. pneumoniae* B5055 mediated croupous pneumonia in mice [44]. The phage suspension was rapidly absorbed by the reticuloendothelial system and phages could not be determined, whereas encapsulated in LSs or bound to nanoparticles phages were detected in the body for a longer time [45]. LSs consisted of PC, cholesterol, Tween-80, and stearylamine in a ratio of 8 : 2 : 1 : 0.5. The average size of LS nanoparticles was 229.83 nm, and the phage encapsulation was 79.2 ± 5.6%. The use of LS encapsulated phage cocktail led to an increased therapeutic effect in the treatment of *K. pneumoniae* mediated burn wounds [46]. The pharmacokinetics of a phage cocktail containing five bacteriophages against *K. pneumoniae* encapsulated in cationic LSs was studied in intraperitoneal administration in BALB/c mice [46]. When studying the circulation time of phages in the blood and the residence time in various organs, LS encapsulated phages were detected in the spleen, liver and blood for almost 48 hours, while free phages were eliminated after 24 hours. An efficacy of LS phage was performed in a model of *K. pneumonia*

mediated burn wound infection in mice. Due to the long circulation time, a number of bacteria in the blood of mice treated with cationic LS phages was reduced more effective in comparison with mice treated with free phage. Furthermore, the use of phages encapsulated in cationic LSs provided a faster infection. LS particles containing phages against *K. pneumoniae* remained in the blood for a longer period than free phage particles, and chitosan-coated small LSs containing phages was detected in the gastrointestinal tract longer than large multilamellar LSs.

Bacteriophages against *Staphylococcus aureus*

S. aureus is a common and virulent human pathogen, which causes a number of serious diseases, including skin abscesses, wound infections, endocarditis, osteomyelitis, pneumonia, and toxic shock syndrome. Like many other infectious agents, *S. aureus* is resistant to a wide range of antibiotics, that increase the interest in the phage therapy. The study of phages is carried out both on various animal models and in a number of human diseases, and the use of phage cocktails allows more targeted treatment [47]. But as mentioned before, there remain many obstacles to phage therapy, especially in terms of their impact on the body *in vivo*, as well as the influence of the external environment of the body on bacteriophages. Naturally, as for other pathogenic agents, scientists turned to the encapsulation of phages in nanoparticles. Thus, LS encapsulated bacteriophages against *S. aureus* (namely, MR-5 and MR-10) were more stable and showed a higher therapeutic effect compared to the free forms in diabetic wound infection in mice [48]. This cationic LSs were prepared from PC, cholesterol, Tween-80, and stearylamine in a ratio of 8 : 2 : 1 : 0.5 by a lipid film method followed by mixing with a phage suspension and sonication the mixture. The average size of LSs was 212 nm, and the phage encapsulation was about 87%. The use of phage loaded LSs led to a reduction in wound healing time by 33%, owing to the more effective capture of phage cocktail in LS form then free phage, that provided twofold increase in the phage titer in damaged tissue, increased rate of the infection resolution and effective treatment of diabetic wound surface.

Two LS preparations of bacteriophages against *E. coli T3* (the size is about 65 nm) and *S. aureus K* (the size of capsid head is 80 nm and tail length — 200 nm) were obtained by microfluidic method [49]. LSs were prepared from 1,2-distearoyl-sn-glycero-3-phosphocholine (DSPC) and cholesterol by the thin film method, followed by dissolution in isopropanol to the concentration of 10 mg/mL. Then, an isopropanol solution of lipids and an aqueous buffer solution were fed through special devices using microfluidic pumps, and the resulting solution was filtered through 0.1 μm syringe filters. Using a co-current microfluidic glass device, the sterile solution was mixed with a concentrated phage suspension to encapsulate two model bacteriophages against *E. coli T3* and *S. aureus K* in submicron-sized LSs. The resulting preparation was dialyzed to remove residual isopropanol, and free phages were separated by ultrafiltration. The average size of LSs varied from 100 to 300 nm. The titer of encapsulated *E. coli T3* phage was 10^9 PFU/ml, but for *S. aureus K* phage it was significantly lower than 10^5 PFU/ml. The effectiveness of the *E. coli T3* phage encapsulation depended on the phage aggregation, while *S. aureus K* phage interacted with the lipid bilayer of LSs, and a large amount of it bound outside the LS nanoparticles rather than encapsulated into them. The authors inactivated LS bound *S. aureus K* phages, while maintaining the activity of the encapsulated phages.

A change in the cholesterol concentration in the LS composition of led to an increase in the average size of LSs and in the particle size distribution. The size of LSs based on only DSPC was 134±13 nm, on the mixture of DSPC and cholesterol in a molar ratio of 5 : 1 — 206±28 nm, and on the mixture of DSPC and cholesterol in a molar ratio of 1 : 1 — 301±32 nm. It should be considered that in the treatment of gastrointestinal infections, nonencapsulated in LS phages can be inactivated by the low acidity of stomach acid (pH 2.5).

Bacteriophages against *Cutibacterium acnes*

C. acnes is a cause of the acne disease, which is a multifactorial disease associated with the colonization of the skin follicles by *C. acnes* of *Propionibacteriaceae* family. The treatment of the acne disease is based on the combination of various products derived from retinoids, antibiotics, and hormonal antiandrogens, which takes a long time, can have side effects, be expensive, and not always effective. in this context, the evaluation of cytotoxicity of free and encapsulated in LSs

Pa.7 bacteriophage from *C. acnes* in HaCaT cells is of interest [50]. LS encapsulated Pa.7 bacteriophage (*Pseudomonas* phage PA7, equivalent to Pa.7 bacteriophage) did not exhibited cytotoxicity to HaCaT cells, which are a spontaneously transformed aneuploid immortal keratinocyte cell line from the adult human skin. It was proposed to use LS encapsulated bacteriophages for skin treatment.

Thus, lipid-based nanovesicles is a universal approach to phage delivery, as well as many other drugs. LSs protect phages from external stress factors such as low gastric pH, reticuloendothelial system, and neutralizing antibodies, increase the circulation time *in vivo*, and also the encapsulation of phages in LSs allows to gain access to intracellular pathogens (Fig. 1). LS phage delivery is safe, the used products are not toxic, and phages in LS form are less immunogenic [32, 44–46, 51, 52]. LSs can provide easier unhindered diffusion of phages through the epithelium [53]. The possibility of modifying the LS surface using conjugation with polymers, sucg as chitosan, alginate, PEG, is also important to note. For example, PEGylated LSs are shielded and less visible [15].

Research on pharmacokinetics and pharmacodynamics of LS forms of phages both for oral and intravenous administration is of particular importance for the creation of drugs for phage therapy. The biodistribution and transcytosis through the intestinal cell layer of orally administered LS encapsulated bacteriophages were analyzed on Caco-2 and HT29 cells (human colorectal adenocarcinoma) [54]. Phage lysate was obtained from *Salmonella enterica* serovar Typhimurium LB5000. The culture was infected with the bacteriophage UAB_Phi20 of the *Podoviridae* family), having an icosahedral head with a size of 60±2.7 nm and a non-contracting tail with a size of 13±0.7 nm. LSs were prepared from DLPC, cholesteryl-PEG600, cholesterol, and cholesteryl-3β-N(dimethylaminoethyl) carbamate hydrochloride in a ratio of 1 : 0.1 : 0.2 : 0.7. The size of the obtained LSs was 341.6±8.6 nm, the zeta potential was between 29 and 34 mV, the final product contained 46% of encapsulated and 54% on non-encapsulated phages. Fluorochrome labeled phages were visualized in the stomach and intestines of mice, and besides, the presence of phages encapsulated in LSs were detected in stomach and other internal organs, including the spleen and liver, and muscles by conventional culture methods. The study of phage adhesion showed that orally administered LS encapsulated phages remained in the stomach, confirming that LS encapsulated phages are protected until their release. Moreover, when the encapsulated phages reach the intestine, the attachment to the intestinal wall temporarily protects them from the action of bile acids and excretion. On the model of *Pseudomonas aeruginosa* phage (PEV20 has s 91 kb genome and a capsid size

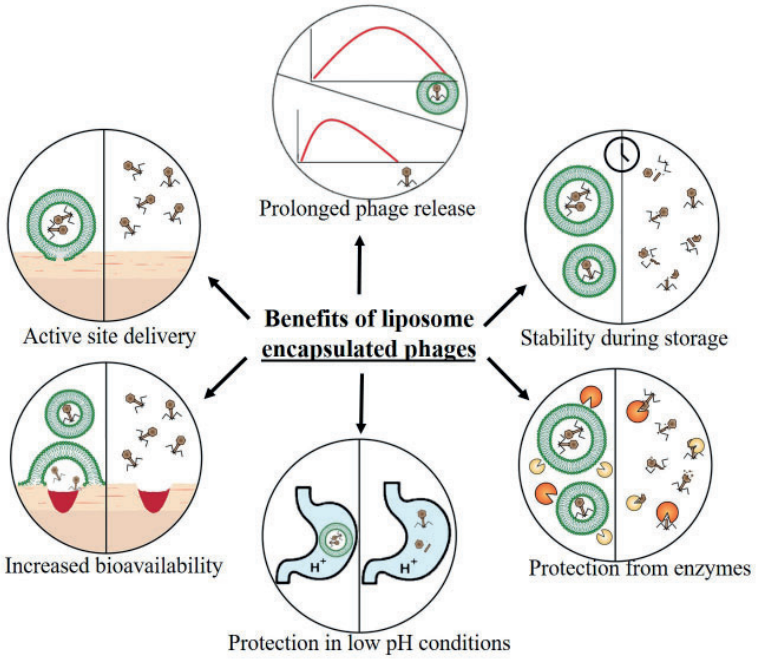

Fig. 1. **The main benefits of the LS encapsulated phages [31]**

of 60 nm), when intravenously administrated to rats, the phages accumulated in the liver, spleen and lymph nodes (where they were absorbed by the mononuclear phagocyte system), and also in lungs and muscles [55]. Renal clearance was limited. The authors found another source of phage inactivation, phage-neutralizing antibodies. When treated with repeated doses of phages, the level of specific phage-neutralizing antibodies increased.

Bacteriophages in the combination antimicrobial therapy

The combination therapy of phages and antibiotics takes a special place in phage therapy. Synergistic effects of a combination of phages and antibiotics have been identified [56, 57], for example, in fighting against *Citrobacter amalonaticus* which causes infections of respiratory and urinary tracts. Eight different antibiotics with different mechanisms of action (cefotaxime, gentamicin, meropenem, tigecyclin, etc.) were used in combination with phage MRM57 to study the effect of the combined treatment on the minimal inhibitory concentration. The authors found that synergism depends on the concentration of antibiotics, notably to varying degrees for a very low amount of phage. And only cefotaxime did not show any synergies.

Considering that the use of phages for compassionate treatment is often used in desperate situations, the absence of side effects in debilitated patients is reassuring [58]. When the introduction of high doses of phages over a long period of time, some phage proteins can apparently elicit an immune response. However, neutralizing anti-phage antibodies have been found in humans who have not been treated with phages, that may limit the success of phage therapy [69]. LS forms of phages can also be used in individual phage therapy for various infections [59]. The antibacterial action of LS nanoparticles themselves should be also taken into account [60].

A significant number of works are devoted to obtaining LSs and studying the stability of the LS forms of phages [51, 61–64].

Conclusions

In conclusion, LS phage drugs makes it possible to create drugs for oral, intravenous, external, and inhalation administration. When administered orally, LS nanoparticles can significantly protect bacteriophages from acid degradation and inactivation by enzymes during transit through the gastrointestinal tract, as well as prolong the residence time of phages in the intestine. At the same time, oral administration leads to low bioavailability of phages. In this regard, the intravenous administration of LS encapsulated phages can provide higher efficacy, because these drugs are safe, and LS forms allows to increase the residence time of the encapsulated product and its antibacterial activity, which is especially important in case of multidrug-resistant infections.

Increasing resistance of pathogenic bacteria to antibiotics has led to a revival of interest in bacteriophage therapy, which was actively used in a number of countries before the era of antibiotics [65]. The search for new forms of phage preparations has begun today in many countries of the world, preclinical and clinical stages of research are underway [66–69]. Current research suggests mechanisms for interaction of phages with nanoparticles, for example, metal nanoparticles, which is based on the value of the zeta potential [70]. The authors believe that particles with a zeta potential below minus 35 mV effectively bind to positively charged phage tails, and particles with a zeta potential above 35 mV effectively bind to negatively charged phages. If particles that do not meet these requirements, the physical interaction of phages with nanoparticle becomes nonspecific.

Using the knowledge of practical use of nanosystems in pharmacy and medicine, it is possible to develop drug delivery system based on nanoparticles, including LSs for phage therapy to overcome the difficulties associated today with the use of phages. Thus, we can talk about the prospects of using LS forms of phages for the treatment of infectious diseases. Perhaps the liposomal form of phages and the liposomal form of antibiotics are especially attractive due to a synergistic effect of these two dosage forms. However, for the licensing and clinical use of phage drugs, a large number of studies, both *in vitro* and *in vivo*, must be conducted to confirm the effectiveness and safety of the treatment.

Funding source. The work was performed within the research program of "Use of biotechnological methods in rational nature management, veterinary medicine and innovative production" (State Registration No. 0121U113717, 2022–2026).

REFERENCES

1. *Ferreira M., Ogren M., Dias J. N. R., Silva M., Gil S., Tavares L., Aires-da-Silva F., Gaspar M. M., Aguiar S. I.* Liposomes as antibiotic delivery systems: a promising nanotechnological strategy against antimicrobial resistance. *Molecules*. 2021, 26(7), 2047. https://doi.org/10.3390/molecules26072047
2. *Gonzalez Gomez A., Hosseinidoust Z.* Liposomes for antibiotic encapsulation and delivery. *ACS Infect. Dis*. 2020, 6(5), 896–908. https://doi.org/10.1021/acsinfecdis.9b00357
3. *Liu P., Chen G., Zhang J.* A review of liposomes as a drug delivery system: current status of approved products, regulatory environments, and future perspectives. *Molecules*. 2022, 27(4), 1372. https://doi.org/10.3390/molecules27041372
4. *Rommasi F., Esfandiari N.* Liposomal nanomedicine: applications for drug delivery in cancer therapy. *Nanoscale Res. Lett*. 2021, (16)1, 95. https://doi.org/10.1186/s11671-021-03553-8
5. *Shvets V. I., Krasnopolskiy Yu. M., Sorokoumova G. M.* Liposomal forms of drugs: technological features of production and use in the clinic. *M.: Remedium*, 2016. 200 p. (In Russian).
6. *Krasnopolsky Y. M., Pylypenko D. M.* Creation of antigen and drug delivery systems based on artificial and natural lipid nanoparticles: Liposomes and Exosomes: monograph. *Kharkiv: Printing House* «Madrid», 2023, 179 p. (In Ukrainian).
7. *Pivnuk V. M., Tymovska Yu. O., Ponomareva O. V., Kulyk G. I., Olyinichenko G. P., Anikusko M. F., Krasnopolsky Yu. M., Chekhun V. F.* Applying of liposomal form of doxorubicin in patients with doxorubicin-resistant breast cancer. *Oncol*. 2007, 9(2), 120–124. (In Ukrainian).
8. *Krasnopolsky Y., Pylypenko D.* Encapsulation of eucalyptus leaves phytoproducts into liposomal nanoparticles and study of their antibacterial activity against Staphylococcus aureus in vivo. *JMBFS*. 2023, 12(5), e9445. https://doi.org/10.55251/jmbfs.9445
9. *Allen T. M., Cullis P. R.* Liposomal drug delivery systems: from concept to clinical applications. *Adv. Drug Deliv. Rev*. 2013, (65(1), 36–48. https://doi.org/10.1016/j.addr.2012.09.037
10. *Krasnopolskii Y. M., Grigor'eva A. S., Katsai A. G., Konakhovich N. F., Prokhorov V. V., Stadnichenko A. V. Balaban'yan V. Yu., Lyutik A. I., Shvets V. I.* Technologies and perspectives of liposomal drug application in clinical practice. *Nanotechnol. Russ*. 2017, 12 (7-8), 461–470. http://doi.org/10.1134/s1995078017040139
11. *Zhang J., Pan Y., Shi Q., Zhang G., Jiang L., Dong X., Gu K., Wang H., Zhang X., Yang N., Li Y., Xiong J., Yi T., Peng M., Song Y., Fan Y., Cui J., Chen G., Tan W., Zang A., Guo Q., Zhao G., Wang Z., He J., Yao W., Wu X., Chen K, Hu X., Hu C., Yue L., Jiang D., Wang G., Liu J., Yu G., Li J., Bai J., Xie W., Zhao W., Wu L., Zhou C.* Paclitaxel liposome for injection (Lipusu) plus cisplatin versus gemcitabine plus cisplatin in the first-line treatment of locally advanced or metastatic lung squamous cell carcinoma: A multicenter, randomized, open-label, parallel controlled clinical study. *Cancer Commun. (Lond)*. 2022, 42(1), 3–16. https://doi.org/10.1002/cac2.12225
12. *Seo B. J., Song E. T., Lee K., Kim J. W., Jeong C. G., Moon S. H., Son J. S., Kang S. H., Cho H. S., Jung B. Y., Kim W. I.* Evaluation of the broad-spectrum lytic capability of bacteriophage cocktails against various Salmonella serovars and their effects on weaned pigs infected with Salmonella Typhimurium. *J. Vet. Med. Sci*. 2018, 80(6), 851–860. https://doi.org/10.1292/jvms.17-0501
13. *Chang R. Y. K., Chen K., Wang J., Wallin M., Britton W., Morales S., Kutter E., Li J., Chan H. K.* Proof-of-principle study in a murine lung infection model of antipseudomonal activity of phage PEV20 in a dry-powder formulation. *Antimicrob. Agents Chemother*. 2018, 62(2), e01714-17. https://doi.org/10.1128/AAC.01714-17
14. *Nabil N. M., Tawakol M. M., Hassan H. M.* Assessing the impact of bacteriophages in the treatment of Salmonella in broiler chickens. *Infect. Ecol. Epidemiol*. 2018, 8(1), 1539056. https://doi.org/10.1080/20008686.2018.1539056
15. *Wright A., Hawkins C. H., Anggard E. E., Harper D. R.* A controlled clinical trial of a therapeutic bacteriophage preparation in chronic otitis due to antibiotic-resistant Pseudomonas aeruginosa; a preliminary report of efficacy. *Clin. Otolaryngol*. 2009, 34(4), 349–357. https://doi.org/10.1111/j.1749-4486.2009.01973.x
16. *Kortright K. E., Chan B. K., Koff J. L., Turner P. E.* Phage therapy: a renewed approach to combat antibiotic-resistant bacteria. *Cell Host Microbe*. 2019, 25(2), 219–232. https://doi.org/10.1016/j.chom.2019.01.014
17. *Aminov R., Caplin J., Nino C., Coffey A., Cooper I., De Vos D., Doskar J., Friman V-P., Kurtboke I., Pantucek R.* Application of bacteriophages. *Microbiol. Australia*. 2017, 38(2), 63-66.
18. *Cui H., Yuan L., Lin L.* Novel chitosan film embedded with liposome-encapsulated phage for biocontrol of *Escherichia coli* O157:H7 in beef. *Carbohydr. Polym*. 2017,

177, 156–164. https://doi.org/10.1016/j.carbpol.2017.08.137
19. *Gonzalez-Menendez E., Fernandez, L., Gutierrez D., Pando D., Martinez B., Rodríguez A., García P.* Strategies to encapsulate the Staphylococcus aureus bacteriophage phiIPLA-RODI. *Viruses*. 2018, 10(9), 495. https://doi.org/10.3390/v10090495
20. *Balasubramanian S., Sorokulova I. B., Vodyanoy V. J., Simonian A. L.* (2007). Lytic phage as a specific and selective probe for detection of Staphylococcus aureus--A surface plasmon resonance spectroscopic study. *Biosens. Bioelectron*. 2007, 22(6), 948–955. https://doi.org/10.1016/j.bios.2006.04.003
21. *Sorokulova I., Olsen E., Vodyanoy V.* Bacteriophage biosensors for antibiotic-resistant bacteria. *Expert Rev. Med. Devices*. 2014, 11(2), 175–186. https://doi.org/10.1586/17434440.2014.882767
22. *Pardo-Freire M., Domingo-Calap P.* Phages and nanotechnology: new insights against multidrug-resistant bacteria. *BioDesign Res*. 2023, 5. https://doi.org/10.34133/bdr.0004
23. *Briot T., Kolenda C., Ferry T., Medina M., Laurent F., Leboucher G., Pirot F.* Paving the way for phage therapy using novel drug delivery approaches. *J. Controlled Release. 2022*. 347, 414–424. https://doi.org/10.1016/j.jconrel.2022.05.021
24. *Azimi T., Mosadegh M., Nasiri M. J., Sabour S., Karimaei S., Nasser A.* Phage therapy as a renewed therapeutic approach to mycobacterial infections: a comprehensive review. *Infect. Drug Resist*. 2019, 12, 2943–2959. https://doi.org/10.2147/IDR.S218638
25. *Abedon S. T., Kuhl S. J., Blasdel B. G., Kutter E. M.* Phage treatment of human infections. *Bacteriophage*. 2011, 1(2), 66–85. https://doi.org/10.4161/bact.1.2.15845
26. *Wilson T., Papahadjopoulos D., Taber R.* Biological properties of poliovirus encapsulated in lipid vesicles: antibody resistance and infectivity in virus-resistant cells. *Proc. Natl. Acad. Sci. USA*. 1977, 74(8), 3471–3475. https://doi.org/10.1073/pnas.74.8.3471
27. *Faller D. V., Baltimore D.* Liposome encapsulation of retrovirus allows efficient superinfection of resistant cell lines. *J. Virol*. 1984, 49(1), 269–272. https://doi.org/10.1128/JVI.49.1.269-272.1984
28. *Mendez N., Herrera V., Zhang L., Hedjran F., Feuer R., Blair S. L., Trogler W. C., Reid T. R., Kummel A. C.* Encapsulation of adenovirus serotype 5 in anionic lecithin liposomes using a bead-based immunoprecipitation technique enhances transfection efficiency. *Biomaterials*. 2014, 35(35), 9554–9561. https://doi.org/10.1016/j.biomaterials.2014.08.010
29. *Wang Y., Huang H., Zou H., Tian X., Hu J., Qiu P., Hu H., Yan G.* Liposome encapsulation of oncolytic virus M1 to reduce immunogenicity and immune clearance in vivo. *Mol. Pharm*. 2019, 16(2), 779–785. https://doi.org/10.1021/acs.molpharmaceut.8b01046
30. *Rosner D., Clark J.* Formulations for bacteriophage therapy and the potential uses of immobilization. *Pharmaceuticals (Basel)*. 2021, 14(4), 359. https://doi.org/10.3390/ph14040359
31. *Loh B., Gondil V. S., Manohar P., Khan F. M., Yang H., Leptihn S.* Encapsulation and delivery of therapeutic phages. *Appl. Environ. Microbiol*. 2021, 87(5), e01979-20. https://doi.org/10.1128/AEM.01979-20
32. *Colom J., Cano-Sarabia M., Otero J., Cortes P., Maspoch D., Llagostera M.* Liposome-encapsulated bacteriophages for enhanced oral phage therapy against Salmonella spp. *Appl. Environ. Microbiol*. 2015, 81(14), 4841–4849. https://doi.org/10.1128/AEM.00812-15
33. *Cortes P., Cano-Sarabia M., Colom J., Otero J., Maspoch D., Llagostera M.* Nano/Micro formulations for bacteriophage delivery. *Methods Mol. Biol*. 2018, 1693, 271–283. https://doi.org/10.1007/978-1-4939-7395-8_20
34. *Dedrick R. M., Guerrero-Bustamante C. A., Garlena R. A., Russell D. A., Ford K., Harris K., Gilmour K. C., Soothill J., Jacobs-Sera D., Schooley R. T., Hatfull G. F., Spencer H.* Engineered bacteriophages for treatment of a patient with a disseminated drug-resistant Mycobacterium abscessus. *Nat. Med*. 2019, 25(5), 730–733. https://doi.org/10.1038/s41591-019-0437-z
35. *Zeynali Kelishomi F., Khanjani S., Fardsanei F., Saghi Sarabi H., Nikkhahi F., Dehghani B.* Bacteriophages of Mycobacterium tuberculosis, their diversity, and potential therapeutic uses: a review. *BMC Infect. Dis*. 2022, 22(1), 957. https://doi.org/10.1186/s12879-022-07944-9
36. *Nieth A., Verseux C., Barnert S., Süss R., Römer W.* A first step toward liposome-mediated intracellular bacteriophage therapy. *Expert Opin. Drug Deliv*. 2015, 12(9), 1411–1424. https://doi.org/10.1517/17425247.2015.1043125
37. *Avdeev V. V., Kuzin V. V., Vladimirsky M. A., Vasilieva I. A.* Experimental studies of the liposomal form of lytic mycobacteriophage D29 for the treatment of tuberculosis

infection. *Microorganisms*. 2023, 11(5), 1214. https://doi.org/10.3390/microorganisms11051214
38. *Vladimirsky M., Lapenkova M., Alyapkina Y., Vasilyeva I.* Efficiency of bacterial activity of liposomal Mycobacteria tuberculosis in the model of macrophages RAW264-7. *Europ. Respiratory J*. 2019, 54, PA4607 https://doi.org/10.1183/13993003.congress-2019.PA4607
39. *Lapenkova M. B., Alyapkina Y. S., Vladimirsky M. A.* (2020). Bactericidal Activity of Liposomal Form of Lytic Mycobacteriophage D29 in Cell Models of Tuberculosis Infection In Vitro. Bull. Exp. Biol. Med., 169(3), 361–364. https://doi.org/10.1007/s10517-020-04887-6
40. *Manohar P., Tamhankar A. J., Lundborg C. S., Nachimuthu R.* Therapeutic characterization and efficacy of bacteriophage cocktails infecting Escherichia coli, Klebsiella pneumoniae, and Enterobacter species. *Front. Microbiol*. 2019, 10, 574. https://doi.org/10.3389/fmicb.2019.00574
41. *Anand T., Virmani N., Kumar S., Mohanty A. K., Pavulraj S., Bera B. C., Vaid R. K., Ahlawat U., Tripathi B. N.* Phage therapy for treatment of virulent Klebsiella pneumoniae infection in a mouse model. *J. Glob. Antimicrob. Resist*. 2020, 21, 34–41. https://doi.org/10.1016/j.jgar.2019.09.018
42. *Hung C. H., Kuo C. F., Wang C. H., Wu C. M., Tsao N.* Experimental phage therapy in treating Klebsiella pneumoniae-mediated liver abscesses and bacteremia in mice. *Antimicrob. Agents Chemother*. 2011, 55(4), 1358–1365. https://doi.org/10.1128/AAC.01123-10
43. *Taha O. A., Connerton P. L., Connerton I. F., El-Shibiny A.* Bacteriophage ZCKP1: a potential treatment for Klebsiella pneumoniae isolated from diabetic foot patients. *Front. Microbial*. 2018, 9, 2127. https://doi.org/10.3389/fmicb.2018.02127
44. *Singla S., Harjai K., Katare O. P., Chhibber S.* Bacteriophage-loaded nanostructured lipid carrier: improved pharmacokinetics mediates effective resolution of Klebsiella pneumoniae-induced lobar pneumonia. *J. Infect. Dis*. 2015, 212(2), 325–334. https://doi.org/10.1093/infdis/jiv029
45. *Singla S., Harjai K., Raza K., Wadhwa S., Katare O. P., Chhibber S.* Phospholipid vesicles encapsulated bacteriophage: A novel approach to enhance phage biodistribution. *J. Viirol. Methods*. 2016, 236, 68–76. https://doi.org/10.1016/j.jviromet.2016.07.002
46. *Chadha P., Katare O. P., Chhibber S.* Liposome loaded phage cocktail: Enhanced therapeutic potential in resolving *Klebsiella pneumoniae* mediated burn wound infections. *Burns*. 2017, 43(7), 1532–1543. https://doi.org/10.1016/j.burns.2017.03.029
47. *Plumet L., Ahmad-Mansour N., Dunyach-Remy C., Kissa K., Sotto A., Lavigne J. P., Costechareyre D., Molle V.* Bacteriophage therapy for *Staphylococcus aureus* infections: a review of animal models, treatments, and clinical trials. *Front. Cell. Infect. Microb*. 2022, 12, 907314. https://doi.org/10.3389/fcimb.2022.907314
48. *Chhibber S., Kaur J., Kaur S.* Liposome entrapment of bacteriophages improves wound healing in a diabetic mouse MRSA infection. *Front. Microbiol*. 2018, 9, 561. https://doi.org/10.3389/fmicb.2018.00561
49. *Cinquerrui S., Mancuso F., Vladisavljević G. T., Bakker S. E., Malik D. J.* Nanoencapsulation of bacteriophages in liposomes prepared using microfluidic hydrodynamic flow focusing. *Front. Microbial*. 2018, 9, 2172. https://doi.org/10.3389/fmicb.2018.02172
50. *Torres Di Bello D., Narváez D. M., Groot de Restrepo H., Vives M. J.* Cytotoxic evaluation in HaCaT cells of the Pa.7 bacteriophage from Cutibacterium (Propionibacterium) acnes, free and encapsulated within liposomes. *Phage (New Rochelle)*. 2023, 4(1), 26–34. https://doi.org/10.1089/phage.2022.0038
51. *Malik D. J., Sokolov I. J.,Vinner G. K., Mancusi F., Cinquerrui S., Vladisavlevic G. T., Clokie M. R. J., Garton N. J., Stapley A. G. F., Kirpichnikova A.* Formulation, stasbilisation and encapsulation of bacteriophage for phage therapy. *Adv. Colloid Interface Sci*. 2017, 249, 100–133. https://doi.org/10.1016/j.cis.2017.05.014
52. *Kaur S., Kumari A., Kumari Negi A., Galav V., Thakur S., Agrawal M., Sharma, V.* Nanotechnology based approaches in phage therapy: overcoming the pharmacological barriers. *Front. Pharmacol*. 2021, 12, 699054. https://doi.org/10.3389/fphar.2021.699054
53. *Sarker S. A., Berger B., Deng Y., Kieser S., Foata F., Moine D., Descombes P., Sultana S., Huq S., Bardhan P. K., Vuillet V., Praplan F., Brüssow H.* Oral application of Escherichia coli bacteriophage: safety tests in healthy and diarrheal children from Bangladesh. *Environ. Microbial*. 2017, 19(1), 237–250. https://doi.org/10.1111/1462-2920.13574
54. *Otero J., García-Rodríguez A., Cano-Sarabia M., Maspoch D., Marcos R., Cortés P., Llagostera M.* Biodistribution of liposome-

encapsulated bacteriophages and their transcytosis during oral phage therapy. *Front. Microbiol*. 2019, 10, 689. https://doi.org/10.3389/fmicb.2019.00689
55. *Lin Y. W., Chang R. Y., Rao G. G., Jermain B., Han M. L., Zhao J. X., Chen K., Wang J. P., Barr J. J., Schooley R. T., Kutter E., Chan H. K., Li J.* Pharmacokinetics/pharmacodynamics of antipseudomonal bacteriophage therapy in rats: a proof-of-concept study. *Clin. Microbiol. Infect.* 2020, 26(9), 1229–1235. https://doi.org/10.1016/j.cmi.2020.04.039
56. *Lev K., Kunz Coyne A. J., Kebriaei R., Morrisette T., Stamper K., Holger D. J., Canfield G. S., Duerkop B. A., Arias C. A., Rybak M. J.* Evaluation of bacteriophage-antibiotic combination therapy for biofilm-embedded MDR Enterococcus faecium. *Antibiotics (Basel)*. 2022, 11(3), 392. https://doi.org/10.3390/antibiotics11030392
57. *Manohar P., Madurantakam Royam M., Loh B., Bozdogan B., Nachimuthu R., Leptihn S.* Synergistic effects of phage-antibiotic combinations against Citrobacter amalonaticus. *ACS Infect. Dis*. 2022, 8(1), 59–65. https://doi.org/10.1021/acsinfecdis.1c00117
58. *Patey O., McCallin S., Mazure H., Liddle M., Smithyman A., Dublanchet A.* Clinical indications and compassionate use of phage therapy: personal experience and literature review with a focus on osteoarticular infections. *Viruses*. 2018, 11(1), 18. https://doi.org/10.3390/v11010018
59. *Desgranges F., Bochud P. Y., Resch G.* Customised infectiology — Phage therapy: from theory to clinical evidence. *Rev. Med. Suisse*. 2019, 15(646), 771–775. (In French).
60. *Grigorieva G. S., Krasnopolsky Yu. M.* Liposomes per se pharmacotherapeutic status. *Pharmacol. Drug Toxicol.* 2020, 14(4), 264–271. https://doi.org/10.33250/14.04.264 (In Ukrainian).
61. *González-Menéndez E., Fernández L., Gutiérrez D., Rodríguez A., Martínez B., García P.* Comparative analysis of different preservation techniques for the storage of Staphylococcus phages aimed for the industrial development of phage-based antimicrobial products. *PloS One*. 2018, 13(10), e0205728. https://doi.org/10.1371/journal.pone.0205728
62. *Vandenheuvel D., Lavigne R., Brüssow H.* Bacteriophage therapy: advances in formulation strategies and human clinical trials. *Annu. Rev. Virol*. 2015, 2(1), 599–618. https://doi.org/10.1146/annurev-virology-100114-054915
63. *Malik D. J.* Bacteriophage encapsulation using spray drying for phage therapy. *Curr. Issues Mol. Biol*. 2021, 40, 303–316. https://doi.org/10.21775/cimb.040.303
64. *Leung S. S. Y., Morales S., Britton W., Kutter E., Chan H. K.* Microfluidic-assisted bacteriophage encapsulation into liposomes. *Int. J. Pharm*. 2018, 545(1-2), 176–182. https://doi.org/10.1016/j.ijpharm.2018.04.063
65. *Myelnikov D.* An alternative cure: the adoption and survival of bacteriophage therapy in the USSR, 1922-1955. *J. Hist. Med. Allied Sci*. 2018, 73(4), 385–411. https://doi.org/10.1093/jhmas/jry024
66. *Magar K. T., Boafo G. F., Li X. T., Chen Z. J., He W*. Liposome-based delivery of biological drugs. *Chin. Chem. Lett*. 2022, 33(2), 587–596. https://doi.org/10.1016/j.cclet.2021.08.020
67. *Strathdee S. A., Hatfull G. F., Mutalik V. K., Schooley R. T*. Phage therapy: From biological mechanisms to future directions. *Cell*. 2023, 186(1), 17–31. https://doi.org/10.1016/j.cell.2022.11.017
68. *Chhibber S., Kaur J., Kaur S.* Liposome entrapment of bacteriophages improves wound healing in a diabetic mouse MRSA infection. *Front. Microbiol*. 2018, 9, 561. https://doi.org/10.3389/fmicb.2018.00561
69. *Diacon A. H., Guerrero-Bustamante C. A., Rosenkranz B., Rubio Pomar F. J., Vanker N., Hatfull G. F.* Mycobacteriophages to treat tuberculosis: dream or delusion?. *Respiration*. 2022, 101(1), 1–15. https://doi.org/10.1159/000519870
70. *Stachurska X., Cendrowski K., Pachnowska K., Piegat A., Mijowska E., Nawrotek P.* Nanoparticles influence lytic phage T4-like performance in vitro. *Int. J. Mol. Sci*. 2022, 23(13), 7179. https://doi.org/10.3390/ijms23137179

ПЕРСПЕКТИВИ СТВОРЕННЯ ЛІПОСОМАЛЬНИХ АНТИМІКРОБНИХ ПРЕПАРАТІВ НА ОСНОВІ ФАГІВ

Пилипенко Д. М.[1], *Григор'єва Г. С.*[2], *Краснопольський Ю. М.*[3]

[1] Державний біотехнологічний університет, Харків,Україна
[2] Державна установа «Інститут фармакології та токсикології Національної академії медичних наук України»
[3] Національний технічний університет «Харківський політехнічний інститут», Україна

E-mail: pdmforwork@gmail.com

Поява великої кількості патогенних мікроорганізмів, резистентних до відомих антибіотиків, вказує на необхідність пошуку нових стратегій боротьби з ними.

Мета. Стаття присвячена аналізу сучасних досліджень ліпосомальних форм фагів як перспективної стратегії боротьби з мікробними інфекціями.

Методи. Аналіз сучасної вітчизняних та іноземних досліджень, присвячених інкапсуляції бактеріофагів у ліпосоми та оцінці ефективності цієї системи доставлення ліків у протимікробній терапії.

Результати. Інкапсуляція бактеріофагів у ліпосомальні наночастинки захищає фаги від негативного впливу зовнішніх факторів, збільшує період циркуляції в організмі, забезпечує підвищену біодоступність фагових частинок і, як наслідок, підвищує ефективність протимікробного лікування. Ліпосомальні форми фагів продемонстрували свою ефективність у боротьбі з багатьма поширеними патогенними бактеріями, зокрема *Staphylococcus aureus*, *Klebsiella pneumoniae*, *Mycobacterium tuberculosis*, *Salmonella* та ін.

Висновки. Ліпосомальні фаги мають перспективи як протимікробні препарати, проте для широкого застосування у клінічній практиці потребують проведення доклінічних та клінічних досліджень для підтвердження їхньої ефективності та безпечності.

Ключові слова: нанобіотехнологія; система доставлення ліків; ліпосома; бактеріофаг; фагова терапія; антимікробний препарат.

EXPERIMENTAL ARTICLES

UDC 616.091:576.31

https://doi.org/10.15407/biotech16.04.034

KAN0438757: A NOVEL PFKFB3 INHIBITOR THAT INDUCES PROGRAMMED CELL DEATH AND SUPPRESSES CELL MIGRATION IN NON-SMALL CELL LUNG CARCINOMA CELLS

Deniz Özdemir
Seher Saruhan
Can Ali Agca

Department of Molecular Biology and Genetics of the Bingol University,TÜRKİYE

E-mail: c.aliagca@gmail.com

Received 2023/09/15
Revised 2023/10/10
Accepted 2023/10/31

Aim. PFKFB3 is glycolytic activator that overexpressed in human lung cancer and plays a crucial role in multiple cellular functions including programmed cell death. Despite the many small molecules described as PFKFB3 inhibitors, some of them have shown disappointing results *in vitro* and *in vivo*. On the other hand KAN0438757, selective and potent, small molecule inhibitor has been developed. However, the effects of KAN0438757, in non-small cell lung carcinoma cells remain unknown. Herein, we sought to decipher the effect of KAN0438757 on proliferation, migration, DNA damage, and programmed cell death in non-small cell lung carcinoma cells

Methods. The effects of KAN0438757 on cell viability, proliferation, DNA damage, migration, apoptosis, and autophagy in non-small cell lung carcinoma cells were tested by WST-1, real-time cell analysis, comet assay, wound-healing migration test, and MMP/JC-1 and AO/ER dual staining assays as well as western blot analysis.

Results. Our results revealed that KAN0438757 significantly suppressed the viability and proliferation of A549 and H1299 cells and inhibited migration of A549 cells. More importantly, KAN0438757 caused DNA damage and triggered apoptosis and this was accompanied by the up-regulation of cleaved PARP in A549 cells. Furthermore, treatment with KAN0438757 resulted in increased LC3 II and Beclin1, which indicated that KAN0438757 stimulated autophagy.

Conclusions. Overall, targeting PFKFB3 with KAN0438757 may be a promising effective treatment approach, requiring further *in vitro* and *in vivo* evaluation of KAN0438757 as a therapy in non-small cell lung carcinoma cells.

Key words: PFKFB3; KAN0438757; Apoptosis; Autophagy; Lung Cancer.

Transformed cells more than non-transformed cells exert heavy demands on glycolysis to support their increased energy consumption owing to their rapid rates of cell division. The glycolysis pathway is the basic enzymatic process in cell metabolism. However, under limited oxygen, normal cells respond physiologically by increasing glycolysis. The dysregulation of glucose metabolism is one of the hallmarks of cancer cells. High glucose consumption by tumors was first reported by Warburg in the 1920s and later suggested that cancer cells exhibit a respiratory disorder [1, 2]. Cancer cells choose the aerobic glycolysis (known as "Warburg" effect), which is an efficient way of rapidly synthesizing nucleotides, amino acids and lipids required to form biomass [3] 6-phosphofructo-2-kinase/fructose-2, 6-bisphosphatases (PFKFBs) are enzyme family, best known for its role in the glycolysis. PFKFBs enzyme family consists of four homologs are encoded by separate genes: PFKFB1, PFKFB2, PFKFB3, and PFKFB4 [4]. Among these members, the

PFKFB3 enzyme exhibit kinase activity higher than phosphatase activity, has the highest Kinase/Biphosphatase activity ratio (740-fold) expressed by PFKFBs [5]. The essential activity of PFKFB3 is to catalyze the synthesis of fructose-2,6-bisphosphate (F2,6BP), which subsequently activates phosphofructokinase-1 (PFK-1) that enables upregulating of the glycolytic flux [6]. Previous findings indicated that PFKFB3 can be regulated by several tumor-related genes, including phosphatase and tensin homolog (PTEN) [7], mitogen activated protein kinase (MAPK) [8], phosphoinositide 3-kinases (PI3K) [9], and hypoxia-inducible factor 1-alpha (HIF-1a) [10], in cancer cell lines. However, in spite of this abundance of potential targets in glycolytic flux, PFKFB3, has received considerable attention. In recent years, potent and selective PFKFB3 inhibitors have been identified and investigated as potential anticancer agents. 3PO (3-(3-pyridinyl)-1-(4-pyridinyl)-2-propen-1-one), a chalcone group, is the first small-molecule inhibitor of PFKFB3 in this class to be evaluated *in vitro* and human-derived tumor studies. 3PO has demonstrated impressive single-agent activity via prohibit tumorigenic growth of breast, leukemia, and lung adenocarcinoma cells [11]. Moreover, it exhibits synergistic activity when administered in combination with a multi-kinase inhibitor Sunitinib L-malate in preclinical studies in Human endothelial cells (HUVECs) [12]. On the other hand, PFK15, also a potent and selective PFKFB3 inhibitor, displayed a more (aprx.100-fold) potent effect than 3PO in preclinical studies [13]. PFK15 inhibit cell migration and invasion in HNSCC cell culture and block the metastasis to lung in the xenograft mice models [14]. PFK158, an PFK15-based synthetic inhibitor assessed through active phase I clinical trials, exhibits a high affinity to the ATP binding site and elicits a significant antitumor effect on lung, glioblastoma, melanoma, pancreatic, and colon cancer. In more recent study, Gustafsson et al. revealed that RNAi or pharmacological inhibition of PFKFB3 is involved in DNA damage response and deoxynucleotide incorporation upon DNA repair. In addition, the results showed that PFKFB3 inhibition plays a critical role in homologous recombination and defective nucleotide incorporation. KAN0438757 is a newly developed small molecule inhibitor of PFKFB3 that impairs DNA repair by disrupting deoxynucleotide incorporation and inhibits survival of transformed cells [15]. Previous studies have found that PFKFB3 expression is increased significantly in some cancers [16] including lung cancer; however, whether KAN0438757, a novel and specific small molecule inhibitor of PFKFB3, has anti-neoplastic activity on lung cancer is unknown. Since lung cancer is very resistant to chemotherapy, and PFKFB3 has been shown to crucial effects on its survival, the objective of the study was to reveal the potential therapeutic role of KAN0438757 by targeting PFKFB3.

In this study, we found that the pharmacological inhibition of PFKFB3 It also arrested the migration and induced DNA damage and apoptosis *in vitro*. Furthermore, KAN0438757 disrupted Mitochondrial Membrane Potential (MMP) and induced Autophagy biomarkers; LC3 and Beclin1. Overall, KAN0438757 treatment may be a novel approach to suppressing Lung cancer.

Materials and Methods

Main reagents, Antibodies, and KAN0438757

Protease-phosphatase inhibitor cocktail, trypan blue, Tris HCl, trypsin-EDTA, dimethyl sulfoxide (DMSO), TEMED, Sodium azide (NaN3), luminol, Skim milk powder, P-coumaric acid, bovine serum albumin (BSA) and others was obtained from Sigma Aldrich company. Dulbecco's modified Eagle's medium (DMEM) fetal bovine serum (FBS), penicillin/streptomycin, and phosphate buffered saline (PBS) were purchased from Gibco. WST-1 assay was obtained from Boster (USA). Mouse anti-GAPDH, p62, Beclin 1, LC3, PARP antibodies used in Western blot studies were obtained from SantaCruz Biotechnology (USA), and Anti-mouse antibody horseradish peroxidase conjugated was obtained from Invitrogen (USA).

PFKFB3 inhibitor KAN0438757 (Cat No: S0400) was purchased from Selleck Chemicals GmbH (Houston, TX 77014 USA). It was dissolved in sterile dimethyl sulfoxide (DMSO, sterile-filtered, suitable for cell culture) at a final concentration of 1 mM, and then stored in aliquots at –80 °C and working concentrations were diluted in culture medium.

Cell Lines and Culture Conditions

All cell lines used (A549, H1299, and COS7) were provided by ATCC (American Type Culture Collection, Manassas, USA). A549 and COS7 were maintained in DMEM (Dulbecco's modified Eagle's medium containing with 10%

fetal bovine serum (FBS) and 1% penicillin-streptomycin (Gibco, Grand Island, NY, USA). H1299 cells were cultured in RPMI (Roswell Park Memorial Institute) 1640 medium added with 10% FBS and 1% penicillin-streptomycin. Cell lines used in this study were grown by culturing at 37 ˚C, 95% humidity and 5–6% CO_2.

Cell Viability

The viability of A549, H1299, and COS7 cells was assessed with the WST-1 assay kit (Boster, USA). Briefly, the cells were treated with KAN0438757 at concentrations of 1, 5, 10, 25, 50, and 100 µM) and time point (24, 48, 72h). Then, 10µl WST-1 solution was added into the wells. The plates were kept out of light and incubated in a 37 °C CO_2 (5%) incubator for 3h. After that, it was measured spectrophotometrically at 420–480 nm using an ELISA microplate reader (Spectra Max 384 Plus).

Real-Time Cell Analysis (RCTA)

A549 and H1299 cells (1.5×10^4 cells/well) and A549 cells (1×10^4 cells/well) were plated into the E-Plate16 and then incubated in xCELLigence RTCA instrument (ACEA Bioscience, CA, USA) at 37 °C and %5 CO_2. E-16 plates have microelectrodes to measure the cellular impedance which was recorded every 15 min for 96 h by xCELLigence RTCA. After attaching them to the plate, the cells were given different doses of KAN0438757 and then incubated for 48 hours. Recorded data were analyzed by RTCA Software (v1.2, ACEA Biosciences Inc.).

Single Cell Gel Electrophoresis (Comet Assay)

A549 cells were seeded in 6-well plates (2×10^5) and treated with incubated with indicated doses of KAN0438757 for 48 h. At the end of the incubation, the wells were washed with PBS and the cells were dissociated using trypsin. The cells were then centrifuged and re-suspended with PBS and mixed with 0.5% low melting point agarose (LMA). After taking 20 µl of this mixture, it was spread on a slide covered with normal melting point agarose (NMA) and the agarose was frozen at 4 °C by covering the coverslip for 45 minutes. Coverslips were removed and placed in cold lysis solution (2.5M NaCl, 100mM EDTA, 10 mM Tris, 10% DMSO, 1% Triton X-100, (pH 10)) at 4 °C for 60 min. Slides were rinsed with PBS and placed in a buffer-filled gel electrophoresis. Electrophoresis was performed at 28V, 300 mA for 25 minutes and slides were neutralized with solution (pH 7.5) and rinsed with PBS. Slides were stained with Ethidium bromide (10 µg/mL) for 15 minutes and viewed under a fluorescent microscope. Opencomet program was used for analysis.

Wound-Healing Assay

Cells were seeded in 6-well cell culture dishes at 25×10^4 in each well. After the cells adhered to the surface, the cells were scraped to form a straight line with the help of a 20 µl pipette tip. Each well was washed twice with PBS so that the removed cells would not re-adhere to the surface. Wound areas were observed with an inverted microscope and photographed at 0, 24, and 48 hour time periods [17].

Acridine Orange And Ethidium Bromide double staining

Acridine orange and Ethidium bromide (EtBr/AO) staining was performed according to the protocol described previously [18]. A549 cells were treated with the indicated doses of KAN0438757 and then EtBr/AO(1:1) and added to the wells for 15 minutes at room temperature. Stained cells were observed with a fluorescence microscope (Olympus, Japan).

Mitochondrial membrane potential ($\Delta\Psi m$) Assay

Monolayers cells in the logarithmic growth stage were inoculated into glass-bottom culture plates at 2×10^5 cells per well. Then, cells were treated with KAN0438757 for 48 h. Slides were then washed and stained with the cationic dye JC-1 (5 mg/mL) for 15 min at 37 ℃. The stained cells were analyzed by fluorescence microscope (Olympus, Japan). After staining, seven areas per well were randomly captured by the microscope. Each experiment was repeated at least three times.

Cell lysate preparation and Western Blot Analysis

Cells were collected with a plastic scraper by washing three times with cold PBS after 48 hours of treatment and transferred to numbered microcentrifuge tubes. After centrifugation at 6600 rpm for 10 minutes, it was dissolved in lysis (RIPA) buffer and then incubated on ice for 60 minutes. After the incubation period, it was centrifuged for 10 minutes at 14,000 rpm at 4 °C. Protein content in the supernatants was measured by their absorbance at 595 nm in the spectrophotometer using BSA as a

standard. (Biomethod-GBC (Bradford)). With the help of electrophoresis system (Bio-RadTrans-Blot cell, BioRad, USA), protein samples and marker were fractionated on SDS-PAGE (10–12%) gel. Then, the proteins separated in the gel were transferred to Polyvinylidenedifluoride (PVDF) membrane. Blockage was made with BSA. The membrane was incubated overnight with primary antibodies first and then with secondary antibodies. Subsequently, washing was done with TBS-T. The results were determined by chemiluminescence method so that the membranes were visualized by X-Ray device.

Statistical Analysis

A statistical analysis were performed using the GraphPad Prism 8.0.2 software (USA). Data were obtained from three separate experiments. The multiple comparison Post-Hoc Tests in "One-way ANOVA" method or independent two-sample Student's t-test were performed. $P < 0.05$ was accepted as significant in the analyzes.

Results and Discussion

The PFKFB3 inhibitor KAN0438757 effectively blocked the proliferation of non-small cell lung carcinoma cells

Colorimetric assay (WST-1 based) and Real-Time Cell Analysis (RCTA) was carried out to investigate the effect of KAN0438757 on cell viability and the proliferation of cell lines. The Non-small cell lung cancer cell lines (NSCLC H1299 and A549) or COS7 were treated with increasing concentrations of KAN0438757 (0, 5, 10, 25, 50 and 100 μM). The WST-1 results showed that KAN0438757 inhibited cell viability in a dose-time dependent manner (supplementary data, 24/48/72 h) when compared to untreated control and the cell viability of the A549 and H1299 cell lines with KAN0438757 for 48 h were shown in Fig. 1, *A* and *B*. The IC50s of A549 for KAN0438757 was pronouncedly lower (35.2 μM) than that of H1299 (52.4 μM) for 48h. RCTA was performed to further confirm the effect of KAN0438757 on the inhibition of lung cancer cells proliferation for 48 h. The RCTA results of A549 cells (Fig. 1, *D*) further proved that

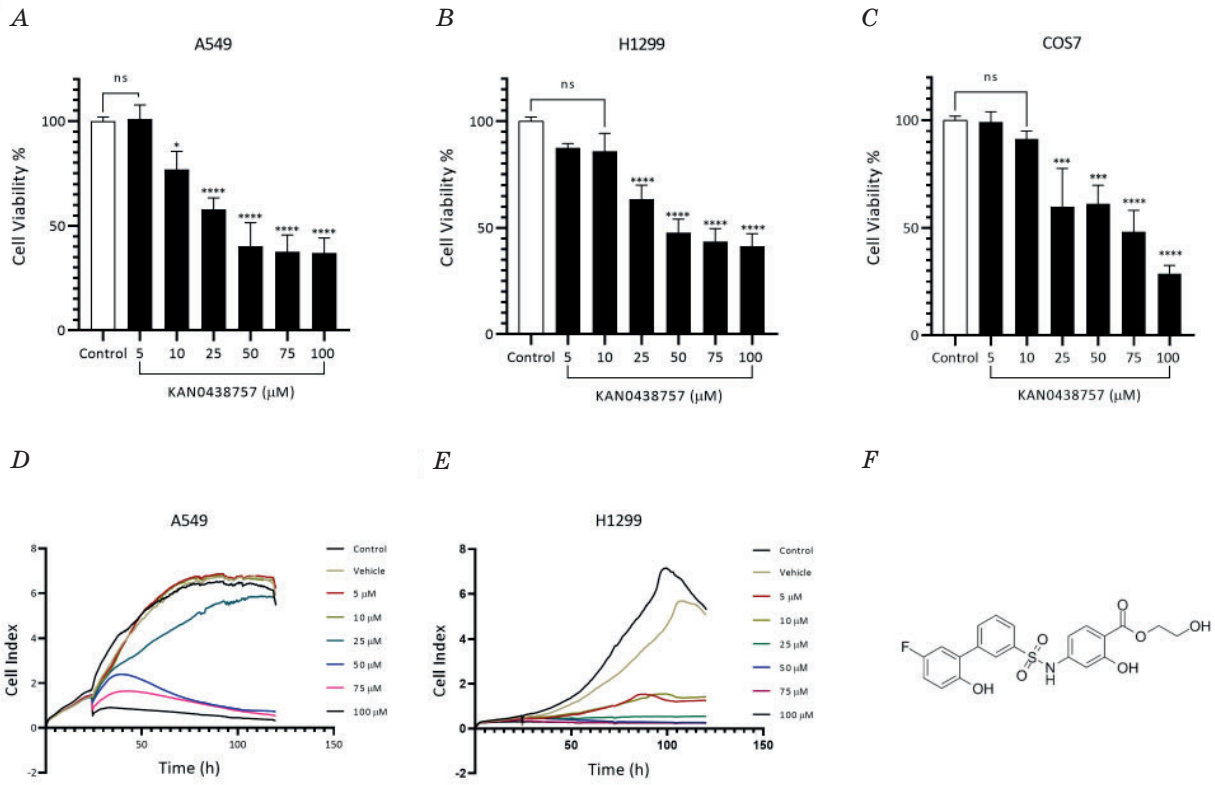

Fig. 1. **KAN0438757 inhibits the proliferation and viability of human non-small cell lung carcinoma cell:**
A, *B* and *C* — A549, H1299 and COS7 cells were treated with KAN0438757 (0, 5, 10, 25, 50, and 100 μM) for 48 h, and cell viability was examined using WST-1 assays;
D and *E* — A549 and H1299 were seeded in the xCELLigence system plate for 24 h and were then exposed to increasing concentrations of KAN0438757 for 120 h; *F* —the chemical structure of KAN0438757

KAN0438757 had a stronger antiproliferative activity. Similar results also observed in H1299 cells (Fig. 1, *E*).

KAN0438757 stimulate DNA damage

In order to investigate the effects of KAN0438757 on DNA damage, the Comet Assay was performed in A549 cell line using alkaline single-cell gel electrophoresis (Fig. 2). Almost all of comets in the control and 5, 10 μM -treated cells showed no fluorescent tails, which indicates that the nuclear DNA was intact. In contrast, the exposure of the cells to 25 and 50 μM concentrations of KAN0438757 for increased the number of typical comets with tails of different fluorescence intensities, which is an evident indicator of DNA strand breakage (Fig. 2, *A*). The values of the% tail DNA, the tail length, were significantly increased in the KAN0438757 treated groups compared with the control group (Fig. 2, *B*, *C*). These results suggest that KAN0438757 can induce DNA damage in A549 cells.

KAN0438757 inhibits migration of A549 lung cancer cells

Furthermore, having established that a low dose of KAN0438757 has no effect on cell viability, we used a wound-healing assay in order to investigate whether these concentrations affect cell migration in the A549 cell line. The data showed that a low concentration of KAN0438757 (less than 25 μM) effectively inhibited the cell migration (Fig. 3, *A*). The distance was found to be wide in A549 cells treated with KAN0438757 compared with the control (Fig. 3, *A*), indicating that KAN0438757 effectively inhibits cell migration ability in A549 cells (Fig. 3, *B*).

AO/EB double-staining in KAN0438757 treated-lung adenocarcinoma cells

After treatment with KAN0438757 inhibitors for 48 h, apoptotic cell death was determined by using Double-Staining with Acridine Orange-Ethidium Bromide on A549 lung cancer cells. As shown Fig.4, *A*, in the untreated control group, the green color labeled cells were visible. On the other hand, KAN0438757 treated groups, the intensity of the orange color also increased, illustrating a higher rate of apoptosis, which had the highest number of apoptotic cells in the 25 μM group.

PFKFB3 inhibitor KAN0438757 triggers mitochondrial membran instability in A549 cells

The mitochondrial membrane potential (ΔΨm) is crucial for mitochondrial homeostasis which is a fundamentally important determinant of cell predestination.

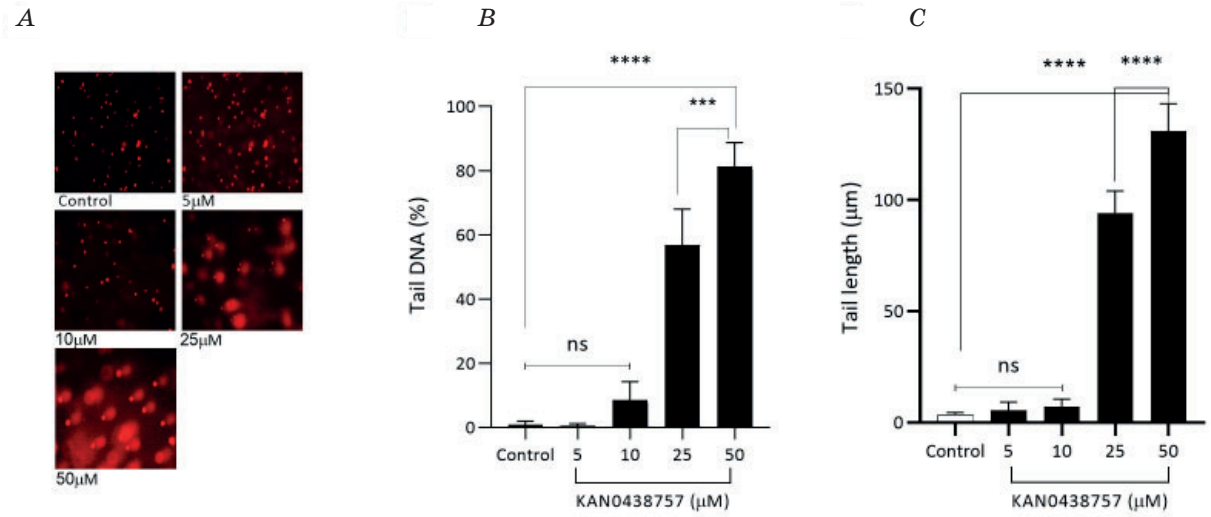

Fig. 2. **Single-cell gel electrophoresis for effects of KAN0438757 on DNA damage in A549 cells**
DNA damage was detected by the alkaline single-cell gel electrophoresis in A549 cells exposed to KAN0438757 at 5, 10, 25, 50 μM for 48h. DNA fragments were stained with Ethidium bromide (20 μg/mL) for 10 minutes and images (*A*) obtained under a fluorescent microscope. Opencomet program was used for analysis; *B* — Tail DNA; *C* — Tail length

To investigate whether KAN0438757 induces A549 cell mitochondrial membrane instability, we used JC-1 staining which is the cationic dye; red-colored cells indicate healthy mitochondria while green-colored indicate loss of mitochondrial membrane potential. As depicted in Fig. 4, *B*, with increasing the KAN0438757 concentration, the intensity of green color also increased, indicating a higher rate of loss of mitochondrial membrane potential in A549 cells. Furthermore, the results showed a significant positive correlation between the loss of mitochondrial membrane potential and the KAN0438757 concentration indicating that KAN0438757 triggers mitochondrial membrane instability.

KAN0438757 induces autophagy in lung adenocarcinoma cell

To further assess whether KAN0438757 affects autophagy, which are key events that maintains cellular homeostasis. To investigate the underlying mechanism of autophagy induced by KAN0438757, the expression of p62/SQSTM1, LC3 I-II, and Beclin1 was measured by western blotting. Results showed that KAN0438757 in A549 cells did not change the protein expression level of p62/SQSTM1. As shown in Fig. 4, *D*, the protein expression of LC3 I was down-regulated and LC3 II was up-regulated in A549 cell line. Besides, KAN0438757 treatment increased the Beclin1 protein expression level. Collectively, these findings indicated that KAN0438757 treatment could induce autophagy in A549 cells.

PFKFB3 is a member of a the bifunctional enzyme family of 4 such proteins of which are known a rate-limiting enzyme and essential control point in the glycolytic pathway. Beyond its glycolytic activities, PFKFB3 is involved in numerous biological processes such as promoting cell cycle progression [13], inhibiting apoptosis [19], stimulating migration/invasion [29] and having a critical factor for homologous recombination [15]. Previous studies have revealed that PFKFB3 expression is increased significantly both non-small cell lung cancer (NSCLC) [16] and small-cell lung cancer (SCLC) [20]. It identified that PFKFB3 has a crucial role in homologous recombination and developed a selective PFKFB3 small molecule inhibitor-KAN0438757 [15]. However, to the best of our knowledge, there is currently no study available that describes the effects of KAN0438757 on lung cancer. Moreover, the properties of KAN0438757 regarding anti-neoplastic and induction of programmed cell death and the underlying mechanism(s) in lung cancer cells are unclear. Therefore, we assessed the effect of KAN0438757 in human lung cancer and normal cells.

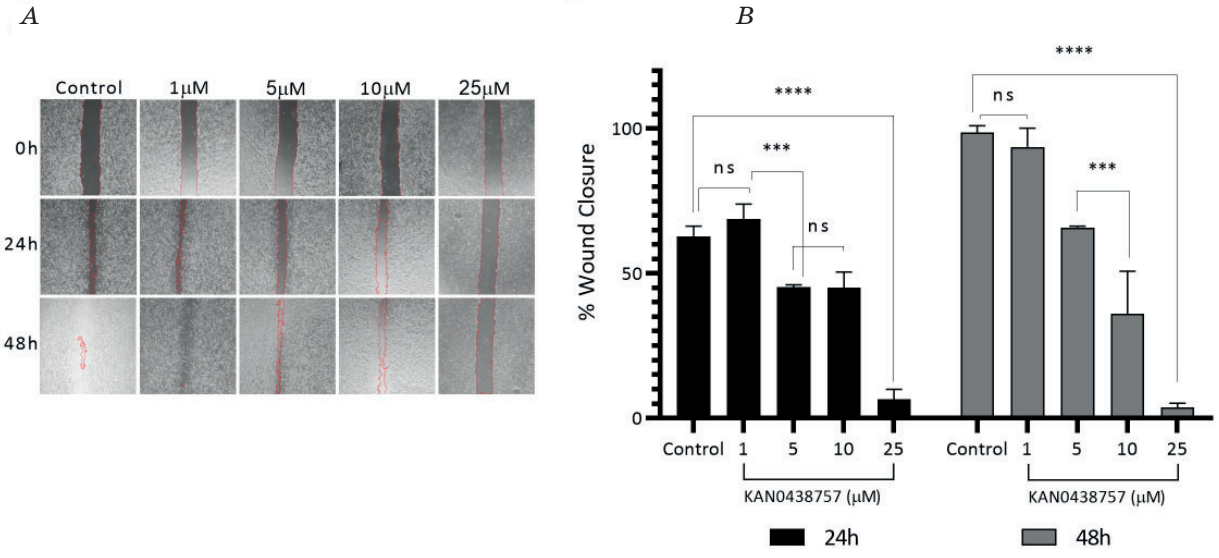

Fig. 3. **KAN0438757 inhibits cell migration**
The A549 cells were treated with KAN0438757 (1–25 μM) for 48 h, and the migration of cells was determined by the wound-healing assay:
A — Microscopic images of A549 cells after different treatments of KAN0438757; *B* — Wound closure. All results are representative of three separate experiments, and representative results are shown

In this study, we investigated the potential anti-neoplastic effect of KAN0438757 in lung cancer cell lines, and the possible mechanisms for it by determining cell viability, cell proliferation, DNA damage, and cell migration, the morphological analysis of apoptosis, apoptosis, and autophagy protein expression.

Firstly, the anti-proliferative effects of KAN0438757 were analyzed on A549 and H1299 cells. Similar to previous research [21], our results demonstrated that KAN0438757 effectively reduced cell viability and inhibited the growth of A549 and H1299 lung cancer cells.

A small molecule inhibitor were reported inhibition of PFKFB3 could lead to DNA

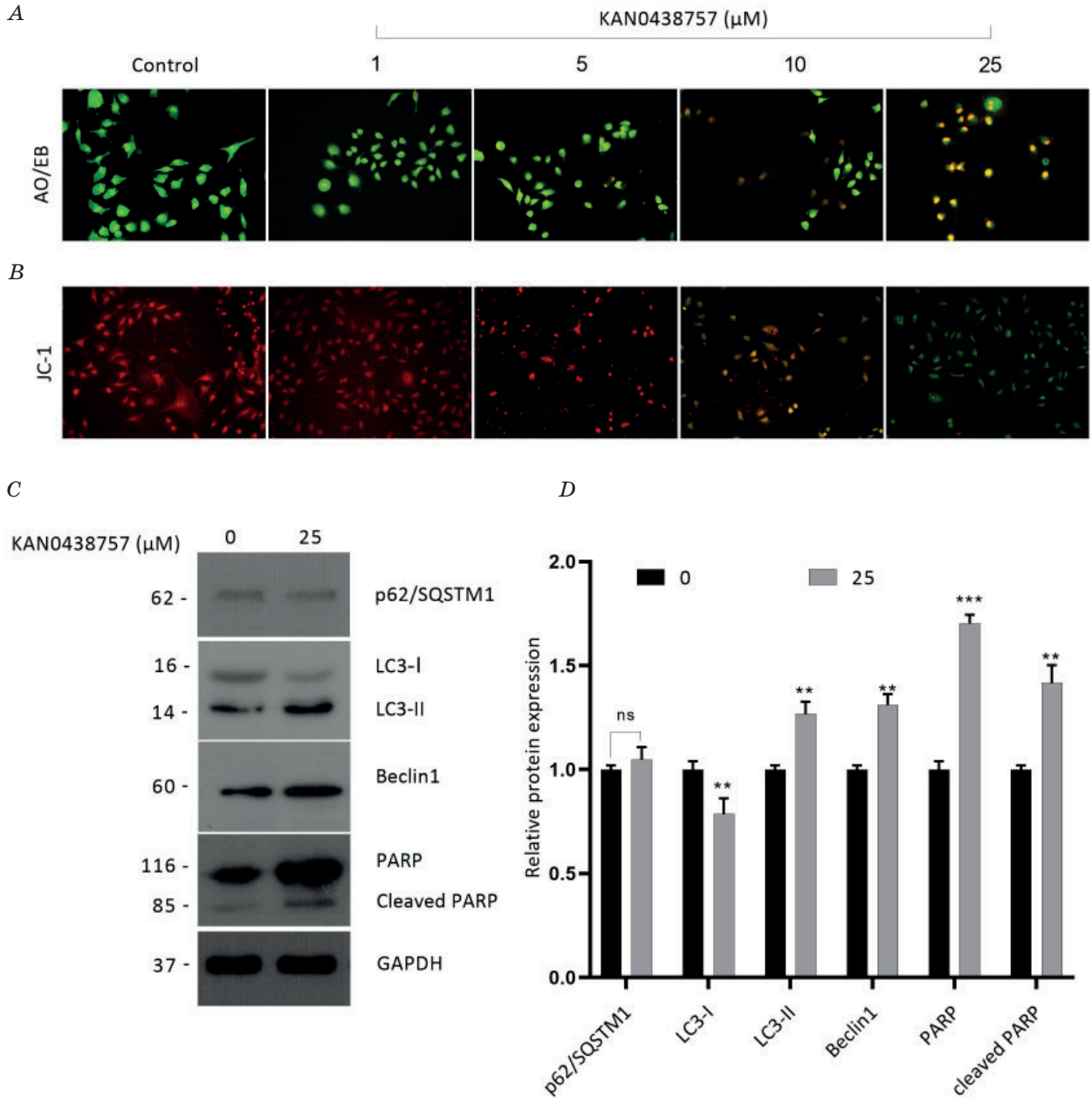

Fig. 4. **KAN0438757 induce apoptosis and causes the activation of autophagy-related markers in A549 lung cancer cells**

Representative fluorescence inverted microscopic images of AO/EB (*A*) and Δψm labeled with JC-1 (*B*). Expression of p62/SQSTM1, LC3 I-II, Beclin1, PARP, and GAPDH were examined by Western Blotting analysis (C–D). The experiment was repeated at least 3 times.
$n = 3$, $^{*}P < 0.05$ and $^{**}P < 0.01$ compared with that of control

damage and cell death. PFK15, a PFKFB3 inhibitor, cause DNA damage impairing DNA repair through AKT in HCC cells [22]. In this study, a comet assay quantitatively detected KAN0438757-induced DNA damage in A549 cells. In line with previous reports, our results showed that the Tail DNA and Tail length of the KAN0438757 treatment groups (25 and 50 μM) were higher than those of the other groups, indicating more severe DNA damage. These results indicated that KAN0438757 triggered DNA damage at the single-cell level, which may lead to apoptosis in lung cancer cell line.

The disruption of mitochondrial membrane potential (Δψm) can lead to the activation of the caspase cascade including caspase-9 and caspase-3 is activated, which are crucial effectors of apoptosis [25]. Once the caspase-3 is activated, the downstream effector proteins are cleaved such as PARP, which plays essential roles in DNA repair and the programmed cell death process [26]. In the current study, it was observed that treatment with KAN0438757 induced cleavage of PARP. In addition, KAN0438757 treatment of A549 cells significantly increased the red fluorescence intensity, indicating loss of Δψm, which is an early event in the apoptotic process. Furthermore, our AO/EB dual staining data confirmed that KAN0438757 treatment increased the apoptosis at 10 and 25 μM dose of KAN0438757. These results are consistence with the former results that either siRNA silencing [19] or the pharmacological inhibition of PFKFB3 [27] induces cell apoptosis. All the results discussed above directly suggest that KAN0438757 induces A549 cell apoptosis via mitochondria-mediated pathway.

PFKFB3 also plays a role in angiogenesis and metastasis, which can indirectly promote tumor growth [28]. Previous *in vivo* and *in vitro* studies have indicated that PFKFB3 is involved in the migration in nasopharyngeal carcinoma [29], breast cancer [28], non-small-cell lung cancer [16], gastric cancer[30], and osteosarcoma Saos-2 cells [31]. In the present study, KAN0438757 was applied as an PFKFB3 inhibitor in lung cancer cell line. The results indicated that KAN0438757 significantly blocked migration of A549 cells. This result was in accordance with previous reports, where KAN0438757 was observed to reduced the migration capabilities of HCT-116 and HT-29 cell line, as well as HUVECs cells [21].

Autophagy may play different roles not only in the degradation of macromolecules and damaged organelles, but also in different steps of tumor development. It may play a role in inhibiting proliferation and metastasis of cancer cells during tumorigenesis by autophagic activity. On the other hand, as a pro-survival mechanism, cancer cells initiate autophagy by breaking down intracellular organelles and proteins, thus providing the most important energy support of cancer cells [32, 33]. Previous *in vitro* experiments showed that either knockdown of PFKFB3 or pharmacological inhibition, including PFK158, and 3-PO, participated in autophagic flux and markers of autophagy induction [34, 35]. Knockdown of PFKFB3 resulted in the degradation of p62/SQSTM1. Meanwhile, PFKFB3 siRNA transfection, led to a significant increase LC3-II which involved in the assembly of autophagosomes in the inner and outer membrane [35]. Indeed, we found that the inhibiting of PFKFB3 after KAN0438757 treatment is positively connected with autophagy in A549 cells. Western blotting results revealed that the protein expression LC3 II and Beclin1 were significantly increased in the KAN0438757 treatment, while the expression of p62/SQSTM1 was not significantly increased in A549, suggesting that the KAN0438757 treatment promotes autophagy. Accumulating evidence has shown that autophagy can promote cell survival and maintenance of cellular homeostasis by degrading damaged organelles and macromolecules in cells, but it should not be overlooked that autophagy can also promote cell death due to its tight association with apoptosis [36]. In conjunction with analysis of AO/EB, Δψm, and western blotting demonstrated that KAN0438757 treatment (25 μM, 48 h) induced cell death.

Conclusions

KAN0438757 may hold great promise as a novel small molecules agent for lung cancer treatment. Further investigation is needed to validate the contribution of KAN0438757 to lung cancer therapy *in vitro* and *in vivo*.

Declaration of competing interest

Authors have no conflict of interest.

Acknowledgment

This study was supported by BUBAP (Grant Numbers: BAP-FEF.2021.004 and BAP-FEF.2021.005). Deniz Özdemir and Seher Saruhan are equal contributors to this work.

REFERENCES

1. *WARBURG O.* On the origin of cancer cells. Science. New York, 1956, 123(3191), 309–314. https://doi.org/10.1126/science.123.3191.309
2. *Koppenol W. H., Bounds P. L, Dang C. V.* Otto Warburg's contributions to current concepts of cancer metabolism. Nature Reviews Cancer. 2011, 11(5), 325–337. https://doi.org/10.1038/nrc3038
3. *Boroughs L. K., Deberardinis R. J.* Nisan 30. Metabolic pathways promoting cancer cell survival and growth. Nature Cell Biology Nature Publishing Group. 2015. https://doi.org/10.1038/ncb3124
4. *Lu L., Chen Y., Zhu Y., Lu L., Chen Y., Zhu Y.* The molecular basis of targeting PFKFB3 as a therapeutic strategy against cancer. Oncotarget 2017, 8(37), 62793–62802. https://doi.org/10.18632/oncotarget.19513
5. *Chesney J., Telang S., Yalcin A., Clem A., Wallis N., Bucala R.* Targeted disruption of inducible 6-phosphofructo-2-kinase results in embryonic lethality. Biochemical and Biophysical Research Communications. 2005, 331(1), 139–146. https://doi.org/10.1016/j.bbrc.2005.02.193
6. *Yalcin Abdullah, Telang S., Clem B., Chesney J.* Regulation of glucose metabolism by 6-phosphofructo-2-kinase/fructose-2,6-bisphosphatases in cancer. Experimental and Molecular Pathology. 2009, 86(3), 174–179. https://doi.org/10.1016/j.yexmp.2009.01.003
7. *Cordero-Espinoza L., Hagen T.* Increased Concentrations of Fructose 2,6-Bisphosphate Contribute to the Warburg Effect in Phosphatase and Tensin Homolog (PTEN)-deficient Cells. Journal of Biological Chemistry. 2013, 288(50), 36020–36028. https://doi.org/10.1074/jbc.M113.510289
8. *Bolaños J. P.* Adapting glycolysis to cancer cell proliferation: the MAPK pathway focuses on PFKFB3. Biochemical Journal. 2013, 452(3), e7–e9. https://doi.org/10.1042/BJ20130560
9. *N. L, S.M. D., L. L., J. C., Y. I.F.* PFKFB3 Inhibition Impairs Erlotinib-Induced Autophagy in NSCLCs. Cells. 2021, 10(7). https://doi.org/10.3390/cells10071679
10. *Obach M., Navarro-Sabaté A., Caro J., Kong X., Duran J., Gómez M., Bartrons R.* 6-Phosphofructo-2-kinase (pfkfb3) Gene Promoter Contains Hypoxia-inducible Factor-1 Binding Sites Necessary for Transactivation in Response to Hypoxia. Journal of Biological Chemistry. 2004, 279(51), 53562–53570. https://doi.org/10.1074/jbc.M406096200
11. *Clem B., Telang S., Clem A., Yalcin A., Meier J., Simmons A., Chesney J.* Small-molecule inhibition of 6-phosphofructo-2-kinase activity suppresses glycolytic flux and tumor growth. Molecular cancer therapeutics. 2008, 7(1), 110–120. https://doi.org/10.1158/1535-7163.MCT-07-0482
12. *Horváthová J., Moravčík R., Boháč A., Zeman M.* Synergic effects of inhibition of glycolysis and multikinase receptor signalling on proliferation and migration of endothelial cells. General physiology and biophysics. 2019, 38(2), 157–163. https://doi.org/10.4149/gpb_2018047
13. *Clem B.F., O'Neal J., Tapolsky G., Clem A. L., Imbert-Fernandez Y., Kerr D. A., Chesney J.* Targeting 6-phosphofructo-2-kinase (PFKFB3) as a therapeutic strategy against cancer. Molecular Cancer Therapeutics. 2013, 12(8), 1461–1470. https://doi.org/10.1158/1535-7163.MCT-13-0097
14. *Li H. M., Yang J. G., Liu Z. J., Wang W. M., Yu Z. L., Ren J. G., Jia J.* Blockage of glycolysis by targeting PFKFB3 suppresses tumor growth and metastasis in head and neck squamous cell carcinoma. Journal of Experimental and Clinical Cancer Research. 2017, 36(1), 1–12. https://doi.org/10.1186/s13046-016-0481-1
15. *Gustafsson N. M. S., Färnegårdh K., Bonagas N., Ninou A. H., Groth P., Wiita E., Helleday T.* Targeting PFKFB3 radiosensitizes cancer cells and suppresses homologous recombination. Nature Communications. 2018, 9(1). https://doi.org/10.1038/s41467-018-06287-x
16. *Li X., Liu J., Qian L., Ke H., Yao C., Tian W., Zhang J.* Expression of PFKFB3 and Ki67 in lung adenocarcinomas and targeting PFKFB3 as a therapeutic strategy. Molecular and Cellular Biochemistry. 2018, 445(1–2), 123–134. https://doi.org/10.1007/s11010-017-3258-8
17. *Cory G.* Scratch-wound assay. Methods in Molecular Biology (Clifton, N.J.). 2011, 769, 25–30. https://doi.org/10.1007/978-1-61779-207-6_2
18. *Liu K., Liu Pcheng, Liu R., Wu X.* Dual AO/EB staining to detect apoptosis in osteosarcoma cells compared with flow cytometry. Medical science monitor basic research. 2015, 21, 15–20. https://doi.org/10.12659/MSMBR.893327
19. *Yalcin A,. Clem BF., Imbert-Fernandez Y., Ozcan S. C., Peker S., O'Neal J., Chesney J.* 6-Phosphofructo-2-kinase (PFKFB3) promotes cell cycle progression and suppresses apoptosis via Cdk1-mediated phosphorylation of p27. *Cell Death & Disease*, 2014, *5*(7), e1337–e1337. https://doi.org/10.1038/cddis.2014.292

20. *Thirusangu P., Ray U., Sarkar Bhattacharya S., Oien D. B., Jin L., Staub J., Shridhar V.* PFKFB3 regulates cancer stemness through the hippo pathway in small cell lung carcinoma. Oncogene. 2022, 41(33), 4003–4017. https://doi.org/10.1038/s41388-022-02391-x
21. *De Oliveira T., Goldhardt T., Edelmann M., Rogge T.., Rauch K, Kyuchukov N. D., Conradi L. C.* Effects of the Novel PFKFB3 Inhibitor KAN0438757 on Colorectal Cancer Cells and Its Systemic Toxicity Evaluation In Vivo. Cancers. 2021, 13(5), 1–24. https://doi.org/10.3390/cancers13051011
22. *Shi W. K., Zhu X. D., Wang C. H., Zhang Y. Y., Cai H., Li X. L., Sun H. C.* PFKFB3 blockade inhibits hepatocellular carcinoma growth by impairing DNA repair through AKT. Cell Death & Disease. 2018, *9*(4), 1–12. https://doi.org/10.1038/s41419-018-0435-y
23. *Ninou A. H.., Lehto J, Chioureas D., Stigsdotter H., Schelzig K., Åkerlund E., Gustafsson N. M. S.* PFKFB3 Inhibition Sensitizes DNA Crosslinking Chemotherapies by Suppressing Fanconi Anemia Repair. Cancers. 2021, 13(14). https://doi.org/10.3390/cancers13143604
24. *Agca C. A., Kırıcı M., Nedzvetsky V. S., Gundogdu R., Tykhomyrov A. A.* The Effect of TIGAR Knockdown on Apoptotic and Epithelial-Mesenchymal Markers Expression in Doxorubicin-Resistant Non-Small Cell Lung Cancer A549 Cell Lines. Chemistry and Biodiversity. 2020, 17(9). https://doi.org/10.1002/cbdv.202000441
25. *Ly J. D., Grubb D. R., Lawen A.* The mitochondrial membrane potential (δψm) in apoptosis; an update. Apoptosis. 2003, *8*(2), 115–128. https://doi.org/10.1023/a:1022945107762
26. *Herceg Z., Wang Z. Q.* Functions of poly(ADP-ribose) polymerase (PARP) in DNA repair, genomic integrity and cell death. Mutation Research — Fundamental and Molecular Mechanisms of Mutagenesis. 2001, 477(1–2), 97–110. https://doi.org/10.1016/s0027-5107(01)00111-7
27. *Zhu W., Ye L., Zhang J., Yu P., Wang H., Ye Z., Tian J.* PFK15, a Small Molecule Inhibitor of PFKFB3, Induces Cell Cycle Arrest, Apoptosis and Inhibits Invasion in Gastric Cancer. 2016, 11(9), e0163768. https://doi.org/10.1371/journal.pone.0163768
28. *Peng F., Li Q., Sun J. Y., Luo Y., Chen M., Bao Y.* PFKFB3 is involved in breast cancer proliferation, migration, invasion and angiogenesis. International journal of oncology. 2018, 52(3), 945–954. https://doi.org/10.3892/ijo.2018.4257
29. *Gu M., Li L., Zhang Z., Chen J., Zhang W., Zhang J., You Y.* PFKFB3 promotes proliferation, migration and angiogenesis in nasopharyngeal carcinoma. Journal of Cancer. 2017, 8(18), 3887–3896. https://doi.org/10.7150/jca.19112
30. *Han J., Meng Q., Xi Q., Wang H., Wu G.* PFKFB3 was overexpressed in gastric cancer patients and promoted the proliferation and migration of gastric cancer cells. Cancer biomarkers : section A of Disease markers. 2017, 18(3), 249–256. https://doi.org/10.3233/CBM-160143
31. *Zheng W. D., Zhou F. L., Lin N.* MicroRNA-26b inhibits osteosarcoma cell migration and invasion by down-regulating PFKFB3 expression. Genetics and molecular research : GMR. 2015, 14(4), 16872–16879. https://doi.org/10.4238/2015.Aralık.14.14
32. *Zhang D. M., Zhang T., Wang M. M., Wang X. X., Qin Y. Y., Wu J., Qin Z. H.* TIGAR alleviates ischemia/reperfusion-induced autophagy and ischemic brain injury. Free Radical Biology and Medicine. 2019, 137, 13–23. https://doi.org/10.1016/j.freeradbiomed.2019.04.002
33. *Yun C. W., Lee S. H.* The Roles of Autophagy in Cancer. International Journal of Molecular Sciences. 2018, 19(11). https://doi.org/10.3390/ijms19113466
34. *Mondal S., Roy D., Sarkar Bhattacharya S., Jin L., Jung D., Zhang S., Shridhar V.* Therapeutic targeting of PFKFB3 with a novel glycolytic inhibitor PFK158 promotes lipophagy and chemosensitivity in gynecologic cancers. International Journal of Cancer. 2019, 144(1), 178. https://doi.org/10.1002/ijc.31868
35. *Klarer A. C., O'neal J., Imbert-Fernandez Y., Clem A., Ellis S. R., Clark J., Telang S.* Inhibition of 6-phosphofructo-2-kinase (PFKFB3) induces autophagy as a survival mechanism. 2014, 2, 1–14. https://doi.org/10.1186/2049-3002-2-2
36. *Xi H., Wang S., Wang B., Hong X., Liu X., Li M., Dong Q.* The role of interaction between autophagy and apoptosis in tumorigenesis (Review). Oncology reports, 2022, 48(6), 1–16. https://doi.org/10.3892/or.2022.8423

KAN0438757 — ИНГИБИТОР PFKFB3, ЯКИЙ ІНДУКУЄ ЗАПРОГРАМОВАНУ КЛІТИННУ СМЕРТЬ І ПРИГНІЧУЄ КЛІТИННУ МІГРАЦІЮ В КЛІТИНАХ НЕДРІБНОКЛІТИННОЇ КАРЦИНОМИ ЛЕГЕНІВ

Deniz Özdemir[1], *Seher Saruhan*[2], *Can Ali Agca*[3]

Department of Molecular Biology and Genetics, Bingol University, Bingol, TÜRKİYE

E-mail: c.aliagca@gmail.com

Мета. PFKFB3 є гліколітичним активатором, який надмірно експресується при раку легенів людини і відіграє вирішальну роль у багатьох клітинних функціях, включаючи запрограмовану клітинну смерть. Незважаючи на велику кількість малих молекул, описаних як інгібітори PFKFB3, деякі з них продемонстрували невтішні результати *in vitro* та *in vivo*. З іншого боку, булол розроблено KAN0438757, селективний і потужний маломолекулярний інгібітор. Однак вплив KAN0438757 на клітини недрібноклітинної карциноми легень залишається невідомим. Ми намагалися розшифрувати вплив KAN0438757 на проліферацію, міграцію, пошкодження ДНК і запрограмовану клітинну смерть у клітинах недрібноклітинної карциноми легенів.

Методи. Вплив KAN0438757 на життєздатність клітин, проліферацію, пошкодження ДНК, міграцію, апоптоз і аутофагію в клітинах недрібноклітинної карциноми легені було перевірено за допомогою WST-1, клітинного аналізу в реальному часі, кометного аналізу, тесту міграції загоєння ран, аналізів подвійного фарбування MMP/JC-1 і AO/ER, а також вестерн-блоту.

Результати. Показано, що KAN0438757 значно пригнічував життєздатність і проліферацію клітин A549 і H1299 і пригнічував міграцію клітин A549. Що ще важливіше, KAN0438757 викликав пошкодження ДНК і апоптоз, і це супроводжувалося посиленням розщепленого PARP у клітинах A549. Крім того, лікування KAN0438757 призвело до збільшення LC3 II і Beclin1, що вказувало на те, що KAN0438757 стимулював аутофагію.

Висновки. Загалом, націлювання на PFKFB3 за допомогою KAN0438757 може бути багатообіцяючим ефективним підходом до лікування, що потребує подальшої *in vitro* та *in vivo* оцінки KAN0438757 як терапії клітин недрібноклітинної карциноми легенів.

Ключові слова: PFKFB3; KAN0438757; апоптоз; аутофагія; рак легенів.

UDC 612.8: 573.7 https://doi.org/10.15407/biotech16.05.045

ASSESSMENT OF ACUTE NEUROTOXICITY OF NITROGEN-DOPED MULTILAYER GRAPHENE NANOPARTICLES AND THEIR CAPABILITY TO CHANGE Cd^{2+}/Pb^{2+}/Hg^{2+}-INDUCED INJURY IN BRAIN CORTEX NERVE TERMINALS

Marina Dudarenko[1]
Nataliya Krisanova[1]
Natalia Pozdnyakova[1]
Artem Pastukhov[1]
Olena Pariiska[2]
Yaroslav Kurys[2]
Svitlana Sotnik[2]
Sergey V. Kolotilov[2]
Vyacheslav Koshechko[2]
Tatiana Borisova[1]

[1] Palladin Institute of Biochemistry of the National Academy of Sciences of Ukraine, Kyiv

[2] Pisarzhevskii Institute of Physical Chemistry of the National Academy of Sciences of Ukraine, Kyiv

E-mail: pastukhovart@gmail.com

Received 2023/09/14
Revised 2023/10/11
Accepted 2023/10/31

Graphene materials are widely used in different technologies and certainly released into aquatic and air surroundings being environmental pollution components. Nitrogen-doped graphene nanomaterials have great potential for application, in particular, in energy storage, as electrochemical sensors and waste water treatment. The neurotoxic risk of nitrogen-doped multilayer graphene is unknown.

Aim. To evaluate neurotoxic risk of nitrogen-doped multilayer graphene.

Methods. Here, nitrogen-doped multilayer graphene nanoparticles (N-MLG) were synthesized by means of electrochemical exfoliation of high-purity graphite rods in NaN_3-based electrolyte and characterised using TEM, AFM and UV-vis spectroscopy. Neuroactive features of N-MLG were assessed in isolated cortex nerve terminals (synaptosomes) analysing the extracellular level of excitatory neurotransmitter L-[^{14}C] glutamate and inhibitory one [^{3}H]GABA.

Results. It was revealed that N-MLG did not affect the extracellular synaptosomal levels of L-[^{14}C]glutamate and [^{3}H]GABA within the concentration range 0.01–0.5 mg/ml, and an increase in a concentration up to 1 mg/ml caused an insignificant increase (tendency to increase) in these levels for both neurotransmitters. To analyse a capability of interaction with heavy metals in biological system, N-MLG was investigated using model of acute Cd^{2+}/Pb^{2+}/Hg^{2+}-induced neurotoxicity in nerve terminals. It was revealed that Cd^{2+}/Pb^{2+}/Hg^{2+}-induced increase in the extracellular level of L-[^{14}C] glutamate and [^{3}H]GABA was not changed by N-MLG.

Conclusions. N-MLG does not possess neurotoxic signs and is biocompatible within the concentration range 0.01^{-1} mg/ml. In biological system, N-MLG did not mitigate/aggravate Cd^{2+}/Pb^{2+}/Hg^{2+}-induced neurotoxicity in nerve terminals.

Key words: nitrogen-doped multilayer graphene; nanoparticles; heavy metals; neurotoxicity; glutamate; GABA; brain nerve terminals.

Graphene is a carbon 2D crystal consisting of a two dimensional honeycomb-lattice structure made of sp^2-hybridized carbon atoms. Graphene and its derivatives due to their two-dimensional shape and special mechanical, electronic, optical and catalytic properties are widely used in diverse fields, e.g. nanoelectronics, catalysis, and water technologies. Graphene is considered one of the most promising nanomaterials for biomedical applications and nanomedicine [1, 2]. Nitrogen-doped graphene exhibits excellent electrochemical parameters and has great potential for applications in energy storage, as a high-performance catalyst support for fuel cell electrocatalysis and sensor electrochemical applications [2, 3]. Nitrogen-doped graphene nanomaterials are effective for removing toxic species, e.g. organic pollutants, dyes, heavy metal ions from wastewater [4, 5]. In particular, nitrogen-doping enhances the interaction between the active sites and organic or ionic species, thereby improving removal efficiency of these pollutants [2].

Graphene materials during production and application can find ways into the environment in the form of nanoparticles because of its high dispersity in many solvents [6, 7]. In this context, graphene materials can widely pollute water resources and air around the world.

Nowadays, it is clear that carbonaceous airborne particulate matter is the most abandon environmental pollutant that can reach the nervous system of humans and trigger development of neurological and neurodegenerative disorders/diseases [8–10]. Expansion of these disorders/diseases is one of the main reasons of disability and premature death in Europe and linked to air pollution with particulate matter [8, 11–13]. From one hand, particulate matter can reach human organism through lungs and gut to the circulatory system and possibly cross the blood-brain barrier [14–18]. From the other hand, particulate matter can get to the human nervous system along the olfactory axon and overcome the blood-brain barrier [19, 20]. Recently, we have characterised neuroactivity of carbon-based nanoparticles, such as carbon nanodots, nanodiamonds, fullerene C60, carbonaceous smoke particulate matter from combustion of plastics and wood samples. Transport kinetics of key excitatory neurotransmitters, L-[^{14}C] glutamate and inhibitory one [^{3}H] GABA, were changed by above nanoparticles that in turn can provoke presynaptic malfunction and development of neuropathology [21, 22]. Carbonaceous airborne particulate matter possesses adhesive surface and can bind potentially toxic molecules, including heavy metals [23, 24].

The neurotoxic potential of nitrogen-doped multilayer graphene is unknown. In neurobiology study of other graphene derivatives, it was demonstrated that few-layer pristine graphene and monolayer graphene oxide flakes were in contact with the neuronal membrane and free in the cytoplasm, but did not have significant impact on neuron viability. Graphene oxide exposure inhibited excitatory transmission, reduced the number of excitatory synaptic contacts, and concomitantly enhanced the inhibitory activity. This was accompanied by altered Ca^{2+} dynamics in excitatory and inhibitory neurons. So, it was suggested that both graphene preparations affected neuronal transmission [1]. Taking into account abovementioned facts, the aims of the present study were (*) to synthesize nitrogen-doped multilayer graphene nanoparticles (N-MLG) by means of electrochemical exfoliation of high-purity graphite rods; (**) to assess neuromodulatory features of N-MLG in isolated presynaptic rat cortex nerve terminals (synaptosomes) analysing the extracellular level of neurotransmitters L-[^{14}C] glutamate and [^{3}H]GABA; and (***) to examine the effects of N-MLG on the neurotoxic injury caused by heavy metal ions Cd^{2+}, Pb^{2+}, and Hg^{2+} in the nerve terminals.

Materials and Methods

HEPES, EGTA, EDTA, NaN_3, Ficoll 400, High Performance LSC Cocktail salts of the analytical grade were obtained from Sigma, USA; L-[^{14}C] glutamate; [^{3}H] GABA– Perkin Elmer, Waltham, MA, USA. The high-purity graphite rods (99.9995%) were obtained from Alfa Aesar.

Transmission electron microscopy (TEM) images of the synthesized graphene material were recorded using a microscope TEM125K (Selmi) with an accelerating voltage 100 kV. Atomic force microscopy (AFM) of thin film N-MLG samples on the surface of silicon wafers coated with silicon nitride (Agar Scientific) was performed on a Nanoscope IIIa Dimension 3000TM (Digital) instrument. UV-vis-spectra of N-MLG dispersions were registered via UV-visible spectrometer 4802 (Unico).

Synthesis of multilayer graphene doped with nitrogen

Multilayer graphene doped with nitrogen (N-MLG) was synthesized according to previous published procedure by means of electrochemical exfoliation of high-purity graphite rods (Alfa Aesar, 99.9995%) in 1.0 M aqueous solution of NaN_3 using three-electrode undivided cell and potentiostat PI-50-1.1 [25]. Graphite rods were used as working and auxiliary electrodes and Ag/AgCl as reference electrode. Exfoliation procedure was carried out during 20 h via polarization of graphite electrode by +4.0 V (50 s) and 0.0 V (50 s) with multiple changing of polarization potential (pulse mode of electrolysis).

N-MLG particles from the obtained aqueous dispersion were separated on a nylon membrane filter with a pore diameter 0.2 μm (SUPELCO®), rinsed with water, and dried in oven at 60 °C. If necessary, the regeneration of N-MLG dispersion was performed by short-term ultrasound treatment (2 min) of the dried graphene material in appropriate solvent (for example, water) using the ultrasonic washing bath.

Animals and Ethics

Wistar rats (males), 3 months' age, were kept in the vivarium of Palladin Institute of Biochemistry, NAS of Ukraine in a quiet and temperature-controlled room at 22–23 °C. Animals were provided with dry food pellets and water *ad libitum*. All animal-involving procedures were performed in accordance with the guidelines of the European Community (2010/63/EU); "Scientific Requirements and Research Protocols"; "Research Ethics Committees" of Declaration of Helsinki; and "ARRIVE guidelines for reporting experiments involving animal" [26, 27]; and also local Ukrainian laws and policies. The experimental protocols were approved by the Animal Care and Use Committee of Palladin Institute of Biochemistry (Protocol # 1 from 10/01/2023). The total number of animals was 9.

Isolation of the synaptosomes from the rat cortex

The synaptosomes represented ~87% of the particles in electron micrographs of preparations, and did not contain nerve cell bodies and functional glial fragments [28–30]. Nerve terminals were isolated from the cortex regions of rat brain. Isolation procedures were conducted at + 4 °C. The cortex regions were removed and homogenized in the following ice-cold solution: sucrose 0.32 M; HEPES-NaOH 5 mM, pH 7.4; EDTA 0.2 mM. One synaptosome preparation was obtained from one rat. The synaptosomes were isolated according to Cotman method with minor modifications [9, 31–33] by differential/Ficoll-400 density gradient centrifugation. The synaptosomes were fitting for experiments for 2–4 hours after isolation. The standard saline solution contained: NaCl 126 mM; KCl 5 mM; $MgCl_2$ 2.0 mM; NaH_2PO_4 1.0 mM; HEPES 20 mM, pH 7.4; and D-glucose 10 mM. Protein concentrations were monitored according to Larson [34].

The extracellular synaptosomal level of L-[^{14}C] glutamate

The synaptosomes were diluted up to a concentration of 2 mg of protein/ml, and then the synaptosomes were pre-incubated at 37 °C for 10 min, and loaded with L-[^{14}C] glutamate, 1 nmol per mg of protein, 238 mCi/mmol, at 37 °C for 10 min. The synaptosomes after loading were washed with 10 volumes of the ice-cold standard saline solution and centrifuged (10,000×g, 20 s) at +4 °C; the pellets were re-suspended in the standard saline solution up to 1 mg protein/ml. The extracellular L-[^{14}C] glutamate level was assessed in the synaptosome suspensions (125 μl, 0.5 mg of protein/ml). The synaptosome aliquots were preincubated for 8 min to restore the ion gradients, and then Cd^{2+} (1 mM $CdCl_2$), Pb^{2+} (2.5 mM Pb acetatate (PbAc)), and Hg^{2+} (2.5 μM $HgCl_2$) were added to the synaptosomes and they were further incubated at 37 °C during 0 and 6 min; then centrifuged at 10,000 × *g* for 20 s at room temperature. The values of L-[^{14}C] glutamate release were monitored in the supernatant aliquots (100 μl), and the pellets preliminary treated with SDS (100 μl of 10% SDS stock solution) by liquid scintillation counting using the scintillation cocktail ACS (1.5 ml) and liquid scintillation counter Hidex 600SL (Finland) [35]. The experimental data were collected from "*n*" independent experiments carried out in triplicate using different synaptosome preparations.

The extracellular synaptosomal level of [^{3}H] GABA

The synaptosomes were diluted up to 2 mg of protein/ml; after pre-incubation at 37 °C for 10 min, the synaptosomes were preloaded with [^{3}H]GABA (50 nM, 4.7 μCi/ml) in the standard saline solution at 37 °C for 10 min. Aminooxyacetic acid (100 μM) was added

to the incubation medium throughout [^{3}H] GABA experiments. After pre-loading, the suspension was washed with 10 volumes of the ice-cold standard saline solution. The pellets were re-suspended in the standard saline solution up to 1 mg of protein/ml. The synaptosome aliquots were pre-incubated for 8 min to restore the ion gradients, and then Cd^{2+} (1 mM $CdCl_2$), Pb^{2+} (1 mM PbAc) and Hg^{2+} (2.5 μM $HgCl_2$) were added and further incubated at 37 C during 0 and 5 min; then centrifuged at 10,000 × g for 20 s at room temperature [36]. [^{3}H] GABA was measured in the supernatant aliquots (90 μl) by liquid scintillation counting with Sigma-Fluor® High Performance LSC Cocktail (1.5 ml) using liquid scintillation counter Hidex 600SL (Finland), and the extracellular level was expressed as the percentage of total accumulated [^{3}H] GABA [37]. The data were collected from "n" independent experiments performed in triplicate with different synaptosome preparations.

Statistical analysis

The experimental data were expressed as the mean ± S.E.M. of *n* independent experiments. One-way and two-way ANOVA were applied; the accepted significance level was $P < 0.05$. Two-way ANOVA followed by Tukey's post hoc test was applied to assess the interactions between N-MLG and Cd^{2+}, Pb^{2+}, and Hg^{2+} (N-MLG treatment and Cd^{2+}/Pb^{2+}/Hg^{2+} treatment were the independent factors).

Results and Discussion

Characterization of multilayer graphene doped with nitrogen

During pulse mode of electrolysis, multiple (cyclic) azide anions (N_3^-) intercalation/deintercalation into graphite interlayer space occurs, also associated with N_2, NH_3 and O_2 evolution due to partial anodic/cathodic decomposition of N_3^-. This provides exfoliation of the graphite electrode, forming multilayer packages of graphene, doped with nitrogen, and its transition in the electrolyte volume [25].

The obtained graphene material was characterized by several instrumental analysis methods. On the TEM images of N-MLG (Fig. 1, *A*) graphene sheets with lateral size from several hundred nanometers to several microns, forming multiple-layered lamellar structures, can be observed.

According to the data of AFM experiment, shown on the Fig. 1b, the lateral size of N-MLG particles, taken from a dilute dispersion in ethanol, is consistent with the data obtained by TEM. From the cross-sectional profile analysis (Fig. 1, *B*) it can be seen that the thickness of the N-MLG particles present in the AFM image is 4.2 nm. Earlier, on the basis of AFM data, we showed that the thickness of the monolayer in the N-MLG was 0.6 nm [25]. Taking this into account, it can be assumed that the obtained N-MLG particles are multilayered, consisting of the packages of ~7 graphene layers. At the same time, we cannot rule out the presence of a small number of N-MLG particles of both smaller (< 7 graphene layers) and larger (up to 9 graphene layers) thicknesses obtained by the electrochemical approach used herein [25]. Thus, AFM data also confirm the multilayered nature of the obtained graphene material.

UV–vis spectrum of N-MLG dispersions in ethanol is provided on Fig. 2. The presence of a band with an absorption maximum at 267 nm, corresponding to the ππ* transition in the C=C bonds of graphene, indicates in favor of a slight oxidation of the resulting N-MLG.

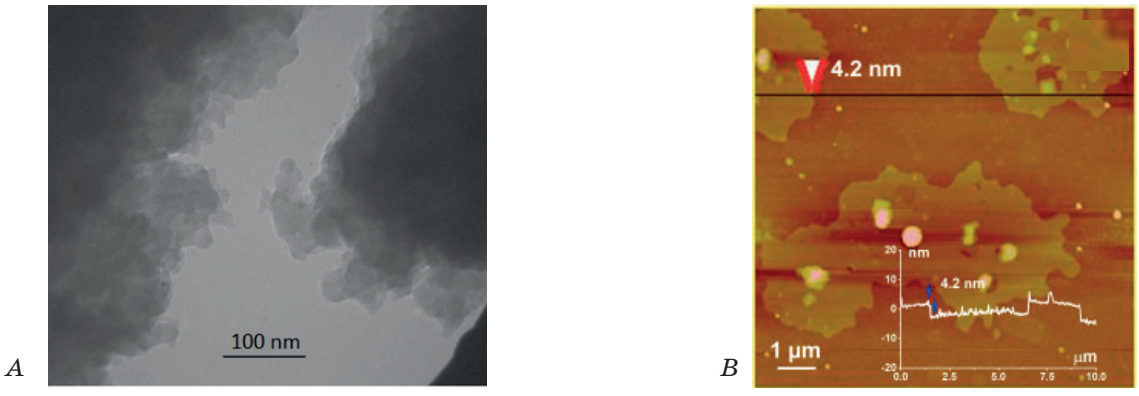

Fig. 1. **TEM image (*A*) and AFM image with corresponding cross-sectional profile (*B*) of N-MLG particles**

Neurotoxicity studies using rat brain nerve terminals

The extracellular levels of neurotransmitters glutamate and GABA are essential synaptic characteristics which show a balance of transporter-mediated uptake and tonic release of neurotransmitters [38, 39].

In the first series of the experiments, the effects of N-MLG on the extracellular levels of excitatory neurotransmitter L-[^{14}C] glutamate and inhibitory one [^{3}H]GABA were assessed in the nerve terminals. It was revealed that N-MLG did not affect the extracellular levels of L-[^{14}C] glutamate and [^{3}H]GABA within the concentration range 0.01–0.5 mg/ml, while an increase in a concentration up to 1 mg/ml caused an insignificant elevation (tendency to increase) of these levels for both neurotransmitters (Fig. 3). Therefore, N-MLG did not possess neurotoxic signs and was biocompatible within the concentration range 0.01^{-1} mg/ml.

In the next series of the experiments, it was investigated whether N-MLG could modulate a Cd^{2+}/Pb^{2+}/Hg^{2+}-induced increase in the extracellular levels of L-[^{14}C] glutamate and [^{3}H]GABA in nerve terminals. Based on above data, a N-MLG concentration of 0.5 mg/ml was chosen for further experiments with heavy metals. It was found that N-MLG (0.5 mg/ml) did not change Cd^{2+}/Pb^{2+}/Hg^{2+}-induced increase in the extracellular levels of L-[^{14}C] glutamate and [^{3}H]GABA in nerve terminals (Fig. 4), and so N-MLG was inert regarding modulation/aggravation of Cd^{2+}/Pb^{2+}/Hg^{2+}-induced neurotoxic effects in nerve terminals.

Two-way ANOVA revealed no interaction between Cd^{2+} and N-MLG [$F_{(1,32)}$ = 0.009; p = 0.92; n = 9], between Pb^{2+} and N-MLG [$F_{(1,32)}$ = 1.55; p = 0.22; n = 9] and between Hg^{2+} and N-MLG [$F_{(1,32)}$ = 1.22; p = 0.27; n = 9] in L-[^{14}C] glutamate experiments.

Two-way ANOVA revealed no interaction between Cd^{2+} and N-MLG [$F_{(1,32)}$ = 0.69; p = 0.41; n = 9], between Pb^{2+} and N-MLG [$F_{(1,32)}$ = 0.22; p = 0.63; n = 9] and between Hg^{2+} and N-MLG [$F_{(1,32)}$ = 0.13; p = 0.72; n = 9] in [^{3}H] GABA experiments.

Graphene and its derivatives have a potential to make a very significant impact on society with applications in the biomedical field. A possibility to engineer graphene-based medical devices at the neuronal interface is of particular interest, making it imperative to determine the biocompatibility of graphene materials with neuronal cells [1]. However, wide production and application of neuroactive graphene and its derivatives can increase

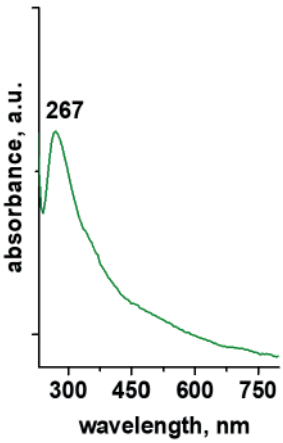

Fig. 2. **UV-vis spectra of N-MLG dispersion in ethanol**

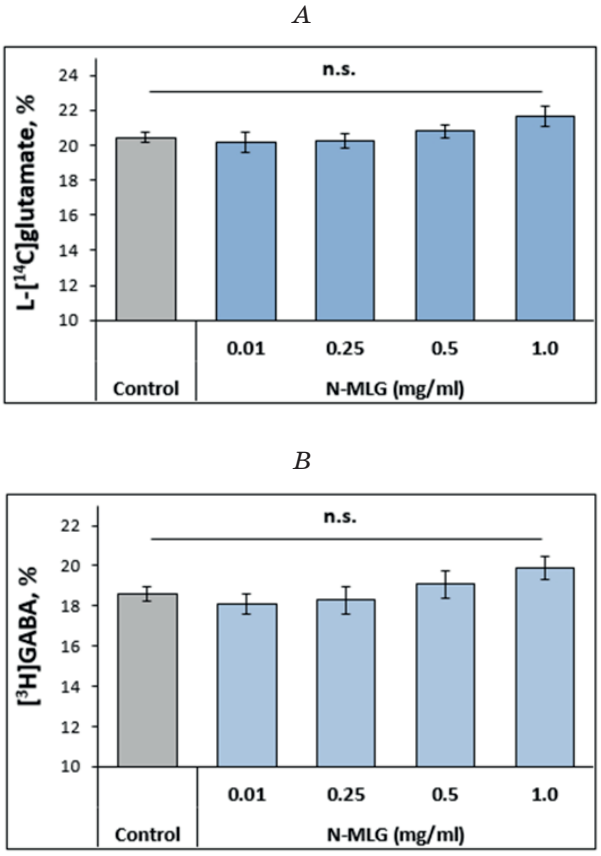

Fig. 3. **The extracellular levels of neurotransmitters L-[^{14}C] glutamate (*A*) and [^{3}H]GABA (*B*) in the nerve terminals in the presence of N-MLG (0.01–1.0 mg/ml)**

Data are the mean ± SEM. n.s., no significant differences as compared to the appropriate control, n = 9

uncontrolled environment pollution with these nanoparticles increasing risks to nervous system. To avoid the problem, technological-oriented graphene and its derivatives should be analysed regarding their neurotoxicity as single pollutants and also in combination with other pollutants, e.g. heavy metals, using multipollutant approach.

Here, we showed that N-MLG did not affect the extracellular synaptosomal levels of L-[^{14}C] glutamate and [^{3}H]GABA within the concentration range 0.01–1 mg/ml. Therefore, N-MLG can be applied in different technologies, including neurotechnologies and waste water treatment, because N-MLG did not possess neurotoxic signs and is biocompatible within this concentration range and it is safe when become environmental pollution component. Among other carbon-based nanoparticles that we have investigated regarding changes in the extracellular levels of L-[^{14}C] glutamate and [^{3}H]GABA in nerve terminals, N-MLG was less neurotoxic as compared to carbon dots [40], nanodiamonds [35], fullerene C_{60} [41], plastic and wood smoke particulate matter [21, 22, 42]. In this contex, N-MLG is more promising for neurotechnologies then other carbon nanoparticles because of absence of neurotoxic signs and its neurocompatibility.

Literature data have demonstrated that due to weak hydrophobic interactions, the negatively charged surfaces of graphene oxide were favorable to interact through electrostatic attractions with organic and inorganic cations [43, 44]. Graphene oxide could remove heavy metal ions as carriers due to its large surface area, pore size and abundant oxygen-containing functional groups [45–47]. In the present study, we revealed that N-MLG did not change Cd^{2+}/Pb^{2+}/Hg^{2+}-induced increase in the extracellular level of L-[^{14}C] glutamate and [^{3}H]GABA and so the nanoparticles did not mitigate/aggravate Cd^{2+}/Pb^{2+}/Hg^{2+}-induced neurotoxicity in nerve terminals. It also means that despite potential application in technologies, in particulate in waste water treatment against heavy metals, N-MLG was

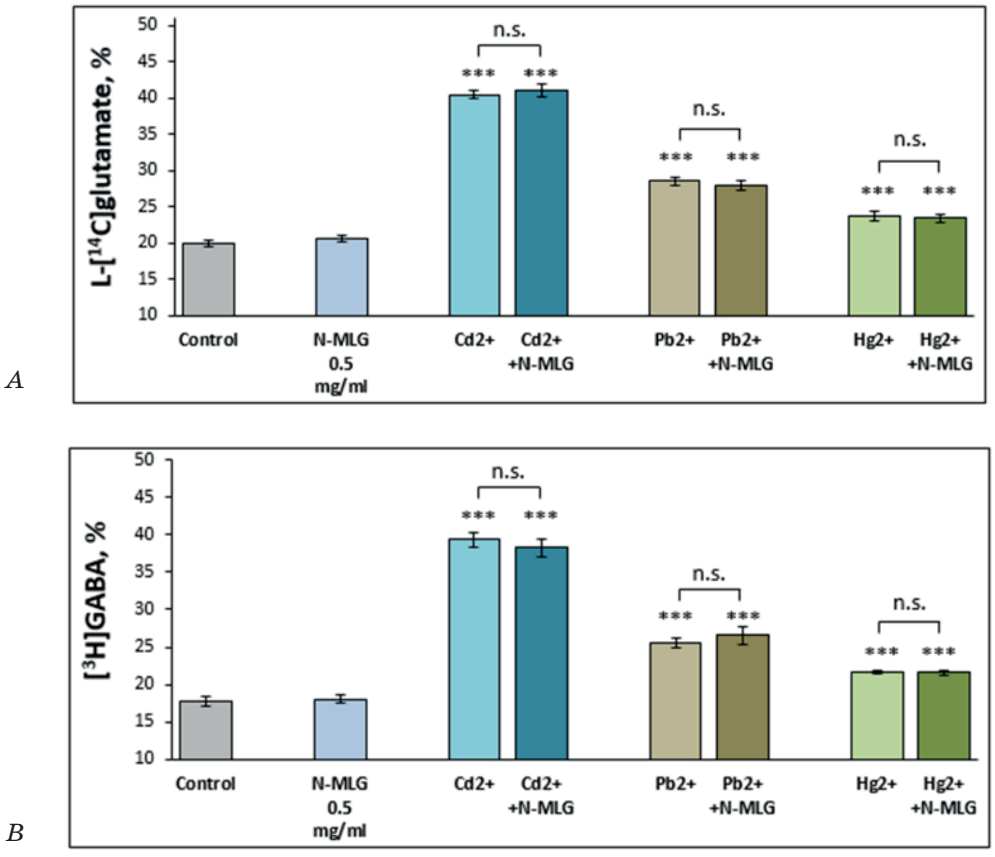

Fig. 4. **Effects of N-MLG (0.5 mg/ml) on Cd^{2+}/Pb^{2+}/Hg^{2+}-induced increase in the extracellular levels of L-[^{14}C] glutamate (*a*) and [^{3}H]GABA (*b*)**

Data are the mean ± SEM. ***, $P < 0.001$; as compared to the control; n.s., no significant differences as compared to Cd^{2+}/Pb^{2+}/Hg^{2+} effects, $n = 9$

not effective against prevention/mitigation of Cd^{2+}/Pb^{2+}/Hg^{2+}-induced neurotoxicity in biological system such as nerve terminals.

Conclusions

N-MLG, prepared by exfoliation of the graphite electrode in azide-containing electrolyte, did not influence the extracellular levels of L-[^{14}C] glutamate and [^{3}H] GABA in the nerve terminals. Cd^{2+}/Pb^{2+}/Hg^{2+}-induced increase in the extracellular levels of L-[^{14}C] glutamate and [^{3}H]GABA was not changed by N-MLG that was shown using model of acute neurotoxicity in nerve terminals. Therefore, N-MLG did not possess neurotoxic signs and is neurocompatible. In biological system, N-MLG did not mitigate or aggravate Cd^{2+}/Pb^{2+}/Hg^{2+}-induced neurotoxicity in nerve terminals.

Competing interests

The authors declare no financial and non-financial competing interests exist.

Authors contributions

N-MLG synthesis and characterisation — OP, YK; synaptosome preparations were obtained by AP & MD, L-[^{14}C] glutamate experiments — AP & KN, [^{3}H] GABA experiments — NP & MD; data analysis and figure preparation — OP, YK, SS, NP, KN, TB, SK; funding acquisitions, project leading, data analysis and paper writing — TB, VK.

Ethical Approval

Animal-involved experiments were performed according to the "Scientific Requirements and Research Protocols" & "Research Ethics Committees" of Declaration of Helsinki; the "ARRIVE guidelines for reporting experiments involving animal" [26, 27], and were preliminary approved by Institutional Animal Care and Use Committee (Protocol # 1 from 10/01/2023).

Consent to Participate

Not applicable.

Consent to Publish

Not applicable.

Availability of data and materials

All data generated or analyzed during this study are included in this published article.

Acknowledgements and Funding

This work was supported by the National Research Foundation of Ukraine: NRFU grant #2021.01/0061 «Cumulative neurotoxic effect of multicomponent pollution by airborne particles and neuroactive pharmaceuticals, biomaterials (including SARS-CoV-2), toxic metals and its prevention», PI of the Project: Prof. T. Borisova.

REFERENCES

1. *Brami ni M., Sacchetti S., Armirotti A., Rocchi A., Vázquez E., León Castellanos V., Bandiera T., Cesca F., Benfenati F.* Graphene Oxide Nanosheets Disrupt Lipid Composition, Ca 2+ Homeostasis, and Synaptic Transmission in Primary Cortical Neurons. *ACS Nano*. 2016, 10 (7), 7154–7171. https://doi.org/10.1021/acsnano.6b03438
2. *Yokwana K., Ntsendwana B., Nxumalo E. N., Mhlanga S. D.* Recent advances in nitrogen-doped graphene oxide nanomaterials: Synthesis and applications in energy storage, sensor electrochemical applications and water treatment. 2023, 38 (13), 3239–3263. https://doi.org/10.1557/S43578-023-01070-1
3. *Xiong B., Zhou Y., Zhao Y., Wang J., Chen X., O'Hayre R., Shao Z.* The use of nitrogen-doped graphene supporting Pt nanoparticles as a catalyst for methanol electrocatalytic oxidation. *Carbon N Y*. 2013, 52 (52), 181–192. https://doi.org/10.1016/j.carbon.2012.09.019
4. *Chen F., Guo L., Zhang X., Leong Z. Y., Yang S., Yang H. Y.* Nitrogen-doped graphene oxide for effectively removing boron ions from seawater. *Nanoscale*. 2016, 9 (1), 326–333. https://doi.org/10.1039/C6NR07448K
5. *Liu Y., Liu H., Zhou Z., Wang T., Ong C. N., Vecitis C. D.* Degradation of the Common Aqueous Antibiotic Tetracycline using a Carbon Nanotube Electrochemical Filter. *Environ Sci Technol*. 2015, 49 (13), 7974–7980. https://doi.org/10.1021/ACS.EST.5B00870
6. *Zhao J., Wang Z., White J. C.., Xing B.* Graphene in the aquatic environment: Adsorption, dispersion, toxicity and transformation. *Environ Sci Technol*. 2014, 48 (17), 9995–10009. https://doi.org/10.1021/ES5022679
7. *Bussy C., Ali-Boucetta H., Kostarelos K.* Safety Considerations for Graphene: Lessons Learnt from Carbon Nanotubes. *Acc Chem Res*. 2013, 46 (3), 692–701. https://doi.org/10.1021/ar300199e
8. *Landrigan P. J., Fuller R., Acosta N. J. R. R., Adeyi O., Arnold R., Basu N. (Nil)., Baldé A. B., Bertollini R., Bose-O'Reilly S., Boufford J. I., Breysse P. N., Chiles T., Ma-*

hidol C., Coll-Seck A. M., Cropper M. L., Fobil J., Fuster V., Greenstone M., Haines A., Hanrahan D., Hunter D., Khare M., Krupnick A., Lanphear B., Lohani B., Martin K., Mathiasen K. V., McTeer M. A., Murray C. J. L. L., Ndahimananjara J. D., Perera F., Potočnik J., Preker A. S., Ramesh J., Rockström J., Salinas C., Samson L. D., Sandilya K., Sly P. D., Smith K. R., Steiner A., Stewart R. B., Suk W. A., van Schayck O. C. P. P., Yadama G. N., Yumkella K., Zhong M. The Lancet Commission on pollution and health. *Lancet*. 2018, 391 (10119), 462–512. https://doi.org/10.1016/S0140-6736(17)32345-0

9. *Borisova T.* Nervous System Injury in Response to Contact With Environmental, Engineered and Planetary Micro- and Nano-Sized Particles. *Front Physiol*. 2018, 9, 728. https://doi.org/10.3389/fphys.2018.00728
10. *Tranvik LJ*. New light on black carbon. *Nat Geosci*. 2018, 11 (8), 547–548. https://doi.org/10.1038/s41561-018-0181-x
11. *Deuschl G., Beghi E., Fazekas F., Varga T., Christoforidi K. A., Sipido E., Bassetti C. L., Vos T., Feigin V. L.* The burden of neurological diseases in Europe: an analysis for the Global Burden of Disease Study 2017. *Lancet Public Heal*. 2020, 5 (10), e551–e567. https://doi.org/10.1016/S2468-2667(20)30190-0
12. *The Lancet Neurology*. Long COVID: understanding the neurological effects. *Lancet Neurol*. 2021, 20 (4), 247. https://doi.org/10.1016/S1474-4422(21)00059-4
13. *Jarrahi A., Ahluwalia M., Khodadadi H., Da Silva Lopes Salles E., Kolhe R., Hess D. C., Vale F., Kumar M., Baban B., Vaibhav K., Dhandapani K. M.* Neurological consequences of COVID-19: what have we learned and where do we go from here? *J Neuroinflammation*. 2020, 17 (1), 286. https://doi.org/10.1186/s12974-020-01957-4
14. *Jew K., Herr D., Wong C., Kennell A., Morris-Schaffer K., Oberdörster G., O'Banion MK., Cory-Slechta D. A., Elder A.* Selective memory and behavioral alterations after ambient ultrafine particulate matter exposure in aged 3xTgAD Alzheimer's disease mice. *Part Fibre Toxicol*. 2019, 16 (1), 45. https://doi.org/10.1186/s12989-019-0323-3
15. *Morris-Schaffer K., Merrill A., Jew K., Wong C., Conrad K., Harvey K., Marvin E., Sobolewski M., Oberdörster G., Elder A., Cory-Slechta D. A.* Effects of neonatal inhalation exposure to ultrafine carbon particles on pathology and behavioral outcomes in C57BL/6J mice. *Part Fibre Toxicol*. 2019, 16 (1), 10. https://doi.org/10.1186/s12989-019-0293-5
16. *Kim E. A.* Particulate matter (fine particle) and urologic diseases. *Int Neurourol J*. 2017, 21 (3), 155–162. https://doi.org/10.5213/INJ.1734954.477
17. *Gładka A., Rymaszewska J., Zatoński T.* Impact of air pollution on depression and suicide. *Int J Occup Med Environ Health*. 2018, 31 (6), 711–721. https://doi.org/10.13075/IJOMEH.1896.01277
18. *Klocke C., Allen J. L., Sobolewski M., Mayer-Pröschel M., Blum J. L., Lauterstein D., Zelikoff J. T., Cory-Slechta D. A.* Neuropathological consequences of gestational exposure to concentrated ambient fine and ultrafine particles in the mouse. *Toxicol Sci*. 2017, 156 (2), 492–508. https://doi.org/10.1093/TOXSCI/KFX010
19. *Oberdörster G., Sharp Z., Atudorei V., Elder A., Gelein R., Kreyling W., Cox C.* Translocation of Inhaled Ultrafine Particles to the Brain. *Inhal Toxicol*. 2004, 16 (6–7), 437–445. https://doi.org/10.1080/08958370490439597
20. *Oberdörster G., Oberdörster E., Oberdörster J.* Nanotoxicology: an emerging discipline evolving from studies of ultrafine particles. *Environ Health Perspect*. 2005, 113 (7), 823–39. https://doi.org/10.1289/ehp.7339
21. *Borysov A., Tarasenko A., Krisanova N., Pozdnyakova N., Pastukhov A., Dudarenko M., Paliienko K., Borisova T.* Plastic smoke aerosol: Nano-sized particle distribution, absorption/fluorescent properties, dysregulation of oxidative processes and synaptic transmission in rat brain nerve terminals. *Environ Pollut*. 2020, 263, 114502. https://doi.org/10.1016/j.envpol.2020.114502
22. *Tarasenko A., Pozdnyakova N., Paliienko K., Borysov A., Krisanova N., Pastukhov A., Stanovyi O., Gnatyuk O., Dovbeshko G., Borisova T.* A comparative study of wood sawdust and plastic smoke particulate matter with a focus on spectroscopic, fluorescent, oxidative, and neuroactive properties. *Environ Sci Pollut Res Int*. 2022, 29 (25), 38315–38330. https://doi.org/10.1007/s11356-022-18741-x
23. *Islam N., Dihingia A., Khare P., Saikia B. K.* Atmospheric particulate matters in an Indian urban area: Health implications from potentially hazardous elements, cytotoxicity, and genotoxicity studies. *J Hazard Mater*. 2020, 384, 121472. https://doi.org/10.1016/j.jhazmat.2019.121472
24. *Islam N., Saikia B. K.* An overview on atmospheric carbonaceous particulate matter into carbon nanomaterials: A new approach for air pollution mitigation. *Chemosphere*. 2022, 303, 135027. https://doi.org/10.1016/J.CHEMOSPHERE.2022.135027
25. *Ustavytska O., Kurys Y., Koshechko V., Pokhodenko V.* One-Step Electrochemical Preparation of Multilayer Graphene Functionalized with Nitrogen. *Nanoscale Res Lett*. 2017, 12 (1), 175. https://doi.org/10.1186/s11671-017-1957-4

26. *McGrath J., Drummond G., McLachlan E., Kilkenny C., Wainwright C.* Guidelines for reporting experiments involving animals: the ARRIVE guidelines. *Br J Pharmacol*. 2010, 160 (7), 1573–1576. https://doi.org/10.1111/j.1476-5381.2010.00873.x
27. *Kilkenny C., Browne W., Cuthill I. C., Emerson M., Altman D. G.* Animal research: Reporting in vivo experiments: The ARRIVE guidelines. *Br J Pharmacol*. 2010, 160 (7), 1577–1579. https://doi.org/10.1111/j.1476-5381.2010.00872.x
28. *Nicholls D. G.* The glutamatergic nerve terminal. *Eur J Biochem*. 1993, 212 (3), 613–31. https://doi.org/10.1111/j.1432-1033.1993.tb17700.x
29. *Petr G. T., Sun Y., Frederick N. M., Zhou Y., Dhamne S. C., Hameed M. Q., Miranda C., Bedoya E. A., Fischer K. D., Armsen W., Wang J., Danbolt N. C., Rotenberg A., Aoki C. J., Rosenberg P. A.* Conditional deletion of the glutamate transporter GLT-1 reveals that astrocytic GLT-1 protects against fatal epilepsy while neuronal GLT-1 contributes significantly to glutamate uptake into synaptosomes. *J Neurosci*. 2015, 35 (13), 5187–5201. https://doi.org/10.1523/JNEUROSCI.4255-14.2015
30. *Györffy B. A., Kun J., Török G., Bulyáki É., Borhegyi Z., Gulyássy P., Kis V., Szocsics P., Micsonai A., Matkó J., Drahos L., Juhász G., Kékesi K. A., Kardos J.* Local apoptotic-like mechanisms underlie complementmediated synaptic pruning. *Proc Natl Acad Sci U S A*. 2018, 115 (24), 6303–6308. https://doi.org/10.1073/pnas.1722613115
31. *Cotman C. W.* Isolation of synaptosomal and synaptic plasma membrane fractions. *Methods Enzymol*. 1974, 31, 445–452
32. *Borisova T. A., Himmelreich N. H.* Centrifuge-induced hypergravity: [3H]GABA and l-[^{14}C] glutamate uptake, exocytosis and efflux mediated by high-affinity, sodium-dependent transporters. *Adv Sp Res*. 2005, 36 (7), 1340–1345. https://doi.org/10.1016/j.asr.2005.10.007
33. *Krisanova N. V., Trikash I. O., Borisova T. A.* Synaptopathy under conditions of altered gravity: changes in synaptic vesicle fusion and glutamate release. *Neurochem Int*. 2009, 55 (8), 724–731. https://doi.org/10.1016/J.NEUINT.2009.07.003
34. *Larson E., Howlett B., Jagendorf A.* Artificial reductant enhancement of the Lowry method for protein determination. *Anal Biochem*. 1986, 155 (2), 243–248. https://doi.org/10.1016/0003-2697(86)90432-X
35. *Pozdnyakova N., Pastukhov A., Dudarenko M., Galkin M., Borysov A., Borisova T.* Neuroactivity of detonation nanodiamonds: dose-dependent changes in transporter-mediated uptake and ambient level of excitatory/inhibitory neurotransmitters in brain nerve terminals. *J Nanobiotechnology*. 2016, 14 (1), 25. https://doi.org/10.1186/s12951-016-0176-y
36. *Krisanova N., Pozdnyakova N., Pastukhov A., Dudarenko M., Maksymchuk O., Parkhomets P., Sivko R., Borisova T.* Vitamin D3 deficiency in puberty rats causes presynaptic malfunctioning through alterations in exocytotic release and uptake of glutamate/GABA and expression of EAAC-1/GAT-3 transporters. *Food Chem Toxicol*. 2019, 123, 142–150. https://doi.org/10.1016/j.fct.2018.10.054
37. *Borisova T., Krisanova N., Sivko R., Borysov A.* Cholesterol depletion attenuates tonic release but increases the ambient level of glutamate in rat brain synaptosomes. *Neurochem Int*. 2010, 56 (3), 466–478. https://doi.org/10.1016/j.neuint.2009.12.006
38. *Borisova T., Borysov A.* Putative duality of presynaptic events. *Rev Neurosci*. 2016, 27 (4), 377–83. https://doi.org/10.1515/revneuro-2015-0044
39. *Borisova T., Borysov A., Pastukhov A., Krisanova N.* Dynamic Gradient of Glutamate Across the Membrane: Glutamate/Aspartate-Induced Changes in the Ambient Level of L-[(14)C]glutamate and D-[(3)H]aspartate in Rat Brain Nerve Terminals. *Cell Mol Neurobiol*. 2016, 36 (8), 1229–1240. https://doi.org/10.1007/s10571-015-0321-4
40. *Borisova T., Nazarova A., Dekaliuk M., Krisanova N., Pozdnyakova N., Borysov A., Sivko R., Demchenko AP.* Neuromodulatory properties of fluorescent carbon dots: Effect on exocytotic release, uptake and ambient level of glutamate and GABA in brain nerve terminals. *Int J Biochem Cell Biol*. 2015, 59, 203–15. https://doi.org/10.1016/j.biocel.2014.11.016
41. *Krisanova., Dudarenko M. V., Pastukhov A. O., Sivko R. V., Kalynovska L. M., Driuk M. M., Nazarova A. G., Gutich I. I., Shliakhovyi V. V., Pozdnyakova N. G.* Evaluation of the potential neuroactivity in the brain nerve terminals of the C60 fullerene planetary dust component. *Sp Sci Technol*. 2023, 29 (5). https://doi.org/10.15407/knit2023.05.060
42. *Pastukhov A., Paliienko K., Pozdnyakova N., Krisanova N., Dudarenko M., Kalynovska L., Tarasenko A., Gnatyuk O., Dovbeshko G., Borisova T.* Disposable facemask waste combustion emits neuroactive smoke particulate matter. *Sci Rep*. 2023, 13 (1), 17771. https://doi.org/10.1038/s41598-023-44972-0
43. *Madadrang C. J., Kim H. Y., Gao G., Wang N., Zhu J., Feng H., Gorring M., Kasner M. L., Hou S.* Adsorption behavior of EDTA-graphene oxide for Pb (II) removal. *ACS Appl*

Mater Interfaces. 2012, 4 (3), 1186–1193. https://doi.org/10.1021/AM201645G
44. *Mi X., Huang G., Xie W., Wang W., Liu Y., Gao J.* Preparation of graphene oxide aerogel and its adsorption for Cu 2+ ions. *Carbon N Y*. 2012, 50 (13), 4856–4864. https://doi.org/10.1016/J.CARBON.2012.06.013
45. *Deng X., Lü L., Li H., Luo F.* The adsorption properties of Pb(II) and Cd(II) on functionalized graphene prepared by electrolysis method. *J Hazard Mater*. 2010, 183 (1–3), 923–930. https://doi.org/10.1016/J.JHAZMAT.2010.07.117
46. *Zhao G., Jiang L., He Y., Li J., Dong H., Wang X., Hu W.* Sulfonated graphene for persistent aromatic pollutant management. *Adv Mater*. 2011, 23 (34), 3959–3963. https://doi.org/10.1002/ADMA.201101007
47. *Zhao G., Li J., Ren X., Chen C., Wang X.* Few-layered graphene oxide nanosheets as superior sorbents for heavy metal ion pollution management. *Environ Sci Technol*. 2011, 45 (24), 10454–10462. https://doi.org/10.1021/ES203439V

ОЦІНЮВАННЯ ГОСТРОЇ НЕЙРОТОКСИЧНОСТІ БАГАТОШАРОВИХ НАНОЧАСТИНОК ГРАФЕНУ, ЛЕГОВАНИХ АЗОТОМ, ТА ЇХНЬОЇ ЗДАТНОСТІ ВПЛИВАТИ НА $Cd^{2+}/Pb^{2+}/Hg^{2+}$-ІНДУКОВАНІ ЗМІНИ ФУНКЦІОНУВАННЯ НЕРВОВИХ ТЕРМІНАЛЕЙ КОРИ ГОЛОВНОГО МОЗКУ

Марина Дударенко[1], *Наталія Крисанова*[1], *Наталія Позднякова*[1], *Артем Пастухов*[1], *Олена Парійська*[2], *Ярослав Курись*[2], *Світлана Сотник*[2], *Сергій В. Колотілов*[2], *В'ячеслав Кошечко*[2], *Тетяна Борисова*[1]

[1] Інститут біохімії ім. О. В. Палладіна НАН України, Київ
[2]Інститут фізичної хімії ім. Л. В. Писаржевського НАН України, Київ

E-mail: pastukhovart@gmail.com

Графенові матеріали широко використовуються в різних технологіях і, безумовно, потрапляють у водне та повітряне навколишнє середовище та можуть стати його забруднювачами. Графенові наноматеріали, доповані азотом, мають великий потенціал для застосування, зокрема, в накопичувачах енергії, електрохімічних сенсорах і очищенні стічних вод.

Мета. Оцінити нейротоксичний ризик багатошарового графену, допованого азотом.

Методи. У роботі синтезовано наночастинки багатошарового графену, допованого азотом (N-MLG) за допомогою електрохімічної ексфоліації високочистих графітових стрижнів в електроліті на основі NaN_3 та охарактеризовано за допомогою ТЕМ, АСМ і спектроскопії. Нейроактивні властивості N-MLG оцінювали в ізольованих нервових закінченнях кори головного мозку (синаптосомах) шляхом аналізу позаклітинного рівня нейромедіаторів L-[^{14}C] глутамату та [^{3}H]ГАМК.

Результати. Виявлено, що в діапазоні концентрацій 0,5–0,01 мг/мл N-MLG не впливав на позаклітинний синаптосомальний рівень L-[^{14}C] глутамату та [^{3}H]ГАМК, а збільшення концентрації до 1,0 мг/мл викликало незначне підвищення (тенденцію до підвищення) цих рівнів для обох нейромедіаторів. Аналіз здатності N-MLG взаємодіяти з важкими металами в біологічній системі досліджували на моделі гострої $Cd^{2+}/Pb^{2+}/Hg^{2+}$-індукованої нейротоксичності в нервових терміналях. Виявлено, що $Cd^{2+}/Pb^{2+}/Hg^{2+}$-індуковане підвищення позаклітинного рівня L-[$^{2+}$C] глутамату та [$^{2+}$H] ГАМК не змінюється під впливом N-MLG.

Висновки. N-MLG не має нейротоксичних ознак і є біологічно сумісним у діапазоні концентрацій 0,01–1,0 мг/мл. У біологічній системі N-MLG не зменшує/посилює нейротоксичність, спричинену $Cd^{2+}/Pb^{2+}/Hg^{2+}$ у нервових терміналях.

Ключові слова: багатошаровий графен, допований азотом; наночастинки; важкі метали; нейротоксичність; глутамат; ГАМК; нервові терміналі мозку.

UDC 57.088.2 **https://doi.org/10.15407/biotech16.05.055**

APROBATION OF PLATELET AGGREGATION INHIBITOR FROM *Echis multisquamatis* SNAKE VENOM *in vitro, in vivo* AND *ex vivo*

M. A. Zhelavskyi[1, 2]
M. O. Platonov[1]
Y. P. Kucheryavyi[1]
Y. M. Stohnii[1]

[1]Palladin Institute of Biochemistry of the National Academy of Sciences of Ukraine, Kyiv

[2]ZL "Success Academy", Kyiv region, Ukraine

E-mail: bio.cherv@biochem.kiev.ua

Received 2023/07/21
Revised 2023/08/30
Accepted 2023/10/31

Snake venom-derived platelet aggregation inhibitors can be promising antiplatelet medications that can allow to avoid the risk of bleeding and treatment resistance, particularly in aspirin-resistant patients. Our study aimed to assess the effectiveness of a platelet aggregation inhibitor derived from *Echis multisquamatis* snake venom in various settings, including *in vitro, in vivo*, and *ex vivo*.

Methods. We examined a polypeptide from *Echis multisquamatis* venom, purified using a recently developed chromatography protocol, across multiple models. This polypeptide was introduced into platelet-rich blood plasma and administered intravenously to rats. The effects on platelet aggregation were assessed using aggregometry, focusing on ADP-induced aggregation.

Results and Discussion. Our findings revealed that a concentration of 0.040 mg/ml significantly reduced platelet aggregation *in vitro*. Remarkably, this dosage also proved effective when administered intravenously in laboratory animals, reaffirming its potential as a robust antiplatelet agent. In the final phase of our study, the polypeptide demonstrated its ability to inhibit platelet aggregation in blood plasma of pregnant woman with aspirin resistance, presenting a promising avenue for innovative treatment approaches in such cases.

Conclusion. This study underscores the potential of the *Echis multisquamatis* venom-derived polypeptide as a promising antiplatelet agent, effective in diverse scenarios, including aspirin resistance. Further research and clinical trials are imperative to fully harness its therapeutic potential.

Key words: disintegrin; blood plasma; platelets; thrombosis; blood coagulation; platelet aggregation; animal model.

The pursuit of new platelet aggregation inhibitors is an urgent issue, as today's World possesses new challenges: the emergence of patient resistance to antithrombotic agents [1, 2], increased risk of blood loss [3], and genetic resistance to existing drugs [4, 5].

Platelet aggregation inhibitors from snake venoms are small proteins that bind to receptors on platelets surface with high affinity [6, 7]. Due to their specificity, these proteins don't interfering with coagulation factors, which means that platelet aggregation inhibitors from snake venoms have a lower risk of causing excessive bleeding [8, 9]. Also, because they are acting by targeting platelets receptors it helps to avoid the development of treatment resistance [10, 11]. For example, aspirin cannot be successfully applied for the treatment of patients with resistance to aspirin [12] that can be found at least in 20% of population [13].

So, study of novel antiplatelet agents, in particular polypeptides from the venom of snakes, is a promising task for the development of potential drugs with antithrombotic action. Previously platelet aggregation inhibitor was found in the venom of snake *Echis multisquamatis* [14]. The aim of our study was to approbate platelet aggregation inhibitor from *Echis multisquamatis* snake venom *in*

vitro, in vivo and *ex vivo*. In particular our goal was to study the effect of this polypeptide on platelet aggregation after intravenous injection into rat's bloodstream and also to find out whether it can suppress platelet aggregation in platelet rich blood plasma of pregnant women with resistance to aspirin.

Materials and Methods

Polypeptide that effectively inhibited platelet aggregation was purified from the venom of *Echis multisquamatis* by ion-exchange and size-exclusion chromatography and analyzed by SDS-PAGE as it was reported earlier [14].

Male Wistar rats (8 weeks old) with body weight ≅ 200 g were individually housed in separate cages and had ad libitum access to standard food and water. The drug was administered by injection into the tail vein using a 0.3 ml syringe and a needle of diameter 30 g. Rats were anesthetized by sodium thiopental. The procedures were conducted in accordance with the requirements of the European Convention for the Protection of Vertebrate Animals used for Experimental and other Scientific Purposes (Strasbourg, 1986) and the Law of Ukraine On the Protection of Animals from Cruelty No. 3447 of 21.02.2006. Samples of animal blood were collected by heart puncture. 3.8% sodium citrate was added to blood immediately after collection.

Somatically healthy woman with single spontaneous pregnancy with diagnosed aspirin-resistance was enrolled in the study. Blood sample was kindly provided by the Kyiv Perinatal Center and analyzed immediately. Venous blood sampling for testing was collected from a peripheral vein using vacuum systems into sterile plastic 4 ml tubes, containing 3.8% sodium citrate solution. Written informed consent to be included in the study was accepted.

Platelet rich plasma (PRP) for the aggregometry study was obtained from whole blood by centrifuging at 160 g for 30 min at 25 °C [15].

Platelet aggregation was studied by aggregometry using Solar AP2110. PRP was added to the cuvette of the aggregometer and constantly stirred by the magnet mixer. In *in vitro* and *ex vivo* studies the solution of platelet aggregation inhibitor was added to the cuvette (final concentration was 0.04 mg/ml). Platelets were activated by ADP (final concentration 12.5 μM) and $CaCl_2$ (1 mM). Change of the light transmission was monitored. The speed and the rate of platelet inhibitors were measured [16].

Statistical analysis. All measurements were performed in triplicate.

Results and Discussion

Previously, a polypeptide was obtained from the venom of the *Echis multisquamatis* snake, and it was found to be an effective inhibitor of platelet aggregation. It was demonstrated that this polypeptide acts as a disintegrin or an antagonist of integrin receptors. This means that when it interacts with integrin receptors, it hinders the receptors' binding to the fibrinogen molecule, thus complicating the process of platelet aggregation and the formation of a fibrin-platelet thrombus. The researchers suggested a dosage that reduces the degree of platelet aggregation by 50% (IC50), which was 0.040 mg/ml.

In the initial phase of the study, the effect of this dosage of disintegrin was assessed *in vitro*, meaning it was added to a test tube containing platelet rich blood plasma from a control rat. Specifically, 0.01 ml of the disintegrin solution (1.2 mg/ml) was added to 0.24 ml of platelet rich blood plasma and incubated in the aggregometer cuvette, with constant automatic stirring achieved by a rotating magnet. After 3 minutes, platelet aggregation was triggered by adding 0.025 ml of $CaCl_2$ (0.025 M) and 0.025 ml of ADP (0.12 mM). In the control sample, an equivalent volume of physiological saline was added instead of the disintegrin solution. This allowed the determination of ADP-induced platelet aggregation, where platelets activated by ADP aggregated and formed microclots. The device measured the increase in the transparency of the tested suspension. In the case of inhibition of platelet aggregation, this process was delayed, resulting in reduced final transparency of the suspension.

Here we confirmed that the selected dosage effectively inhibited the platelet aggregation *in vitro* (Fig. 1).

The next stage of the research was to determine its effectiveness when administered intravenously (*in vivo*), i.e., to assess whether its efficacy would be maintained. It is confirmed that the blood volume of a rat is approximately 50 ml per kilogram of body weight [17]. Therefore, it is possible to calculate the amount of the polypeptide solution (1.2 mg/ml) needed to be injected into the bloodstream of a 200 g rat to achieve

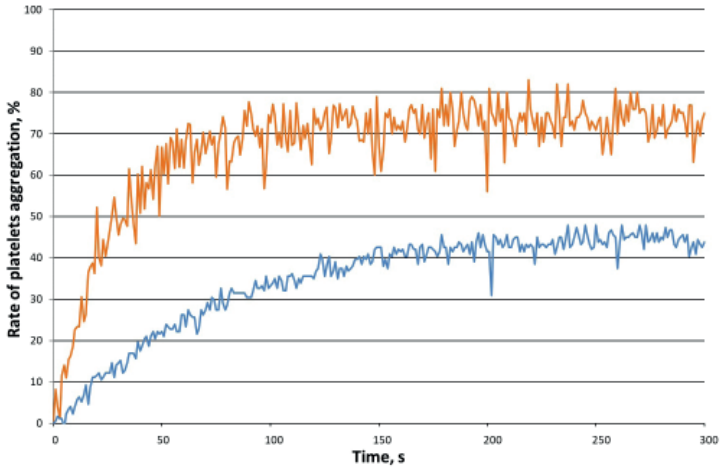

Fig. 1. **ADP-induced aggregation of platelets of a control rat in the presence of disintegrin from the venom of the *Echis multisquamatis* snake (blue line) or an equivalent volume of physiological saline (orange line)**
All measurements performed in triplicate; typical curves are presented

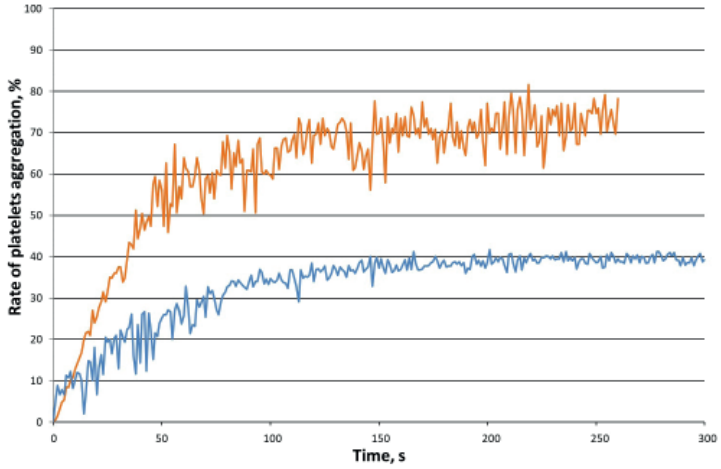

Fig. 2. **ADP-induced aggregation of platelets of a rat after the intravenous administration of disintegrin from the venom of the Echis multisquamatis snake (blue line) or an equivalent volume of physiological saline (orange line)**
All measurements performed in triplicate; typical curves are presented

an effective polypeptide concentration in the bloodstream of 0.04 mg/ml.

The volume of rat blood was 10 ml. The initial concentration of the polypeptide solution was 1.2 mg/ml, and the desired final concentration in the bloodstream was 0.04 mg/ml. Achieving this required diluting the original solution by a factor of 30. Consequently, for 10 ml of blood, 0.33 ml of the solution needed to be injected.

The polypeptide solution was administered through injection into the lateral tail vein of the rats using an insulin syringe. Control rats were injected with 0.33 ml of a physiological saline solution. Blood samples were collected by heart puncture 30 minutes after the injection.

The resulting aggregation shows that the introduction of the polypeptide significantly reduces both the speed and the degree of ADP-induced aggregation of platelets (Fig. 2).

The experiment's results demonstrate that the studied polypeptide from the venom of the *Echis multisquamatis* snake effectively inhibits platelet aggregation even under conditions of intravascular administration. The data obtained suggest promising potential for the use of the investigated disintegrin in future antithrombotic therapy.

As a final step of examinations, we approbated the inhibitory actions of the studied polypeptide *ex vivo* on the platelet rich blood plasma donated by pregnant woman with diagnosed aspirin-resistance.

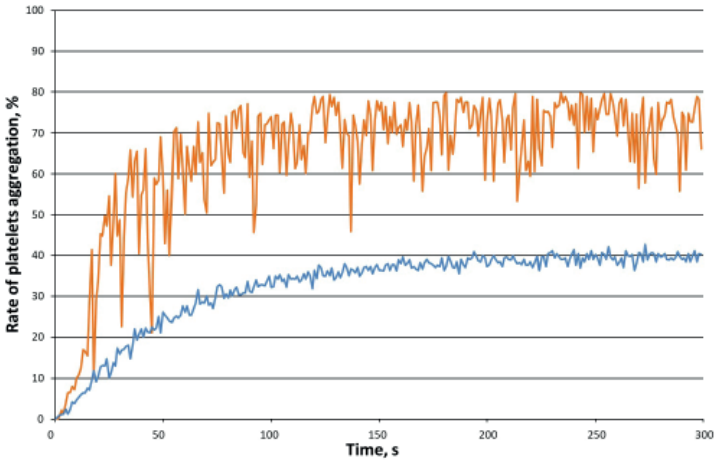

Fig. 3. **ADP-induced aggregation of platelets of a pregnant woman with diagnosed aspirin-resistance after the addition of disintegrin from the venom of the Echis multisquamatis snake (blue line) or an equivalent volume of physiological saline (orange line)**
All measurements performed in triplicate; typical curves are presented

We demonstrated that being the antagonist of integrin receptors the studied polypeptide can be effective for aspirin-resistant patients.

As a result, it can be concluded that the polypeptide derived from the venom of the *Echis multisquamatis* snake effectively reduces the aggregation ability of platelets *in vitro*. Moreover, this antiplatelet effect of the polypeptide remains unaffected under the conditions of intravenous administration to laboratory animals. Notably, it also demonstrated the ability to inhibit platelet aggregation *ex vivo* in patients with aspirin resistance.

In summary, the polypeptide from the venom of the *Echis multisquamatis* snake has the potential to serve as a prototype for an effective antithrombotic agent, capable of inhibiting platelet aggregation.

Authors' contribution

MZ performed aggregometry and analyzed datasets; OP purified polypeptide, performed aggregometry; YK was in aim for animal housing, sample injection and blood collection; YS analyzed results, wrote the manuscript.

Funding source

Study was financed by project 0121U110361 of the National Academy of Sciences of Ukraine.

Acknowledgement

Authors cordially acknowledge Dr. Chernyshenko V.O. (Palladin Institute of biochemistry of the National Academy of Sciences of Ukraine) for his supervising and guidance in the preparation of the manuscript; and Dr. Iryna Us for providing the samples of pregnant women with aspirin resistance.

REFERENCES

1. *Mărginean A., Bănescu C., Scridon A., Dobreanu, M.* Anti-platelet Therapy Resistance — Concept, Mechanisms and Platelet Function Tests in Intensive Care Facilities. *Journal of critical care medicine (Universitatea de Medicina si Farmacie din Targu-Mures)*. 2016, 2(1), 6–15. https://doi.org/10.1515/jccm-2015-0021
2. *Kumar A., Kao J.* Platelet resistance to antiplatelet drugs. *Recent patents on cardiovascular drug discovery*. 2009, 4(2), 98–108. https://doi.org/10.2174/157489009788452959
3. *Ferraris V. A., Ferraris S. P., Saha S. P.* Antiplatelet drugs: mechanisms and risks of bleeding following cardiac operations. *The International journal of angiology : official publication of the International College of Angiology. Inc.* 2011, 20(1), 1–18. https://doi.org/10.1055/s-0031-1272544
4. *Feher G., Feher A., Pusch G., Lupkovics G., Szapary L., Papp E.* The genetics of antiplatelet drug resistance. *Clinical genetics*. 2009, 75(1), 1–18. https://doi.org/10.1111/j.1399-0004.2008.01105.x
5. *Trenk D., Hochholzer W.* Genetics of platelet inhibitor treatment. British journal of clinical pharmacology. 2014, 77(4), 642–653. https://doi.org/10.1111/bcp.12230
6. *Echeverría S. M., Van de Velde A. C., Luque D. E., Cardozo C. M., Kraemer S., Gauna*

Pereira M. D. C., Gay C. C. Platelet aggregation inhibitors from Bothrops alternatus snake venom. *Toxicon : official journal of the International Society on Toxinology*, 2023, 223, 107014. https://doi.org/10.1016/j.toxicon.2022.107014
7. *Chérifi F., Laraba-Djebari F.* Bioactive Molecules Derived from Snake Venoms with Therapeutic Potential for the Treatment of Thrombo-Cardiovascular Disorders Associated with COVID-19. *The protein journal.* 2021, 40(6), 799–841. https://doi.org/10.1007/s10930-021-10019-4
8. *Kuo Y. J., Chung C. H., Huang T. F.* From Discovery of Snake Venom Disintegrins to A Safer Therapeutic Antithrombotic Agent. *Toxins*. 2019, 11(7), 372. https://doi.org/10.3390/toxins11070372
9. *Lazarovici P., Marcinkiewicz C., Lelkes P. I.* From Snake Venom's Disintegrins and C-Type Lectins to Anti-Platelet Drugs. *Toxins*. 2019, 11(5), 303. https://doi.org/10.3390/toxins11050303
10. *Frangieh J., Rima M., Fajloun Z., Henrion D., Sabatier J. M., Legros C., Mattei C.* Snake Venom Components: Tools and Cures to Target Cardiovascular Diseases. *Molecules (Basel, Switzerland.* 2021, 26(8), 2223. https://doi.org/10.3390/molecules26082223
11. *Van den Kerkhof D. L., van der Meijden P. E. J., Hackeng T. M., Dijkgraaf I.* Exogenous Integrin αIIbβ3 Inhibitors Revisited: Past, Present and Future Applications. *International journal of molecular sciences*. 2021, 22(7), 3366. https://doi.org/10.3390/ijms22073366
12. *Khan H., Kanny O., Syed M. H., Qadura M.* Aspirin Resistance in Vascular Disease: A Review Highlighting the Critical Need for Improved Point-of-Care Testing and Personalized Therapy. *International journal of molecular sciences.* 2022, 23(19), 11317. https://doi.org/10.3390/ijms231911317
13. *Lordkipanidzé M., Pharand C., Schampaert E., Turgeon J., Palisaitis D. A., Diodati J. G.* A comparison of six major platelet function tests to determine the prevalence of aspirin resistance in patients with stable coronary artery disease. *European heart journal*. 2007, 28(14), 1702–1708. https://doi.org/10.1093/eurheartj/ehm226
14. *Chernyshenko V., Petruk N., Korolova D., Kasatkina L., Gornytska O., Platonova T., Chernyshenko T., Rebriev A., Dzhus O., Garmanchuk L., Lugovskoy E.* Antiplatelet and anti-proliferative action of disintegrin from Echis multisquamatis snake venom. *Croatian medical journal*. 2017, 58(2), 118–127. https://doi.org/10.3325/cmj.2017.58.118
15. *Chernyshenko V., Shteinberg K., Lugovska N., Ryzhykova M., Platonova T., Korolova D., Lugovskoy E.* Preparation of highly-concentrated autologous platelet-rich plasma for biomedical use. The Ukrainian Biochemical Journal. 2019, 91(2), 19–27. https://doi.org/10.15407/ubj91.02.019
16. *Korolova D. S., Pavlenko A. O., Altorjay A., Zhuk S. I., Us I. V., Tsaryk Y., Suranyi A., Chernyshenko V. O.* Validation of the diagnostics algorithm to monitor coagulation parameters in pregnant women. The Ukrainian Biochemical Journal. 2023, 95(3), 33–41.
17. *Górska P.* Principles in laboratory animal research for experimental purposes. *Medical science monitor : international medical journal of experimental and clinical research*. 2000, 6(1), 171–180.

АПРОБАЦІЯ ІНГІБІТОРА АГРЕГАЦІЇ ТРОМБОЦИТІВ З ОТРУТИ *Echis multisquamatis in vitro, in vivo* ТА *ex vivo*

М. А. Желавський[1, 2], *М. О. Платонов*[1], *Є. П. Кучерявий*[1], *Є. М. Стогній*[1]

[1]Інститут біохімії ім. О.В. Палладіна НАН України, Київ
[2]ЗЛ "Академія Успіху", Київська обл., Україна

E-mail: *bio.cherv@biochem.kiev.ua*

Інгібітори агрегації тромбоцитів, отримані з отрути змій, є перспективними антитромботичними засобами, які водночас зменшують ризик кровотечі та дозволяють уникнути резистентності, як, наприклад, у пацієнтів, стійких до аспірину. Наше дослідження мало на меті оцінити ефективність інгібітора агрегації тромбоцитів, отриманого з отрути змії *Echis multisquamatis*, у різних умовах, включаючи *in vitro, in vivo* та *ex vivo*.

Методи. Досліджено поліпептид з отрути *Echis multisquamatis*, очищений за допомогою розробленого протоколу хроматографії, на кількох моделях. Цей поліпептид додавали до збагаченої тромбоцитами плазми крові або вводили внутрішньовенно щурам. Вплив на агрегацію

тромбоцитів оцінювали за допомогою агрегатометрії, зосереджуючись на індукованій ADP агрегації.

Результати та обговорення. Результати показали, що концентрація порліпептиду 0,040 мг/мл значно знижувала агрегацію тромбоцитів *in vitro*. Примітно, що ця доза також виявилася ефективною при внутрішньовенному введенні лабораторним тваринам, підтверджуючи потенціал поліпептиду як надійного антиагрегантного агента. На завершальному етапі дослідження поліпептид продемонстрував свою здатність пригнічувати агрегацію тромбоцитів у плазмі крові вагітної жінки з резистентністю до аспірину, що є багатообіцяючим для створення інноваційних підходів до лікування в таких випадках.

Висновок. Це дослідження підкреслює потенціал поліпептиду, отриманого з отрути *Echis multisquamatis*, як перспективного антиагрегантного агента, ефективного, зокрема, і за резистентності до аспірину. Для повного використання його терапевтичного потенціалу потребуються подальші дослідження та клінічні випробування.

Ключові слова: дезінтегрин; плазма крові; тромбоцити; тромбоз; зсідання крові; агрегація тромбоцитів; модель на тваринах.

UDC 604.6:577.13 https://doi.org/10.15407/biotech16.05.061

EFFECT OF PHENYLALANINE AND LIGHT ON THE GROWTH OF HAIRY ROOTS OF *Artemisia tilesii* Ledeb.

T.A. Bohdanovych
N.A. Matvieieva

Institute of Cell Biology and Genetic Engineering of the National Academy of Sciences of Ukraine, Kyiv

E-mail: bogdanovych_tais@ukr.net

Received 2023/08/22
Revised 2023/08/30
Accepted 2023/10/31

Aim. To analyze the possibility of using phenylalanine of various concentrations and different lighting modes separately and in combination to boost the biomass accumulation and biosynthesis of flavonoids in two lines of *Artemisia tilesii* Ledeb. hairy roots.

Methods. The roots were grown on solidified medium with phenylalanine at high (1 mM) and low concentrations (0.05 and 0.1 mM) with lighting (3000 lx, 16 h) and in darkness. After four weeks cultivation, weight gain, flavonoid content and DPPH-scavenging activity were determined according to the standard tests.

Results. Roots grown in light were greenish in color, more branched and thick, yet the roots were more elongated after maintenance in the dark. Addition of 1 mM phenylalanine has led to inhibition of growth of all samples. The tolerance to lower concentrations varied among the lines. The flavonoid content for all samples of both lines was higher in the light (up to 3.14 times), regardless of the concentration of phenylalanine. The antioxidant activity was as well higher for the roots grown in light and the values of EC_{50} correlated with the flavonoid content.

Conclusions. Illumination boosted the synthesis of flavonoids and antioxidant activity in all samples of both hairy root lines. The effect of phenylalanine addition on biomass accumulation and flavonoid biosynthesis was line-specific.

Key words: *Artemisia tilesii* Ledeb.; hairy roots; phenylalanine; light mode; elicitors; flavonoids; antioxidant activity.

Hairy roots of medicinal plants are a promising source of biologically active compounds as these cultures carry *rol* genes that are secondary metabolism activators. Hairy roots of *Artemisia tilesii* Ledeb. are of special interest. This is a rare plant adapted to the action of extreme factors [1]. *A. tilesii* is rich in polyphenolic compounds, such as flavonoids, with antioxidant, anti-inflammatory and antiviral effects [2–5]. To increase flavonoids content, different precursors [6–14] of their biosynthesis and various elicitors [15–32] can be added. Their presence and concentration in the nutrient medium can affect the synthesis of flavonoids and, accordingly, the bioactivity of plants.

All polyphenolic compounds originate from the shikimate pathway that leads to phenylalanine and tyrosine — aromatic amino acids. This makes phenylalanine one of possible elicitors for the activation of flavonoids biosynthesis. Indeed, Peng et al. [6] showed the beneficial effect of combination of microwave and L-phenylalanine on the specific activities of phenylalanine ammonia-lyase, chalcone isomerase, and *FLS* flavonol synthase in Tartary buckwheat sprouts. Demirci et al. [7] explored the effect of 24-epibrassinolide and L-phenylalanine on the root growth, total phenolics, total flavonoids, and caffeic acid derivatives accumulation in hairy roots of *Echinacea purpurea*. Treatment with 0.5 mg L^{-1} 24-epibrassinolide for 50 days resulted in the highest fresh root weight, dry root weight, and growth index, while L-phenylalanine had no significant influence on root growth. Cao et al. [8] showed the benefit of combination of 10 mM

phenylalanine and 50 mM chitosan on the dry weight, flavonoid and phenolic contents. Arya and Patni [9] reported significant enhancement of quercetin in callus culture of *Pluchea lanceolata* by incorporation of cinnamic acid and precursor feeding with L-phenylalanine. Syk owska-Baranek et al. [10] determined the effect of L-phenylalanine on PAL activity and production of naphthoquinone pigments in suspension cultures of *Arnebia euchroma*. Andi et al. [11] determined the boosting effect of L-phenylalanine on the synthesis of stilbenes and flavonoids in suspension cultures of *Vitis vinifera*.

The changes in certain cultivation conditions (temperature, lighting, agitation, aeration) can result in the alterations of the secondary metabolites biosynthesis as well. Thus, it is important to determine the parameters essential for the best ratio of biomass accumulation and biosynthesis in plant cultures *in vitro*.

Tusevski et al. [15] showed that dark-grown and photoperiod-exposed hairy root cultures of *Hypericum perforatum* differed in phenolic acids, flavonols, flavan-3-ols, and xanthones accumulation. Light served as the elicitor for the quinic acid, kaempferol, and seven identified xanthones production. On the other hand, dark-grown cultures had a higher content of flavan-3-ols (catechin, epicatechin, and proanthocyanidin dimers). The beneficial effect of light on cyanidin 3-*O*-rutinoside accumulation was also observed in Tartary buckwheat hairy roots [16]. Marsh et al. showed that the American skullcap hairy roots cultivated under continuous illumination in cobination with β-cyclodextrin accumulated flavone glycosides better, while the cultures maintained in the dark with the same treatment had maximum contents of baicalein and wogonin (5.4 mg/g DW and 0.71 mg/g DW, respectively) [17]. Wongshaya et al. showed a better response to elicitation of the *Arachis hypogaea* hairy roots maintained in the dark than those grown in the light [18]. Other researchers [19–25] showed the beneficial effect of different light waves, photoperiod optimization and ultraviolet radiation on the enhancement of flavonoids accumulation.

All these findings suggest that the addition of precursors and changes in cultivation parameters can have different effects on the growth of *in vitro* plant cultures and activity of their biosynthesis. Thus, the research was focused on the possibility of using phenylalanine of various concentrations and different lighting modes separately and in combination to boost the biosynthesis of flavonoids in two lines of *A. tilesii* hairy roots.

Materials and Methods

Plant material

Two *A. tilesii* hairy roots lines from the collection of the Institute of Cell Biology and Genetic Engineering of the National Academy of Sciences of Ukraine were used as the plant material for the study [33]. Both of the lines were obtained by the transformation using *Agrobacterium rhizogenes* A4 wild strain.

Phenylalanine elicitation

The roots were grown for four weeks on the solidified nutrient Murashige and Skoog medium (Duchefa Biochemie, The Netherlands) with halved macrosalt content (½ MS) and the addition of sucrose at a concentration of 20 g/l. Phenylalanine at high (1mM) and lower concentrations (0.05 and 0.1 mM) was added to the nutrient medium. Roots were grown at a temperature of +24 °C with lighting (3000 lx, 16 h) and in darkness. After cultivation, weight gain, flavonoid content and antioxidant activity were determined in both experiments.

Weight gain

After four weeks of cultivation, the grown hairy roots were separated from the medium, washed with distilled water, dried using filter paper and weighed on a Sartorius balance with a standard deviation of ± 0.005 g. Weight gain was determined as the difference between the final and initial weights in terms of one growth point.

Flavonoids content

Determination of the content of flavonoids was carried out according to the method described in [34] with modifications. To prepare the extracts, the roots were separated from the medium, washed with deionized water, dried using filter paper, weighed 0.3 g each and homogenized in 3 ml of 70% ethanol. The homogenate was centrifuged in an Eppendorf Centrifuge 5415 C at 15 000 g for 10 min. The reaction mixture contained 0.25 ml of extract supernatant, 1 ml of deionized water, 0.075 ml of 5% $NaNO_2$ (Merck, Germany) solution. After standing for 5 min, 0.075 ml of 10% $AlCl_3$ (Merck, Germany) solution was added and held for another 5 min. Then 0.5 ml of 1 M NaOH (Merck, Germany) and 0.6 ml of deionized water were added. Absorption was determined

at λ = 510 nm on a Fluorate-02-Panorama spectrofluorimeter. The calculation of the content of flavonoids was carried out in the rutin equivalent (RE) according to the following formula (after calibration graph was plotted), and converted to grams of fresh weight (FW):

$$C = (1.4497 \cdot OD) \cdot V / m, (R^2 = 0.9633)$$

where C — concentration of flavonoids in 1.0 g of fresh weight of plant material, mg RE/g FW; OD – optical density of the investigated solution, U; V — volume of ethanol used to prepare the extract; m — mass of plant material used for research. The total content of flavonoids (in all biomass) was calculated as the multiplication of the concentration of flavonoids and the weight gain per one growth point.

Antioxidant activity (AOA)

The antioxidant activity of ethanol extracts of hairy roots was studied using the DPPH (2,2-diphenyl-1-picrylhydrazyl, Merck, Germany) test according to the method described in [35]. The optical density of the solutions was measured at a wavelength of λ = 515 nm on a Fluorate-02-Panorama spectrofluorimeter. The percentage of inhibition was calculated according to the following formula:

$$\%\ inhibition = (OD_1 - OD_2) / OD_1 \cdot 100,$$

where OD_1 — optical density of the DPPH solution, U; OD_2 — optical density of the of the reaction mixture after carrying out the reaction with DPPH, U.

The effective concentration (EC_{50}) was calculated as the fresh weight of the root (mg FW) required to scavenge 50% of DPPH in the reaction with the radical.

Data analysis

All analyzes were performed in triplicate. Results were calculated in Microsoft Excel and presented as mean ± confidence interval. The data were analyzed for statistical significance using ANOVA followed by Tukey HSD test using R software version 4.0.4. The differences between mean values were considered statistically significant at $P < 0.05$.

Results and Discussion

For both lines cultivated without phenylalanine, hairy roots accumulated more biomass while growing in the dark. Such roots were white, elongated and less branched. Weight gain of the roots No.1 and No. 2 grown in darkness exceeded this parameter of the roots of these lines grown with lighting (2.33 and 3.94 fold, respectively) (Fig. 1, *A*). Therewith, flavonoid content was higher in the roots grown in light. Such roots were greenish in color and highly branched. Flavonoid content in ethanolic extracts obtained from roots No.1 and No.2 grown in light (Fig.1, *B*) was 2.53 ± 0.28 and 5.45 ± 0.37 mg RE/g of FW, respectively. For the samples grown in dark, the values were much lower: 2.3 and 4.74 mg RE/g of FW, respectively. Thus, high increase of biomass correlated with low biosynthesis of flavonoids and vice verse. This result may be explained by the fact that plant cells have limited quantity of all needed precursors and energy both for the root growth and secondary metabolites accumulation. Consequently, as the roots biomass was higher in the dark, their rate of growth was rapid and the flavonoid biosynthesis level was low. Accordingly, roots grown in light had higher biosynthetic activity and flavonoids accumulation, and their growth rate was slower.

All samples grown on the medium with addition of 1 mM phenylalanine (PHE) had drastic inhibition of growth. Line No. 1 tolerated the addition of PHE better and the weight gain was 0.022 ± 0.014 and 0.008 ± 0.003 g per one growth point while grown in light and dark, respectively. Flavonoid content in the ethanolic extracts of these samples was comparable with that of control sample: 2.36 ± 0.17 (grown in light) and 1.84 ± 0.06 (grown in dark) mg RE/g of FW. In addition, total flavonoid content in the whole mass of the hairy root samples was the following: 0 mM PHE light (0.10 mg RE) > 0 mM PHE dark (0.09 mg RE) > 1 mM PHE light (0.05 mg RE) > 1 mM PHE dark (0.01 mg RE). Such result once again confirmed the inhibiting effect of phenylalanine on the growth of *A. tilesii* hairy roots and their biosynthetic activity. Moreover, it was shown that it is better to grow wormwood hairy roots with lighting.

Line No. 2 was more sensitive to the addition of PHE than root line No. 1 (Fig.1, *A*). The inhibition was so drastic, that it was not possible to obtain enough plant material to prepare the extracts for the study of flavonoids accumulation and antioxidant activity.

As phenylalanine at 1 mM concentration was shown to be inhibiting for these *A. tilesii* hairy roots, for the next part of the study lower concentrations were chosen, namely 0.05 and 0.1 mM.

The morphology and growth characteristics of the hairy roots depended

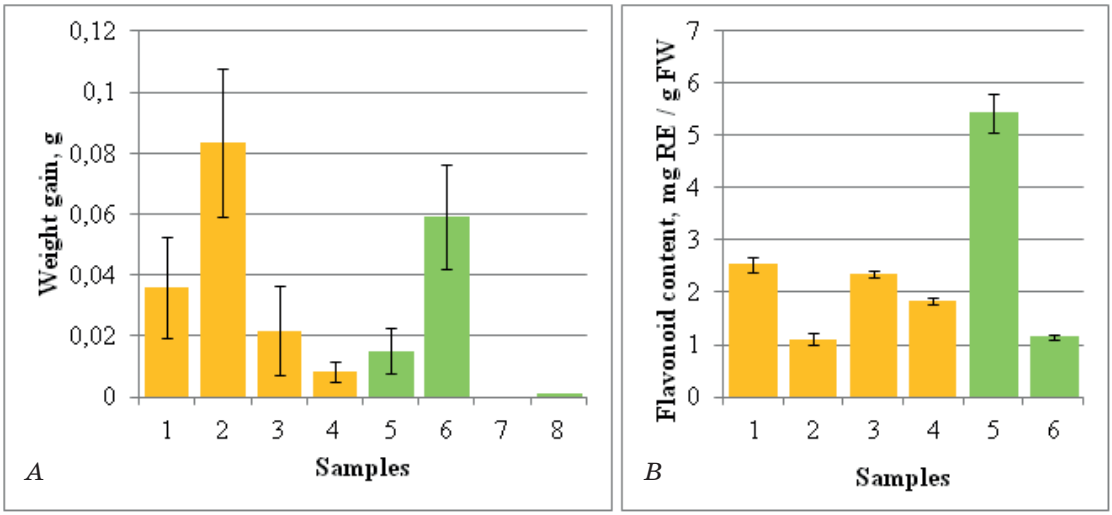

Fig. 1. **Weight gain (*A*) and flavonoid content (*B*) of the *Artemisia tilesii* hairy roots grown on two lighting modes without and with addition of high concentration of phenylalanine:**
orange columns — line No. 1, green columns — line No. 2. Growth conditions: columns 1 and 5 — light, without phenylalanine (controls); 2 and 6 – dark, without phenylalanine; 3 and 7 — light, 1 mM phenylalanine; 4 and 8 — dark, 1 mM phenylalanine

on the presence of lighting (Fig. 2) the same way as in the first experiment. Illumination acted in favor of the color of hairy roots, their branching and thickness. All samples of hairy roots were slightly greenish in the light and white in the dark.

It was established that in this part of experiment for both lines and in all concentrations of phenylalanine the weight gain of hairy roots was higher in the samples grown with lighting (Fig. 3, *A*) that contradicts the data in the previous experiment. Therefore the difference in the effect of lighting on the weight gain may be explained by the thickness of the roots: all root samples grown in light this time were much thicker (up to 1.5 mm), than roots grown in dark. This thickness contributed to the increased weight gain. Weight gain of the roots No.1 and No. 2 grown in light was 1.16–2.91 and 1.26–1.59 times higher respectively than the same parameter of the roots cultivated in darkness. Addition of phenylalanine at any concentrations (0.05 or 0.1 mM) inhibited the growth of the roots. This inhibition varied among the lines in the same manner as in the previous experiment: line No. 1 tolerated phenylalanine better than line No. 2. The weight increase in the roots No. 1, grown under the same lighting conditions, was similar when PHE was added in different concentrations. At the same time, increasing the concentration of PHE led to the inhibition of growth of roots No. 2.

The content of flavonoids (Fig. 3, *B*) in all the samples of both lines was higher in the light, which may prove the possible effect of lighting as flavonoids biosynthesis activator for the wormwood hairy roots that was suggested in the result of the previous experiment. Indeed, regardless of the presence and concentration of phenylalanine in the solid nutrient medium, the flavonoid content was 1.48–2.69 times higher in the roots No. 1 and 1.02–3.14 times higher in the roots No. 2 grown in light. As in the first experiment, even though the biomass accumulation of roots No. 1 was vividly higher than in the line No. 2, the flavonoid content was higher in all the samples when comparing the variants grown at the same conditions. This once more suggests the explanation proposed in the first experiment that biomass accumulation and secondary metabolites biosynthesis often don't occur at the same time and can vary greatly depending on the line of hairy roots.

Similarly, the antioxidant activity in all the samples was higher in the roots grown under lighting conditions. Values of EC_{50} (Fig. 4) correlated with the flavonoid content in the samples. Lower values of EC_{50} and thus higher antioxidant activity was interrelated with higher flavonoid biosynthesis.

As it can be seen from the graph (Fig. 3, *B*), lower concentrations of PHE didn't inhibit the flavonoids biosynthesis, although inhibition was observed when PHE was added at a higher concentration (1 mM, Fig. 1). Nonetheless, such value as the total content of flavonoids calculated per whole biomass gain showed that the inhibition of growth that

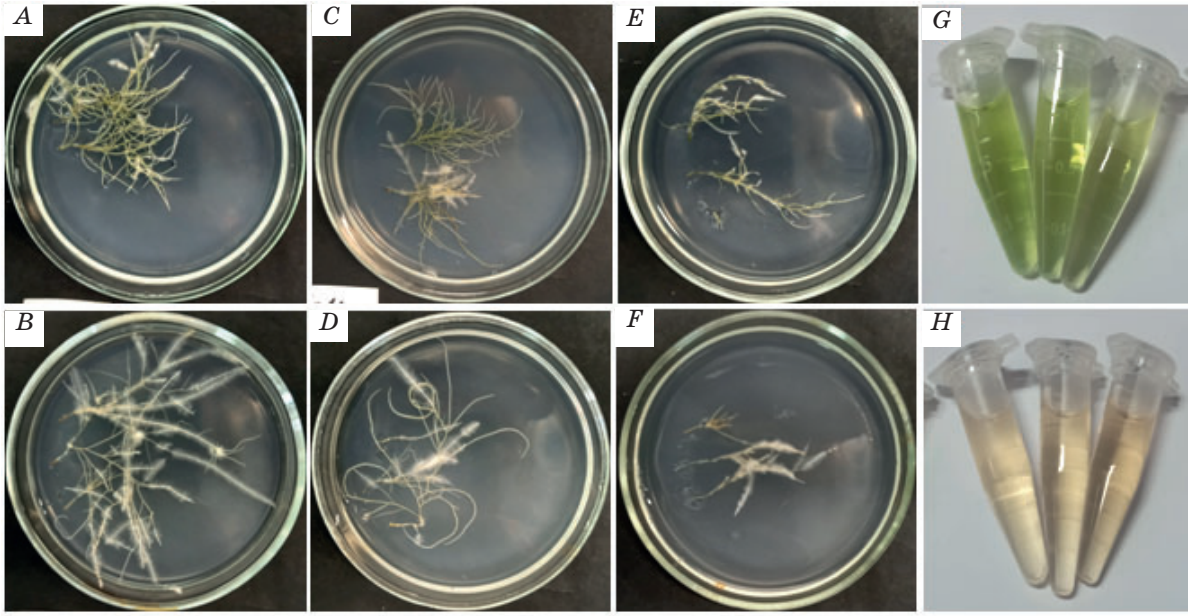

Fig. 2. **Differences in morphology of line No. 2 of *A. tilesii* hairy roots grown in different lighting conditions and phenylalanine addition:**
A — light without phenylalanine addition (control); *B* — dark without phenylalanine; *C* — light, 0.05 mM phenylalanine; *D* — dark, 0.05 mM phenylalanine; *E* — light, 0.1 mM phenylalanine; *F* — dark, 0.1 mM phenylalanine; *G* — ethanolic extracts prepared from the sample of hairy roots grown in light; *H* — ethanolic extracts prepared from the sample of hairy roots grown in dark

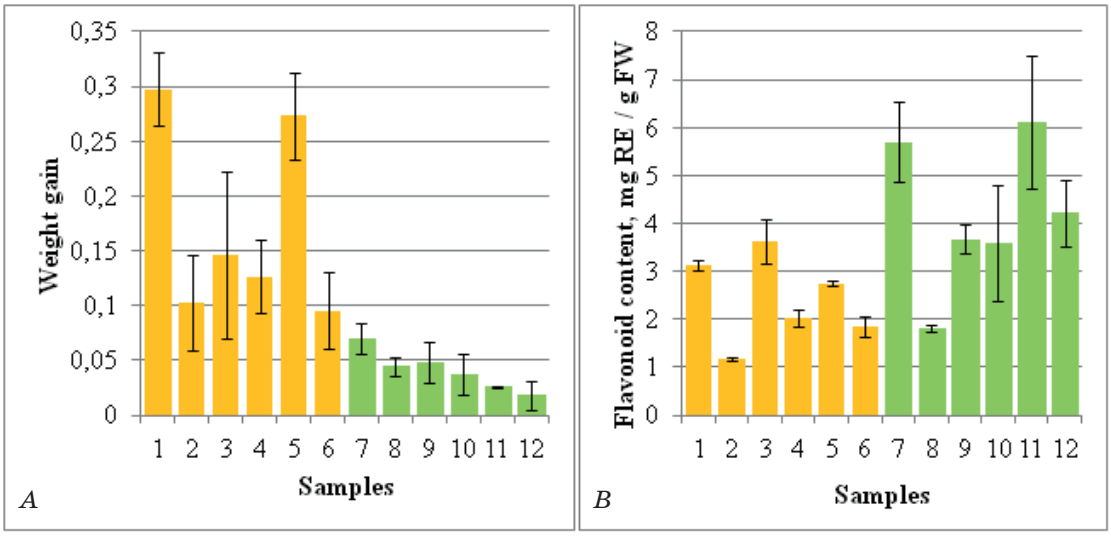

Fig. 3. **Weight gain (*A*) and flavonoid content (*B*) of the *A. tilesii* hairy roots grown on two lighting modes without and with addition of low concentrations of phenylalanine:**
orange columns — line No. 1, green columns — line No. 2. Growth conditions: columns 1 and 7 — light, without addition of phenylalanine (controls); 2 and 8 — dark, without phenylalanine; 3 and 9 — light, 0.05 mM phenylalanine; 4 and 10 — dark, 0.05 mM phenylalanine; 5 and 11 — light, 0.1 mM phenylalanine; 6 and 12 — dark, 0.1 mM phenylalanine

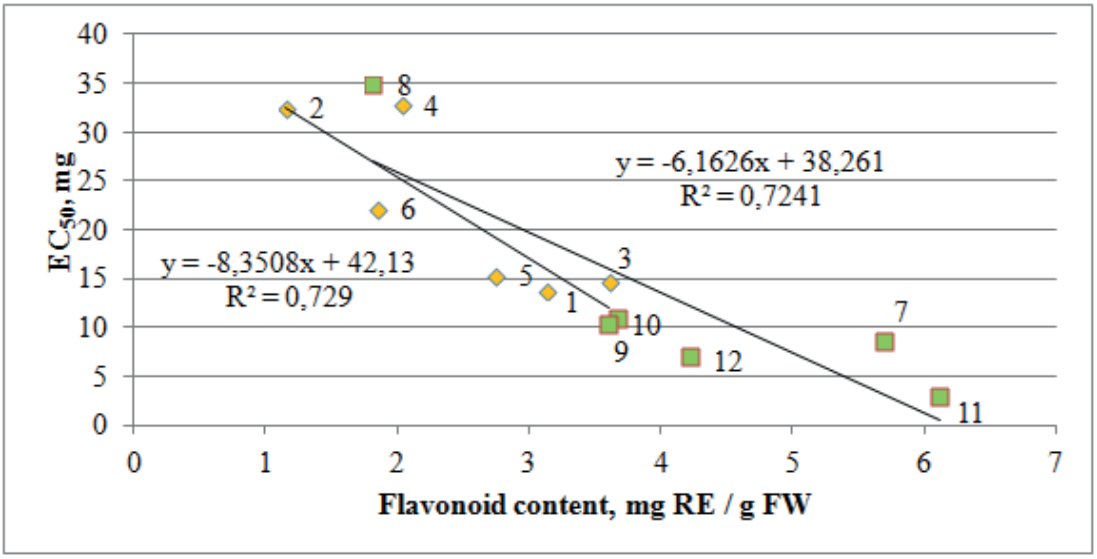

Fig. 4. **Correlation graph of antioxidant activity (EC_{50}) and flavonoid content of the *A. tilesii* hairy roots grown on two lighting modes without and with addition of low concentrations of phenylalanine:** orange markers — line No. 1, green markers — line No. 2. Markers and corresponding conditions: 1 and 7 — light, without addition of phenylalanine (controls); 2 and 8 — dark, without phenylalanine; 3 and 9 — light, 0.05 mM phenylalanine; 4 and 10 — dark, 0.05 mM phenylalanine; 5 and 11 — light, 0.1 mM phenylalanine; 6 and 12 — dark, 0.1 mM phenylalanine

resulted after the addition of phenylalanine was more prominent that the increase in the concentration of flavonoids in the extracts. In none of the samples the value of the total content of flavonoids per whole biomass was higher than in the control root samples (roots grown in light without addition of phenylalanine). This result shows that for both of the *A. tilesii* hairy root lines phenylalanine is not a suitable elicitor, regardless of the chosen concentration. The possibility of stimulating the biosynthesis of metabolites in plants using phenylalanine was previously studied [7, 10]. Obviously, such an effect can be species-specific.

Light is known as an important factor affecting plants including their growth and metabolism of plant cells. It can stimulate secondary metabolism but such an effect may be species-specific and varied in the study of different metabolites. Briefly, greening of *Solanum khasianum* roots under light irradiation and stimulation of biosynthesis was studied [36]. Lighing also increased the concentration of polyphenols in *Echinacea purpurea* [37], *Fagopyrum tataricum* [38], *Scutellaria lateriflora* [17] and *Fagopyrum tataricum* [16]. The results of our study demonstrated the positive effect of lighting on *A. tilesii* hairy roots growth and flavonoid accumulation. The similar stimulating effect was founded in the experiments with other plants of *Artemisia* genus — *A. annua* hairy roots [39]. In that experiment the growth rate and artemisinin accumulation increased in case of cultivation of hairy roots at 3000 lx light irradiation for 16 h.

Conclusions

It was shown that illumination has an impact on *A. tilesii* hairy roots morphology, color, branching, biomass accumulation and flavonoids biosynthesis. For both studied root lines it was found that the presence of lighting is more beneficial than constant maintenance in the dark, as light activated the synthesis of flavonoids and increased antioxidant activity.

In this study, no concentrations of the added precursor were found to be beneficial for the total content of flavonoids in the whole biomass of *A. tilesii* hairy roots. Addition of phenylalanine at a concentration of 1 mM inhibited both the growth of hairy roots of *Artemisia tilesii* and the synthesis of flavonoids. Such effect was observed during cultivation with and without illumination. The degree of inhibition varied in the hairy root lines. One of the lines appeared to be more tolerant to PHE at any concentrations than the other. In addition the line that had worse biomass increase at the same time had higher flavonoid accumulation while cultivating on the medium with the addition

of low concentrations of phenylalanine. This can be the result of the dependence of the ratio of rate of growth and secondary metabolites biosynthesis limited by the scarce resources of the plant cells.

Hereby, the addition of phenylalanine in various concentrations to the nutrient medium during the cultivation can have different effects on the hairy root lines of *A. tilesii*. This can be caused not only by cultivation parameters (different lighting regimes), but also by differences in the genotypes of the obtained lines of the same species.

Funding

This research was partially supported by grant No. 42526.

REFERENCES

1. *Saarela J. M., Sokoloff P. C., Gillespie L. J., Bull R. D., Bennett B. A., Ponomarenko S.* Vascular plants of Victoria Island (Northwest Territories and Nunavut, Canada): a specimen-based study of an Arctic flora. *PhytoKeys*. 2020, 141, 1–330. https://doi.org/10.3897/phytokeys.141.48810
2. *Sharifi-Rad J., Herrera-Bravo J., Semwal P., Painuli S., Badoni H., Ezzat S. M., Farid M. M., Merghany R. M., Aborehab N. M., Salem M. A., Sen S., Acharya K., Lapava N., Martorell M., Tynybekov B., Calina D., Cho W. C. Artemisia* spp.: An Update on Its Chemical Composition, Pharmacological and Toxicological Profiles. *Oxid. Med. Cell. Longev*. 2022, 2022, 5628601. https://doi.org/10.1155/2022/5628601
3. *Ekiert H., Klimek-Szczykutowicz M., Rzepiela A., Klin P., Szopa A.* Artemisia Species with High Biological Values as a Potential Source of Medicinal and Cosmetic Raw Materials. *Molecules*. 2022, 27(19), 6427. https://doi.org/10.3390/molecules27196427
4. *Kshirsagar S. G., Rao R. V.* Antiviral and Immunomodulation Effects of Artemisia. *Medicina*. 2021, 57(3), 217. https://doi.org/10.3390/medicina57030217
5. *Trendafilova A., Moujir L. M., Sousa P. M. C., Seca A. M. L.* Research Advances on Health Effects of Edible *Artemisia* Species and Some Sesquiterpene Lactones Constituents. *Foods*. 2020, 10(1), 65. https://doi.org/10.3390/foods10010065
6. *Peng W., Wang N., Wang S., Wang J., Bian Z.* Effect of co-treatment of microwave and exogenous L-phenylalanine on the enrichment of flavonoids in Tartary buckwheat sprouts. *J Sci Food Agric*. 2023, 103(4), 2014–22. https://doi.org/10.1002/jsfa.12263
7. *Demirci T., Çelikkol Akçay U., Göktürk Baydar N.* Effects of 24-epibrassinolide and L-phenylalanine on growth and caffeic acid derivative production in hairy root culture of *Echinacea purpurea* L. Moench. *Acta Physiol Plant*. 2020, 42, 66. https://doi.org/10.1007/s11738-020-03055-7
8. *Cao D. M., Vu P. T. B., HoangM. T. T., Bui A. L., Quach P. N. D.* Developing a Sufficient Protocol for the Enhancement of α-Glucosidase Inhibitory Activity by *Urena lobata* L. Aeroponic Hairy Roots Using Exogenous Factors, a Precursor, and an Elicitor. *Plants*. 2020, 9(4), 548. https://doi.org/10.3390/plants9040548
9. *Arya D., Patni V.* Pharmacognostic profile and phytochemical investigation of *Pluchea lanceolata* Oliver & Hiern. *vivo and in vitro*. *Int. J. Pharm. Sci. Rev. Res*. 2013, 22, 157–61.
10. *Sykłowska-Baranek K., Pietrosiuk A., Naliwajski M. R., Kawiak A., Jeziorek M., Wyderska S., Lojkowska E., Chinou I.* Effect of L-phenylalanine on PAL activity and production of naphthoquinone pigments in suspension cultures of *Arnebia euchroma* (Royle) Johnst. *In Vitro Cell Dev Biol Plant*. 2012, 48(5), 555–64. doi: https://doi.org/10.1007/s11627-012-9443-2
11. *Andi S.A., Gholami M., Ford C.M., Maskani F.* The effect of light, phenylalanine and methyl jasmonate, alone or in combination, on growth and secondary metabolism in cell suspension cultures of *Vitis vinifera*, *J. Photochem. Photobiol. B.* 2018, 199, 111625. https://doi.org/10.1016/j.jphotobiol.2019.111625
12. *Kwiecień I., Miceli N., D'Arrigo M., Marino A., Ekiert H.* Antioxidant Potential and Enhancement of Bioactive Metabolite Production in In Vitro Cultures of *Scutellaria lateriflora* L. by Biotechnological Methods. *Molecules*. 2022, 27(3), 1140. https://doi.org/10.3390/molecules27031140
13. *Noviyanti R., Sari R. L., Kristanti A. N., Yachya A., Manuhara Y.S.* Biomass and Flavonoid production of *Gynura procumbens* adventitious roots induced by sucrose, Phenylalanine and Tyrosine. *Biosci. Res.* 2017, 14, 934–41.
14. *Fadzliana N. A. F., Rogayah S., Shaharuddin N. A., Janna O. A.* Addition of L-Tyrosine to improve betalain production in red pitaya callus. *Pertanika J. Trop. Agric. Sci*. 2017, 40, 521–32.
15. *Tusevski O., Petreska Stanoeva J., Stefova M., Simic S. G.* Phenolic profile of dark-grown and photoperiod-exposed *Hypericum perforatum* L. hairy root cultures.

ScientificWorldJournal. 2013, 2013, 602752. https://doi.org/10.1155/2013/602752
16. *Thwe A. A., Kim Y., Li X., Kim Y. B., Park N. I., Kim H. H., Kim S.-J., Park S. U.* Accumulation of phenylpropanoids and correlated gene expression in hairy roots of Tartary buckwheat under light and dark conditions. *Appl. Biochem. Biotechnol*. 2014, 174, 2537–47. https://doi.org/10.1007/s12010-014-1203-9.
17. *Marsh Z., Yang T., Nopo-Olazabal L., Wu S., Ingle T., Joshee N., Medina-Bolivar F.* Effect of light, methyl jasmonate and cyclodextrin on production of phenolic compounds in hairy root cultures of *Scutellaria lateriflora*. *Phytochemistry*. 2014, 107, 50–60. https://doi.org/10.1016/j.phytochem.2014.08.020.
18. *Wongshaya P., Chayjarung P., Tothong C., Pilaisangsuree V., Somboon T., Kongbangkerd A., Limmongkon A.* Effect of light and mechanical stress in combination with chemical elicitors on the production of stilbene compounds and defensive responses in peanut hairy root culture. *Plant Physiol. Biochem.* 2020, 157, 93–104. https://doi.org/10.1016/j.plaphy.2020.10.015.
19. *Zhang D., Sun W., Shi Y., Wu L., Zhang T., Xiang L.* Red and Blue Light Promote the Accumulation of Artemisinin in *Artemisia annua* L. *Molecules*. 2018, 23(6), 1329. https://doi.org/10.3390/molecules23061329
20. *Jiao J., Gai Q. Y., Yao L. P., Niu L. L., Zang Y. P., Fu Y. J.* Ultraviolet radiation for flavonoid augmentation in *Isatis tinctoria* L. hairy root cultures mediated by oxidative stress and biosynthetic gene expression. *Ind Crops Prod*. 2018, 118, 347–54. https://doi.org/10.1016/j.indcrop.2018.03.046
21. *Takshak S., Agrawal S. B.* Defence strategies adopted by the medicinal plant *Coleus forskohlii* against supplemental ultraviolet-B radiation: augmentation of secondary metabolites and antioxidants. *Plant Physiol. Biochem.* 2015, 97, 124–38. https://doi.org/10.1016/j.plaphy.2015.09.018
22. *Fazal H., Abbasi B. H., Ahmad N., Ali M., Ali S.* Sucrose induced osmotic stress and photoperiod regimes enhanced the biomass and production of antioxidant secondary metabolites in shake-flask suspension cultures of *Prunella vulgaris* L. *Plant Cell Tissue Organ Cult*. 2016, 124, 573–81. https://doi.org/10.1007/s11240-015-0915-z
23. *Kumar S. S., Arya M., Mahadevappa P., Giridhar P.* Influence of photoperiod on growth, bioactive compounds and antioxidant activity in callus cultures of *Basella rubra* L. *J. Photochem. Photobiol. B.* 2020, 209, 111937. https://doi.org/10.1016/j.jphotobiol.2020.111937
24. *Wu C. H., Murthy H. N., Hahn E. J., Paek K. Y.* Enhanced production of caftaric acid, chlorogenic acid and cichoric acid in suspension cultures of *Echinacea purpurea* by the manipulation of incubation temperature and photoperiod. *Biochem. Eng. J*. 2007, 36, 301–3. https://doi.org/10.1016/j.bej.2007.02.024
25. *de Castro K. M., Batista D. S., Fortini E. A., Silva T. D., Felipe S. H. S., Fernandes A. M., de Jesus Sousa R. M., de Queiroz Nascimento L. S., Campos V. R., Grazul R., Viccini L. F., Otoni W.* Photoperiod modulates growth, morphoanatomy, and linalool content in *Lippia alba* L. (Verbenaceae) cultured in vitro. *Plant Cell Tissue Organ Cult*. 2019, 139, 139–53. https://doi.org/10.1007/s11240-019-01672-w
26. *Tashackori H., Sharifi M., Ahmadian Chashmi N., Safaie N., Behmanesh M.* Induced-differential changes on lignan and phenolic acid compounds in *Linum album* hairy roots by fungal extract of *Piriformospora indica*. *Plant Cell Tiss Organ Cult*. 2016, 127, 187–94. https://doi.org/10.1007/s11240-016-1041-2
27. *Jiao J., Gai Q. Y., Niu L. L., Wang X. Q., Guo N., Zang Y. P., Fu Y. J.* (). Enhanced Production of Two Bioactive Isoflavone Aglycones in *Astragalus membranaceus* Hairy Root Cultures by Combining Deglycosylation and Elicitation of Immobilized Edible *Aspergillus niger*. *J. Agric. Food Chem*. 2017, 65(41), 9078–86. https://doi.org/10.1021/acs.jafc.7b03148
28. *Ghimire B., Thiruvengadam M., Chung I.-M.* Identification of elicitors enhances the polyphenolic compounds and pharmacological potential in hairy root cultures of *Aster scaber*. *S. Afr. J. Bot*. 2019, 125. 92–101. https://doi.org/10.1016/j.sajb.2019.07.006.
29. *Krzemińska M., Owczarek A., Gonciarz W., Chmiela M., Olszewska M. A., Grzegorczyk-Karolak I.* The Antioxidant, Cytotoxic and Antimicrobial Potential of Phenolic Acids-Enriched Extract of Elicited Hairy Roots of *Salvia bulleyana*. *Molecules*. 2022, 27(3), 992. https://doi.org/10.3390/molecules27030992
30. *Gharari Z., Bagheri K., Danafar H., Sharafi A.* Enhanced flavonoid production in hairy root cultures of *Scutellaria bornmuelleri* by elicitor induced over-expression of MYB7 and FNSII2 genes. *Plant Physiol. Biochem.* 2020, 148, 35–44. https://doi.org/10.1016/j.plaphy.2020.01.002
31. *Chung I. M., Rekha K., Rajakumar G., Thiruvengadam M.* (). Influence of silver nanoparticles on the enhancement and transcriptional changes of glucosinolates

and phenolic compounds in genetically transformed root cultures of *Brassica rapa ssp. rapa*. *Bioprocess Biosyst Eng.* 2018, 41(11), 1665–77. https://doi.org/10.1007/s00449-018-1991-3
32. *Nourozi E., Hosseini B., Maleki R., Abdollahi Mandoulakani B.* Iron oxide nanoparticles: a novel elicitor to enhance anticancer flavonoid production and gene expression in *Dracocephalum kotschyi* hairy-root cultures. *J. Sci. Food Agric.* 2019, 99(14), 6418–30. https://doi.org/10.1002/jsfa.9921
33. *Matvieieva N. A., Shakhovsky A. M., Belokurova V. B., Drobot K. O. Artemisia tilesii* Ledeb. hairy roots establishment using *Agrobacterium rhizogenes*-mediated transformation. *Prep. Biochem. Biotechnol.* 2016, 46(4), 342–5. https://doi.org/10.1080/10826068.2015.1031393
34. *Pękal A., Pyrzynska K.* Evaluation of Aluminium Complexation Reaction for Flavonoid Content Assay. *Food Anal. Methods.* 2014, 7, 1776–1782. https://doi.org/10.1007/s12161-014-9814-x
35. *Brand-Williams W., Cuvelier M. E., Berset C.* Use of a free radical method to evaluate antioxidant activity. *LWT — Food Science and Technology*. 1995, 28(1), 25–30. https://doi.org/10.1016/S0023-6438(95)80008-5
36. *Jacob A., Malpathak N.* Green hairy root cultures of Solanum khasianum Clarke — A new route to in vitro solasodine production. *Curr. Sci.* 2004, 1442–7. https://www.jstor.org/stable/24109486
37. *Abbasi B. H., Tian C.-L., Murch S. J., Saxena P. K., Liu C.-Z.* Light-enhanced caffeic acid derivatives biosynthesis in hairy root cultures of *Echinacea Purpurea*. *Plant Cell Rep*. 2007, 26, 1367–1372. https://doi.org/10.1007/s00299-007-0344-5
38. *Park C. H., Park Y. E., Yeo H. J., Park N. I., Park S. U.* Effect of Light and Dark on the Phenolic Compound Accumulation in Tartary Buckwheat Hairy Roots Overexpressing ZmLC. *Int. J. Mol. Sci.* 2021, 22(9), 4702. https://doi.org/10.3390/ijms22094702
39. *Liu C.-Z., Guo C., Wang Y-C., Ouyang F.* Effect of light irradiation on hairy root growth and artemisinin biosynthesis of *Artemisia annua* L. *Process Biochem*. 2002, 38(4), 581–5. https://doi.org/10.1016/S0032-9592(02)00165-6

ВПЛИВ ФЕНІЛАЛАНІНУ ТА ОСВІТЛЕННЯ НА РІСТ «БОРОДАТИХ» КОРЕНІВ *Artemisia tilesii* Ledeb.

Т. А. Богданович, Н. А. Матвєєва

Інститут клітинної біології та генетичної інженерії
Національної академії наук України, Київ

E-mail: bogdanovych_tais@ukr.net

Мета. Проаналізувати вплив фенілаланіну у різних концентраціях та освітлення (окремо та в комбінації) для стимулювання росту біосинтезу флавоноїдів у двох лініях «бородатих» коренів *Artemisia tilesii* Ledeb.

Методи. Корені вирощували на агаризованому середовищі з фенілаланіном високої (1 мМ) і низької (0,05 і 0,1 мМ) концентрацій при освітленні (3000 лк, 16 год) і в темряві. Після чотирьох тижнів культивування приріст ваги, вміст флавоноїдів і активність проти DPPH-радикалу визначали згідно зі стандартними методиками.

Результати. Корені, вирощені на світлі, мали зеленуватий колір, були більш розгалужені та товщі, а після росту в темряві були більш видовженими. Додавання фенілаланіну (1 мМ) пригнічувало ріст усіх зразків. Дві лінії коренів відрізнялися за чутливістю до фенілаланіну у менших концентраціях. Вміст флавоноїдів у всіх зразках обох ліній був вищим на світлі (до 3,14 рази), незалежно від концентрації фенілаланіну. Антиоксидантна активність також була вищою у коренях, вирощених на світлі, причому значення EC_{50} корелювали з вмістом флавоноїдів.

Висновки. Освітлення стимулювало синтез флавоноїдів і підвищувало антиоксидантну активність всіх зразків. Ефект додавання фенілаланіну на накопичення біомаси та біосинтез флавоноїдів залежав від лінії «бородатих» коренів.

Ключові слова: *Artemisia tilesii* Ledeb.; «бородаті» корені; фенілаланін; освітлення; еліситори; флавоноїди; антиоксидантна активність.